UNIVERSITÀ DI PARMA

UNIVERSITÀ DEGLI STUDI DI PARMA

DOTTORATO DI RICERCA IN

Medicina Molecolare

CICLO XXXVI

Role of macrophages in metabolic diseases: focus on atherosclerosis and liver fibrosis

Coordinatore:

Chiar.mo Prof. Prisco Mirandola

Tutore:

Chiar.mo Prof. Francesco Potì

Co-Tutore:

Chiar.mo Dr. Thierry Huby

Dottorando:

Dott. Mattia Dessena

Anni Accademici 2020/2021 – 2022/2023

Table of contents

Chapter 1

Sphingosine 1-phosphate receptors (S1PRs): novel pharmacological targets for modulating lipid transport in macrophages

Chapter 2

Impact of myeloid-Bhlhe40 deficiency in liver fibrosis: exploring Kupffer cells crosstalk with hepatic stellate cells

Abstract

ITA – I macrofagi sono cellule del sistema immunitario caratterizzate da una significativa eterogeneità e plasticità che permette loro di adattarsi alle variazioni dinamiche del microambiente e di contribuire quindi al mantenimento dell'omeostasi. Quasi tutti i tessuti dell'organismo sono popolati da macrofagi residenti (trMacs), i quali, rispondendo a segnali tessuto-specifici, giocano un ruolo chiave nell'infiammazione, nei processi di riparazione, nella difesa dell'ospite contro agenti patogeni e nell'eliminazione delle cellule morte e/o senescenti. I trMacs si sviluppano durante l'embriogenesi e si sostengono attraverso meccanismi di auto-rinnovamento indipendenti dai monociti circolanti. Tuttavia, a seguito di insulti pro-infiammatori o danno tissutale, i monociti sono reclutati nel sito interessato dove differenziano in macrofagi specializzati, aventi fenotipo e funzioni distinguibili rispetto a quelli residenti. Tuttavia, questa risposta omeostatica utile alla guarigione delle ferite, se persistente può innescare o aggravare condizioni patologiche. Negli ultimi anni si è manifestato un crescente interesse per lo studio e lo sviluppo di strategie mirate a modulare la funzione dei macrofagi, proprio per la loro capacità di rispondere dinamicamente all'ambiente circostante.

Il primo obiettivo del presente studio è stato quello di esplorare gli effetti della modulazione farmacologica dell'asse sfingosina 1-fostato (S1P)/recettori di S1P (S1PRs) sul metabolismo del colesterolo nei macrofagi, i quali ricoprono un ruolo centrale nello sviluppo e nella progressione delle lesioni aterosclerotiche. Parallelamente, si è proposto di approfondire il ruolo del fattore di trascrizione Bhlhe40 nelle cellule mieloidi nel contesto della fibrosi epatica, con particolare attenzione al crosstalk tra i macrofagi epatici (Kupffer cells e macrofagi derivati da monociti) e le cellule stellate epatiche.

Il nostro studio suggerisce che la stimolazione farmacologica dei recettori di S1P potrebbe favorire l'omeostasi del colesterolo nei macrofagi, riducendone l'accumulo e promuovendone l'efflusso verso le lipoproteine accettrici. Questa strategia rappresenterebbe, quindi, un nuovo possibile approccio terapeutico per la malattia cardiovascolare aterosclerotica. Inoltre, la nostra ricerca ha rivelato il potenziale coinvolgimento del fattore di trascrizione mieloide Bhlhe40 nella fibrosi epatica. La modulazione dell'infiammazione e la regolazione della produzione di citochine, associate alla carenza di Bhlhe40, sembrano contribuire a una significativa riduzione

dell'infiltrazione di leucociti e all'inibizione dell'attivazione delle cellule stellate epatiche.

ENG – Macrophages are immune cells characterized by significant heterogeneity and plasticity, allowing them to adapt to dynamic changes in the microenvironment and contribute to maintaining homeostasis. Nearly all tissues are populated by resident macrophages (trMacs), which, in response to tissue-specific signals, play a key role in inflammation, repair processes, host defense against pathogens and clearance of dead and/or senescent cells. trMacs develop during embryogenesis and are sustained by self-renewal mechanisms independent of circulating monocytes. However, following injury, monocytes are recruited to the compromised tissue where they differentiate into specialized macrophages with distinct phenotypes and functions compared to resident counterparts. Although this represents a crucial step in the homeostatic response to wound healing, persistent tissue damage can trigger or exacerbate pathological conditions. In the last few years, a growing interest has emerged in studying and developing strategies that directly target macrophages, since their ability to dynamically respond to the surrounding environment makes them key players in many pathogenetic mechanisms.
This study aimed to explore the effects of pharmacological modulation of the sphingosine 1-phosphate (S1P)/S1P receptors (S1PRs) axis on cholesterol metabolism in macrophages, which play a central role in the development and progression of atherosclerotic lesions. Concurrently, our study set out to investigate the role of the transcription factor Bhlhe40 in myeloid cells in the context of hepatic fibrosis, with a specific focus on the crosstalk between hepatic macrophages (Kupffer cells and monocyte-derived macrophages) and hepatic stellate cells.
Our data suggest that the pharmacological stimulation of S1P receptors could promote cholesterol homeostasis in macrophages, reducing lipid accumulation and facilitating efflux to lipoproteins. This strategy would, therefore, represent a new potential therapeutic approach for atherosclerotic cardiovascular disease. Moreover, our investigation has identified a potential implication of the myeloid transcription factor Bhlhe40 in hepatic fibrosis. The modulation of inflammation and the regulation of cytokine production, associated with Bhlhe40 deficiency, seem to be key features in substantially reducing the infiltration of leukocytes and inhibition of hepatic stellate cell activation.

Chapter 1

Sphingosine 1-phosphate receptors (S1PRs): novel pharmacological targets for modulating lipid transport in macrophages

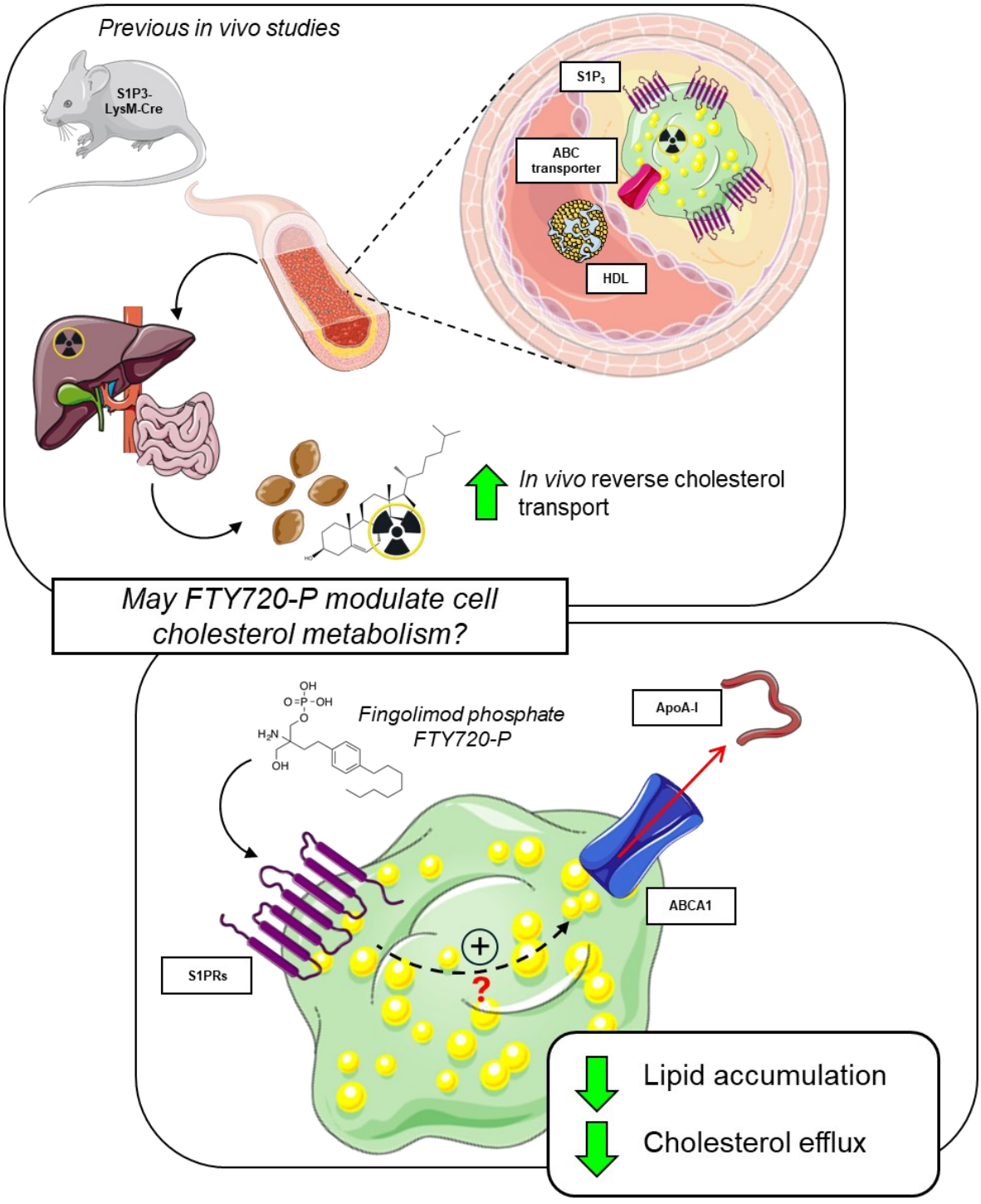

Parts of the figure were drawn by using pictures from Servier Medical Art. Servier Medical Art by Servier is licensed under a Creative Commons Attribution 3.0 Unported License (https://creativecommons.org/licenses/by/3.0/).

Introduction

Sphingosine-1-phosphate (S1P)

Production and metabolism

The role of sphingolipids in regulating many cellular processes, both in physiological and pathological conditions, is widely acknowledged.

Sphingolipids (SLs), essential components of biological membranes of eukaryotic organisms, play important roles in signal transduction pathways, directly contributing to crucial biological functions such as cell motility, growth, differentiation, senescence, as well as survival and cell death[1].

Sphingolipids constitute a wide class of bioactive lipids, including ceramides and sphingosine 1-phosphate, that contain a sphingoid base backbone[2].

De novo SL biosynthesis occurs in the cytoplasmatic side of the endoplasmic reticulum (ER), where a cluster of four enzymes synthesize ceramides with different lengths of acyl chains, which are considered a hub of the SLs metabolism, from non-sphingolipid precursors[3]. The first reaction involves the condensation of a cytosolic serine and palmitoyl-coA to produce 3-ketodihydrosphingosine (KDHSph) catalyzed by serine palmitoyltransferase (SPT). KDHSph is reduced by the enzyme 3-ketodihydrosphingosine reductase (KDHR) in a NADPH dependent manner, leading to the formation of dihydrosphingosine (DHSph), also known as sphinganine, which is N-acetylated with palmitic acid by a ceramide synthase, providing dihydroceramide. Subsequently, the dehydroceramide is dehydrogenated to ceramide by dihydroceramide Δ4-desaturase (DES). Given that ceramides display low solubility within an aqueous environment, they are transported to the Golgi apparatus either through vesicular trafficking or through the cytosolic protein ceramide transfer protein (CERT). Here, this molecule can undergo phosphorylation by ceramide kinase (CERK) to produce ceramide-1-phosphate (C1P), be converted, through the transfer of a phosphocholine headgroup, into sphingomyelin (SM) and diacylglycerol (DAG) by sphingomyelin synthase (SMS), or be deacetylated by the enzyme ceramidase to form sphingosine. Then, sphingosine can be phosphorylated by a sphingosine kinase (SPHK) to form sphingosine-1-phosphate (S1P). S1P levels are rigorously controlled through its rapid synthesis and degradation in multiple compartments. It can undergo

dephosphorylation by sphingosine phosphate phosphatases (SPP-1 and SPP-2), lipid phosphate phosphatases (LPPs) or alkaline phosphatases to generate sphingosine, which can then be recycled for the biosynthesis of new sphingolipids through the "salvage pathway". Alternatively, S1P-lyase (S1PL), a pyridoxal 5'-phosphate-dependent aldehyde-lyase, irreversibly degrade S1P into phosphoetanolamide and hexadecenal[4].

Sphingosine 1-phosphate is a membrane-derived lysosphingolipid that regulates important biological functions by binding to its G protein-coupled receptors, named $S1P_{1-5}$. The specific expression of S1P receptors in different cell types is essential for regulating immune, cardiovascular, and nervous system. S1P is produced by phosphorylating sphingosine, a reaction catalyzed by an enzyme known as sphingosine kinase and acts as an extracellular and intracellular signaling molecule ("inside-out" signaling). Two SK genes, *SPHK1* and *SPHK2*, encode the two enzymatic isoforms (SPHK1 and SPHK2), which exhibit distinct steady-state localizations and functions. SPHK1 is mainly localized in the cytoplasm and translocates to the plasma membrane, endosomal vesicles and/or phagosomes upon cellular stimulation through a mechanism regulated by the ERK1/2 kinase[5]. It has been extensively demonstrated that this enzymatic isoform acts as a cell survival promoter; indeed, SPHK1 activity promotes cell proliferation and survival. On the other hand, SPHK2 is largely localized at the level of the endoplasmic reticulum or associated with mitochondria and can translocate into the nucleus due to the presence of a nuclear localization signal (NLS) and a nuclear exportation signal (NES) in its N-terminal and C-terminal domain. In the nucleus, this isoform induces cell cycle arrest and apoptosis partially achieved by increasing ceramide production[6] and can also inhibit histone deacetylase, thus altering the epigenetic regulation of gene expression.

Platelets, erythrocytes and vascular endothelium are the primary sources of S1P[7]. Thrombocytes exhibit high SPHK, with the primary contribution originating from SPHK1[8], and lack of S1PL[9]. In order to synthesize S1P, platelets incorporate extracellular sphingosine or alternatively degrade SM on the outer leaflet of the plasmalemma due to the very low enzymatic activity of serine palmitoyltransferase. Moreover, it has been shown that they can recycle S1P for the biosynthesis of new ceramides[10]. Similar to platelets, red blood cells also express SPHK, although the enzymatic activity is notably lower, and they are deficient in *de novo* sphingolipid

biosynthesis[11]. Both erythrocytes and platelets efficiently store S1P. However, while the former release it spontaneously without any stimulation into plasma, thrombocytes require activation induced by thrombin, collagen, convulxin or ADP[12,13]. For this reason, it seems that platelets do not have a significant contribution to the regulation of circulating S1P level under physiological conditions, as no changes in plasma S1P levels have been observed in thrombocytopenic mice[14]. The extracellular secretion of the lysosphingolipid is mediated by various transporters, among which the major facilitator superfamily transporter 2b (Mfsd2b) plays a crucial role[15]. The deletion of Mfsd2b in hematopoietic cells drastically reduces plasma levels of S1P, leading to an intracellular increase of the lysosphingolipid in red blood cells and platelets[16]. However, the accumulation of sphingolipids, causing lipotoxicity, results in an alteration of the morphology and functionality of the thrombocytes, exhibiting reduced aggregation[17]. Recent findings have revealed that ATP-binding cassette (ABC) transporters and SPNS2 (Spinster homologue 2) are involved in the export of S1P outside the cells. S1P is released from mast cells independently of degranulation through a mechanism mediated by ABCC1[18]. Moreover, in platelets, S1P is exported via an ABC-mediated process, involving two distinct S1P exporters induced by thrombin or Ca^{2+}[19]. However, in cells expressing both ABC and SPNS2 and Mfsd2b transporters, the former did not export S1P on their own[20]. Indeed, plasma levels of S1P is not changed in ABCA1, ABCA7 or ABCC1 knockout mice[21]. Finally, it has been demonstrated that ABC transporters do not contribute to S1P export from erythroid cells[20,22]. Given their controversial nature, these results emphasize the intricate complexity of S1P transport mechanisms. By contrast, endothelial cells can release S1P through a mechanism mediated by SPNS2, contributing to approximately 30% of plasma S1P levels[23]. Endothelial-specific SPNS2 knockout mice show impaired immune cell trafficking and lymphopenia, underscoring the putative role of endothelial-derived S1P in the regulation of lymphocyte trafficking[24].

S1P concentration in human plasma ranges from 200 nM to 900 nM[7,25, 26,27]. Plasma S1P levels may be influenced by various factors, including gender, age and body composition of the individuals under consideration. Several studies have investigated the correlation between plasma S1P levels and gender differences; however, the data are conflicting[28,29]. This inconsistency is likely associated with differences in the age of the examined populations. Indeed, S1P concentration in plasma markedly

decreases in women after menopause[30] and is negatively correlated with age. Moreover, S1P levels do not change between fasting and non-fasting individuals[29] and are elevated in obese subjects[31].

Gradients of biological molecules are crucial for preserving the homeostasis and development of the organism. It has been estimated that concentrations of S1P in the lymphatic system correspond to approximately 25% of plasma levels[32], while in the interstitial fluid, S1P is found in even lower levels[33]. Substrate availability, metabolic enzyme activity and regulatory factors play crucial roles in establishing and maintaining the S1P gradient. It has been demonstrated that this gradient is functionally relevant in the *in vivo* trafficking of immune cells as they navigate through the vascular and lymphatic compartments. Vascular cells, in particular, are significantly influenced by S1P signaling and actively contribute to the preservation of this gradient, which is essential for the homeostasis of blood vessels[34].

Due to its pronounced hydrophobic characteristics, S1P is preferentially transported in the bloodstream bound to carrier proteins. In plasma, more than half of S1P is carried by HDLs (55%), while the remaining fraction is distributed among albumin (35%) or other lipoproteins, especially LDLs (8%)[25]. Although *in vitro* studies indicated that HDL-bound S1P mediated functions analogous to albumin-bound S1P, it has been demonstrated that the specific plasma distribution reflects distinct biological effects. Wilkerson et al. demonstrated that HDL-bound S1P contributes to endothelial homeostasis much more effectively than the albumin-S1P complex. Moreover, only S1P bound to HDLs reduces the degradation of the $S1P_1$ receptor and promotes its recycling on the cell surface, highlighting the critical influence of the S1P carrier in this process[35]. Discrepancies in half-life demonstrate that HDLs represent a stable plasma reservoir for S1P, exhibiting anti-atherogenic actions by triggering specific signaling pathways in endothelial cells, smooth muscle cells, and macrophages. Conversely, due to its high concentration in plasma, albumin can act both as a reservoir and a molecular trap for S1P, effectively hindering the stimulation of S1P receptors. S1P specifically and selectively binds to the protein component apolipoprotein M (ApoM) of HDLs. The concentration of ApoM in plasma is approximately 0.9 µmol/L, distributed over 95% in HDLs, mainly in the HDL_3 subclass, and to a lesser extent among LDLs and VLDLs. The HDL-bound ApoM/S1P complex plays a crucial role in various anti-atherosclerotic effects linked to HDLs. ApoM-deficient mice exhibit a significant

decrease in both plasma and HDLs S1P level, along with increased permeability of lung capillaries and the blood-brain barrier for albumin[36–38]. Moreover, the ApoM-bound S1P, by interacting with $S1P_1$, promotes transendothelial HDL transport[39]. Recent studies have shown that in animals lacking both ApoM and albumin, the primary protein chaperones for the circulating S1P, immune and vascular functions were not altered, despite a reduction of approximately 25% in plasma S1P levels. This suggested the existence of another carrier for S1P in the blood. Obinata et al. identified ApoA4 in lipoprotein-free protein (LPFP) fractions (protein-rich fractions that elute after lipoproteins) as potential candidates as S1P-binding proteins[40].

Structure and function of S1P receptors

The biological effects mediated by S1P are mainly associated with its interaction with specific G protein-coupled receptors (S1PRs) located in the cytoplasmic membrane. Historically, the first identified S1P receptor was the orphan receptor endothelial differentiation gene 1 (EDG1)[41]. Subsequently, five receptor subtypes were identified: EDG1, EDG5, EDG3, EDG6, EDG8[42]. However, this nomenclature has been replaced by the current classification, namely $S1P_1$, $S1P_2$, $S1P_3$, $S1P_4$, and $S1P_5$[43]. These receptors are expressed ubiquitously, although $S1P_{1,2,3}$ are predominantly distributed in the immune and cardiovascular systems while $S1P_4$ and $S1P_5$ in the lymphatic and nervous systems, respectively[44]. The S1P receptors, upon activation, form complexes with several G proteins that are categorized based on their α-subunit, triggering the activation or inhibition of numerous downstream signaling pathways. The signaling mediated by S1PRs plays a key role in various biological processes, including cell growth, survival, differentiation, angiogenesis[45], lymphocyte trafficking[46], vascular integrity and maturation[47]. $S1P_1$ is exclusively coupled with $G\alpha_{i/o}$ protein, while $S1P_2$ and $S1P_3$ can couple with $G\alpha_{i/o}$, $G\alpha_q$, or $G\alpha_{12/13}$ proteins. On the other hand, S1P4 and S1P5 form complexes with $G\alpha_{i/o}$ or $G\alpha_{12/13}$ proteins. The effects mediated by S1P, therefore, depend on the activated signaling pathway. Signaling through $G\alpha_{i/o}$ can activate three key pathways: the Ras/ERK pathway, promoting cell proliferation; the PI3K/Akt pathway, inhibiting apoptosis and thereby contributing to cell survival; and the PI3K/Rac pathway, facilitating cytoskeletal rearrangements and cell migration. In addition, $G\alpha_{i/o}$ protein can activate phospholipase C (PLC), In addition, the Gαi/o protein can activate phospholipase C (PLC), leading to an increase in intracellular calcium concentration and inhibition of adenylate cyclase. The activation of PLC is

also associated to $G\alpha_q$. Instead, signaling mediated by $G\alpha_{12/13}$ promotes Rho. On one hand, it activates Rho-associated protein kinase (ROCK), thereby reducing the functionality of the endothelial barrier. On the other hand, it inhibits Rac and, consequently, Rac-mediated effects such as cellular migration[48].

S1P$_1$. This receptor plays a crucial role in angiogenesis, neurogenesis, endothelial function and vascular tone. S1P$_1$ is expressed by lymphocytes and regulates their egress from secondary lymphoid organs, guiding their trafficking according to S1P gradient[49]. Additionally, it mediates the recruitment of inflammatory cells, monocytes and macrophages to the site of inflammation. S1P$_1$ full knockout mice are not viable due to impaired development of the vascular system[50].

S1P$_2$. This isoform is particularly expressed in vascular smooth muscle cells and is involved in mast cell degranulation, histamine secretion and contraction of bronchial smooth muscle. Moreover, it mediates opposite effects on endothelium compared to S1P$_1$. It has been observed that depletion of S1P$_2$ in ApoE knockout mice leaded to reduced atherosclerosis but increased pro-inflammatory cytokines (IL-8 and IL-1β) in plasma[51]. However, activation of the isoform inhibits the growth and differentiation of vascular smooth muscle cells[52], suggesting that the activation of S1P/S1P$_2$ axis mediates either pro- or anti-inflammatory effects depending on the site of expression. Finally, although S1P$_2$ depletion is compatible with life, offspring can spontaneously develop lethal seizures and deafness[53].

S1P$_3$. Isoform 3 is widely expressed in heart, lungs, spleen, kidneys, and intestines. It mediates the migration and proliferation of both endothelial and smooth muscle cells and regulates neuronal response and blood pressure. Additionally, a recent study has identified the potential contribution of S1P$_3$ in leukemogenesis[54]. Depletion of S1P$_3$ results in vasodilation due to reduced nitric oxide production *in vitro*[55]. However, the absence of the receptor in ApoE knockout mice does not influence the progression of atherosclerotic plaques, despite reduced leukocyte infiltration[56].

S1P$_4$. This receptor is predominantly expressed by immune cells and smooth muscle cells in the airways. It regulates the production of cytokines in T lymphocytes[56].

S1P$_5$. Isoform 5 is expressed in the brain and spleen and regulates the trafficking of natural killer cells[57].

Fingolimod

Fingolimod (FTY720/Gilenya; Novartis) is an immunosuppressive compound approved by the FDA in 2010 as the first orally administered drug for the treatment of relapsing-remitting multiple sclerosis (RRMS)[58]. Phosphorylated by sphingosine kinase 2 and, to a lesser extent, by sphingosine kinase 1[59], FTY720 is a non-selective modulator of four out of the five S1P receptors (1, 3, 4, and 5). It is a prodrug, requiring phosphorylation to interact with S1PRs. Fingolimod phosphate has a high affinity for $S1P_1$ and the binding to this receptor subtype specifically mediates the immunosuppressive activity of the compound, acting as a functional antagonist. After the binding of S1P or fingolimod phosphate to S1PRs, all receptors undergo internalization, dissociation in endosomes, and return to the cell membrane where they can be reactivated, except for $S1P_1$. Fingolimod phosphate irreversibly downregulates $S1P_1$ since S1P lyase is unable to catabolize this compound. The subsequent desensitization to serum S1P results in the immobilization of lymphocytes in lymphoid organs due to the altered S1P gradient, consequently reducing their infiltration into the central nervous system[49]. Interacting with $S1P_1$ expressed on endothelial cells, fingolimod phosphate preserves vascular integrity by enhancing barrier function, reducing permeability through VEGF inhibition, and promoting adherens junction assembly[60]. However, some studies suggested that the protective effect of the compound on endothelial function may be dose- and exposure time-dependent and other receptor subtypes may be involved[61,62]. Bradycardia induction has been attributed to $S1P_1$ signaling in humans and $S1P_3$ modulation in mice. The first-dose bradycardia observed in some patients is intricately connected to the S1PR-dependent activation of G-protein–coupled inwardly rectifying potassium (GIRK, also known as Kir3) channels on atrial myocytes. This activation leads to hyperpolarization, resulting in a transient reduction in excitability[63,64]. Moreover, activation of the $S1P_1$ signaling pathway results in endothelial NOS activation, NO release and subsequent vasodilation, which could explain the transient hypotension observed in patients at the beginning of fingolimod therapy[65]. Additionally, interaction with $S1P_3$ also induces arterial vasodilation[66]. On the other hand, fingolimod treatment can interfere with $S1P_3$ signaling in macrophages, leading to reduced ROS production, phagocytosis and M2 polarization[67].

A recent systematic review and meta-analysis have highlighted that the use of S1PR modulators increases the risk of cardiovascular events in patients affected by multiple sclerosis. In particular, these individuals have a 2.92- and 2.00-fold higher risk of developing bradyarrhythmia and hypertension, respectively, compared to patients treated with other compounds[68]. Until now, the risk of events related to atherosclerotic progression has not been investigated. Nevertheless, in different patient cohorts receiving fingolimod treatment, an elevation in plasma levels of total cholesterol, HDL cholesterol and ApoE has been observed, while levels of LDL cholesterol and triglycerides remain unchanged[69,70].

Atherosclerosis: an overview

Improved health-care services, widespread vaccinations and the treatment of acute infections have significantly increased life expectancy. However, this has also led to a rise in the incidence of chronic diseases such as atherosclerosis. Cardiovascular diseases (CVDs) represent a leading cause of vascular disease and death worldwide. Over 17.9 million people died from CVDs in 2019, representing 32% of all global deaths[71].

Atherosclerosis is a chronic inflammatory pathological process contributing to the development of pathophysiological conditions such as coronary artery disease (CAD), peripheral artery disease (PAD), and ischemic stroke (IHD). The thickening of arterial walls due to the deposition of fatty and/or fibrous material on the inner side of arteries was initially described by Karl von Rokitansky. The term "atherosclerosis" was introduced by Felix Marchand in 1904, while the first classification of atherosclerotic lesions was proposed by Ludwig Aschoff. It has its origins in the Greek words “athere”, meaning gruel, and “skleros” meaning hardening[72]. The formation of atheromatous plaques represents a critical stage in atherosclerotic progression, characterized by a complex interplay of cellular and structural changes within the arterial walls. The atheroma is characterized by the accumulation of lipid-laden macrophages, T-lymphocytes and fibrous elements, resulting in the protrusion of these components into the vessel lumen. This cause partial or complete occlusion of the affected arteries and consequent disruption of normal blood flow. Moreover, the involvement of fibroblasts in the production of connective tissue and the deposition of calcium within the lesion contribute to the sclerosis or hardening of the arteries. This process further

exacerbates the structural changes, leading to increased stiffness and reduced flexibility of the arterial walls[73].

Atherosclerosis is a silent process that take the first step long before the clinical manifestations. Several studies indicate that subclinical atherosclerosis undergoes a progressive escalation from the early stages of life. The exposure to risk factors during life relates to incidence of future cardiovascular events. Over the past few decades, epidemiological studies have identified several risk factors associated with the progression of atherosclerosis, which can be broadly classified into non-modifiable and modifiable risk factors. Non-modifiable risk factors include age, sex, ethnicity and genetic disorders such as familial hypercholesterolemia, conversely, modifiable risk factors include behavioral risk factors such as unhealthy diet, inactive lifestyle and tobacco smoking, and clinical conditions like hypertension, overweight/obesity, diabetes mellitus and dyslipidemia (not related to genetic factors)[74]. In recent studies, new potential risk factors have been identified, allowing a better identification of individuals at higher cardiovascular risk. Since inflammation plays a critical role in the pathogenesis of atherosclerosis, multiple inflammatory biomarkers have been associated with an increased risk of cardiovascular events including acute phase proteins C-reactive protein (CRP)[75], serum amyloid A (SAA), soluble intercellular adhesion molecule type-1 (sICAM), selectins as well as cytokines and chemokines (TNF-α, IL-6, IL-8, MCP-1)[76].

Pathogenesis of atherosclerosis

Atherosclerotic plaques develop over decades. It is well-known that the earliest visible lesion of atherosclerosis, referred to as fatty streak, are observed in early childhood. These early lesions do not exert significant pathological effects but are precursors of more advanced stages. As atherosclerosis progresses, the fatty streaks can evolve into fibrous plaques, representing a hallmark of established disease. These plaques are characterized by the accumulation of lipids, connective tissue and inflammatory cells within the arterial walls. The fibrous plaque, while contributing to vessel narrowing, may remain stable for an extended period or may become unstable and rupture, resulting in thrombotic occlusion[77].

Blood vessels have a trilaminar structure: the tunica intima (directly interfacing with the bloodstream), the tunica media and the adventitia. Atherogenesis begins in the

tunica intima, a monolayer of endothelial cells (ECs) and few smooth muscle cells (SMCs) that acts as a semipermeable barrier and plays a key role in the regulation of vascular homeostasis, after an initial endothelial damage. Exposure to atherogenic risk factors or an impaired local hemodynamic environment activate ECs, which in turn secrete inflammatory mediators including cytokines and chemotactic factors (CCR2 and CCR5) and express leukocytes adhesion molecules, such as intracellular adhesion molecule-1 (ICAM-1), vascular cell adhesion molecule-1 (VCAM-1), as well as selectins[78]. Once activate, endothelial tight junctions undergo changes that render them “leaky”, promoting the uptake of plasma low-density lipoproteins (LDLs) and triglyceride-rich lipoproteins. As a result of the increased permeability, LDLs start to accumulate at the site of atherosclerosis-prone regions, where undergo different modifications including oxidation, lipolysis, proteolysis or aggregation[79]. Classic monocytes circulate in the bloodstream and have the ability to bind to leukocytes adhesion molecules expressed by activated ECs. Chemoattractant cytokines play a pivotal role in facilitating the migration of these bound monocytes into the artery wall. Upon reaching the intimal region, these monocytes turn into macrophages. This differentiation is orchestrated by locally produced macrophage colony-stimulating factor (M-CSF) and other cytokines. Mouse studies have shown that, in early lesions, the macrophage pool is mainly constituted by monocyte-derived cells, which can later proliferate and expand the population in more advanced stages[80]. Lesional macrophages, therefore, ingest “modified” lipoproteins, above all oxidized LDLs (oxLDLs), through scavenger receptors, such as CD36 and SR-AI[81], resulting in the formation of cholesterol-engorged macrophages commonly referred to as “foam cells”. After the initiation phase, there is a persistent accumulation of lipids and foam cells, actively promoting the progression of atherosclerotic disease. T lymphocytes also infiltrate the intima, playing a regulatory role in the functions of innate immune cells, as well as endothelial and smooth muscle cells (SMCs). Adaptive immune cells exhibit both pro-inflammatory activities (Th1 helper and B2 lymphocytes) and anti-inflammatory activities (TReg and B1 lymphocytes). Th1 lymphocytes are abundant in atherosclerotic plaques and, through the secretion of pro-inflammatory cytokines, can activate macrophages, T lymphocytes, and other cells within the plaque, amplifying the inflammatory response. Furthermore, IL-17 secreted by Th17 lymphocytes promotes the secretion of inflammatory cytokines, chemokines, and growth factors, all of which can be pro-atherogenic. Conversely, Treg cells control the excessive

activation of lymphocyte populations[82]. SMCs in the media undergo a transformation from a contractile to a proliferative state in response to many factors such as platelet-deriver growth factor (PDGF), concurrently migrating into the intima. Here, they secrete pro-inflammatory mediators, reactive oxygen species (ROS) and an extracellular matrix primarily composed of collagen as well as proteoglycans and glycosaminoglycans, contributing to the formation of a protective fibrous cap. Moreover, SMCs can differentiate into macrophage-like cells and take up lipids, leading to the formation of foam cells that deposit calcium phosphate mineral[77].

In the evolution of atherosclerosis, the distinctive feature of an advanced plaque is the development of a “lipid core”, a large pool of extracellular lipids located deep within the intima. Furthermore, cholesterol-laden cells can undergo cell death including by apoptosis contributing to the formation of a necrotic, lipid-rich core. The formation of this necrotic core is promoted by impaired efferocytosis[83]. Efferocytosis, the process of engulfing dying cells, is predominantly mediated by macrophages and plays a pivotal role in limiting the expansion of necrotic cores. Recent studies have revealed that efferocytosis not only reduces inflammation but can also promote noninflammatory macrophage proliferation, contributing to tissue resolution[84]. However, reduced efferocytosis activates the complement and increases the inflammatory state of the plaque.

The fibrous cap acts as a protective barrier, separating the atherosclerotically altered intima from circulating coagulation factors and platelets. Its thickness is crucial for determining plaque vulnerability. SMCs apoptosis results in reduced extracellular matrix production and the release of matrix metalloproteinases (MMP), making the fibrous cap weaker. Upon plaque rupture, the subendothelial space is exposed to the bloodstream, triggering the coagulation process. The activation of the coagulation cascade leads to the development of a thrombus, triggering a series of reactions that could make the lesion more fibrous and stable, reducing the risk of rupture. However, the ongoing growth of the plaque reduces the blood flow, generating ischemic cardiopathies, such as cardiac insufficiency or angina pectoris, or, if the obstruction is complete, myocardial infarction or stroke[85].

Macrophages in atherosclerosis

The identification of specific surface markers chemokine receptors has significantly enhanced our understanding of the remarkable heterogeneity of monocytes and

macrophages in atherosclerosis. Indeed, these cells can adapt their functional phenotype based on the surrounding environment[86].

Aortic-resident macrophages develop during embryogenesis and sustain themselves through self-renewal mechanisms that are independent of circulating monocytes in the steady-state. They exhibit similarities to resident macrophages found in different tissues and organs, playing crucial roles in preserving tissue homeostasis[87,88]. Upon endothelial activation, classical monocytes are the main source of infiltrating macrophages during the early stages of atherosclerotic plaque development, while in the later stages, an additional source of macrophages is represented by locally proliferating macrophages[89].

Leukocyte infiltration and subsequent accumulation of cholesterol-laden macrophages in the vessel wall are distinctive features of atherosclerosis. In response to various stimuli, endothelial cells express different selectins, through which monocyte can adhere to the endothelium. Monocyte can adhere more firmly through the interaction between cell adhesion molecules, VCAM-1 and ICAM-1 expressed by ECs, and the corresponding cell membrane proteins expressed by leukocytes, specifically alpha(4)beta(1) integrin (VLA-4)[90] and lymphocytes function-associated antigen-1 (LFA-1)[91] respectively. Then, diapedesis into the intimal space is mediated by the interaction between various chemokines, such as IL-8, RANTES, and CXCL1, and their respective receptors[92]. Upon reaching the intimal region, macrophage colony-stimulating factor and other cytokines secreted by ECs promote the differentiation of monocytes into macrophages.

Mice circulating monocytes are generally divided into two subsets: conventional Ly6C^{high} monocytes, which exhibit high expression of CCR2 and CD62L, and Ly6C^{low} monocytes, characterized by high expression of CX3CR1 and low expression of CCR2 and CD62L[93]. The primary function of Ly6C^{low} monocytes is to maintain the health of endothelial cells within the arterial system in the steady state. They scavenge lipoproteins, cellular debris and necrotic cells, and differentiate into anti-inflammatory M2-like macrophages in the sites of inflammation[94]. On the other side, Ly6C^{high} monocytes quickly respond to inflammatory signals, infiltrate damaged sites, and differentiate into pro-inflammatory M1-like macrophages. Therefore they could also

turn into M2-like macrophages in a STAT6-dependent manner, resulting in atherosclerosis regression[95].

Based on *in vitro* studies, macrophages are conventionally classified as activated pro-inflammatory M1 and alternatively activated anti-inflammatory M2 macrophages[96]. Differentiation into the M1 phenotype is typically induced by pro-inflammatory cytokines such as IFN-γ and TNF produced by T-helper 1 lymphocytes. Additionally, the accumulation of cholesterol crystals or oxidized lipoproteins further promotes the inflammatory activation of macrophages[97,98]. These phagocytes produce high levels of IL-12 and IL-23[99], low levels of IL-10, and secrete proinflammatory cytokines such as IL-1β, IL-6 and TNF-α[100]. On the other hand, Macrophages M2 are involved in the resolution of inflammation, tissue repair, and modulation of the immune response. These macrophages can be further subdivided into subtypes M2a, M2b, M2c and M2d, each of which performs specific functions within the context of the surrounding tissue environment. M2a macrophages are induced by TH2 cytokines, including IL-4 and IL-13, and express high levels of CD206. Conversely, M2b macrophages respond to immune complexes combined with IL-1β or lipopolysaccharide, exhibiting an additional ability to produce proinflammatory cytokines like IL-1, IL-6 and TNF[101]. M2c macrophages are induced by anti-inflammatory signals such as IL-10, TGF-β or glucocorticoids and exhibit strong anti-inflammatory properties[86]. M2d macrophages express high levels of IL-10, VEGF and iNOS along with low levels of TNF-α, IL-12 and Arg-1. Moreover, they play a crucial role in the growth of atherosclerotic plaques through their angiogenic properties[102]. However, the M1/M2 dichotomy currently has been overcome and this classification has been further expanded with the identification of additional macrophage populations, including M(Hb), Mhem, Mox and M4 macrophages. M(Hb) macrophages express both CD206 and CD163 and demonstrate reduced intracellular iron accumulation, leading to lower production of reactive oxygen species. These macrophages, characterized by increased activity of the transcription factor LXR-α and enhanced cholesterol efflux, are protected against lipid accumulation[103]. However, they promote angiogenesis, vascular permeability and inflammatory cell recruitment via the CD163/HIF1α/VEGF-A pathway, promoting plaque progression[104]. Mhem polarization is driven by heme. The induction of ATF1 and consequently LXR-β promotes the expression of both LXR-α and ABCA1, rendering these macrophages resistant to oxidative stress and preventing the

formation of foam cells[105]. Macrophages give rise to Mox-phenotype, which express proinflammatory markers like COX-2 and IL-1β, upon exposure to oxidized phospholipids. However, these macrophages exhibit diminished phagocytic and chemotactic capacities[106]. Finally, the M4 macrophage phenotype, which shares characteristics with both M1 and M2 phenotypes, is induced by CXCL4 expressed by macrophages and neovascular endothelium. M4 macrophages, identified by the co-expression of MMP7 and the S100A8, exhibit a complete deficiency in phagocytic capacity[107]. Moreover, the significant presence of these macrophages within the intima and the media is strongly associated with plaque instability[108].

Role of HDLs in atherosclerosis

Lipoproteins transport cholesterol and other lipids in the plasma. They consist of a hydrophobic core containing non-polar lipids such as triglycerides and cholesterol esters surrounded by an hydrophilic shell composed of polar lipids including free cholesterol, phospholipids and apolipoproteins. Plasma lipoproteins can be primarily classified into six classes: chylomicrons, very-low-density lipoproteins (VLDLs), low-density lipoproteins (LDLs), intermediate-density lipoproteins (IDLs), high-density lipoproteins (HDLs), and lipoprotein(a) (Lp(a))[109].

HDLs are a heterogeneous class of lipoproteins. Characterized by a density ranging from 1.063 to 1.21 g/mL and a diameter ranging from 5.0 to 12.0 nm, HDLs are the smallest and densest among plasma lipoproteins[110]. Several epidemiological studies have consistently underlined a clear inverse correlation between plasma HDL cholesterol (HDL-C) and the incidence of cardiovascular diseases[111]. However, mendelian randomization studies[112] have questioned the role of HDL in cardiovascular protection, as well as increasing plasma HDL-C levels has not demonstrated any benefits in preventing cardiovascular events[113]. Indeed, several studies have revealed a U-shaped relationship between plasma HDL-C and atherosclerotic cardiovascular events. Furthermore, plasma HDL-C level does not necessarily reflect the efficiency of the HDLs system, which is undoubtedly complex and involves different particles with variable functionalities. Therefore, HDL components, rather than cholesterol, may account for the anti-atherogenic effects attributed to these lipoproteins.

HDLs play several atheroprotective functions, including macrophage reverse cholesterol transport (RCT). RCT is a multi-step process resulting in the movement of

excess cholesterol from peripheral tissues back to the liver for the excretion with bile[114]. It has been extensively demonstrated that the limiting step in this process is the efflux of cholesterol, specifically the movement of free cholesterol from engorged macrophages to serum lipoproteins, which serve as acceptors. This process can occur through simple aqueous diffusion or be mediated by specific transporters. ATP-Binding Cassette, Sub-Family A (ABC1), Member 1 (ABCA1) facilitates the transport of cholesterol and phospholipids by interacting with lipid-free or lipid-poor apolipoproteins, including ApoA-I. This process results in the formation of pre-β-HDL, which, as well as HDLs, can interact with ATP-binding cassette, sub-family G, member 1 (ABCG1) accumulating more cholesterol. Furthermore, the scavenger receptor SR-BI mediates the bidirectional flow of free cholesterol between macrophages and lipoproteins, although its contribution to RCT is rather limited[115]. Finally, ApoE secreted by foam cells can also mediate cholesterol efflux in the absence of additional acceptors through both ABCA1-dependent and independent mechanisms and it has been demonstrated that ABCG1 may promote the movement of free cholesterol to ApoE-enriched lipoproteins[116]. Adorni et al. have shown that both in vitro and in vivo, cholesterol efflux is primarily mediated by ABCA1, to a lesser extent by ABCG1, while SR-BI does not seem to contribute significantly[117]. The enzyme Lecithin-cholesterol acyltransferase (LCAT) catalyzes the esterification of free cholesterol in pre-β-HDL, inhibiting its reverse transfer back into macrophages and leading to the formation of mature HDLs. These HDLs then reach the liver, where hepatic SR-BI extracts cholesterol esters or the enzyme cholesteryl ester transfer protein (CETP) mediates the transfer of cholesterol from HDLs to ApoB-100-containing lipoproteins in exchange for triglycerides[118].

The atheroprotective effects are partly modulated by the other biological activities of HDLs. These activities include countervailing the oxidation of LDL, inhibiting inflammation, platelet activation, apoptosis of ECs and thrombosis. OxLDLs are known for their pro-atherogenic characteristics and their ability to promote atherosclerosis. *In vitro* studies have revealed that isolated HDLs inhibit the oxidation of LDLs[119]. However, it is important to highlight that additional plasma components, including fibrinogen, IgG, albumin and small soluble molecules, also display antioxidative effects. The contribution of HDL to the overall antioxidant capacity of plasma has been estimated at only 1-2%[120]. It has been shown that the interaction

between HDLs and ABCA1, besides its role in RCT, inhibits the polarization of macrophages towards the M1 phenotype, promoting the M2 phenotype and the subsequent secretion of anti-inflammatory cytokines through the activation of JAK2 and STAT3[121]. Furthermore, the activation of the ApoA-I/JAK2/ABCA1 axis suppresses inflammation in endothelial cells through COX-2 expression induction and PGI-2 release[122]. Additionally, the PI3K/Akt pathway, activated through $S1P_1$, SR-BI and $S1P_3$, is involved in the inhibition of TNFα-induced activation of ECs, resulting in reduced expression of adhesion molecules and HDL-induced relaxation through NO synthase (NOS) activation and NO synthesis[123,124]. Through the same pathway, HDLs prevent oxLDL-induced apoptosis of endothelial cells, inhibiting caspase-3 and -9 activation, cytochrome C release and cytoplasm Ca^{2+} production[55]. Nonetheless, S1P-associated HDL induces migration and survival of endothelial cells through the activation of the receptor subtypes $S1P_1$ and $S1P_3$[125]. HDLs also exhibit antithrombotic activity. Indeed, they inhibit the expression of selectins, preserve caveolae (specialized membrane areas where endothelial nitric oxide synthase is located), and act as an eNOS agonist, contributing to NO production. Furthermore, HDLs contribute to prostacyclin synthesis, which induces vascular tone relaxation and platelet inactivation, and reduce thrombin production, which is responsible for platelet activation[126].

S1P and atherosclerosis: focus on sphingolipids metabolism and S1P/S1PRs axis pharmacological modulation

In vitro and *in vivo* studies over the years have elucidated the role of S1P and its receptors in maintaining homeostasis and regulating cellular functions. In particular, the atheroprotective effects of S1P have been widely demonstrated in cellular models involved in atherosclerosis development such as macrophages, endothelial cells and vascular smooth muscle cells. However, *in vivo* studies on athero-prone mouse models have sometimes provided contrasting or unexpected results. Currently, several diets with different composition of fat and cholesterol are commercially available, which can have distinct impacts on the lipid profile and inflammation state of the animal and, consequently, on the progression of atherosclerosis. The availability of fingolimod has generated growing interest in the potential clinical application of compounds that modulate the sphingolipids metabolism or the pathway activated by the interaction between S1P with its receptors in the cardiovascular context.

Regardless of the athero-prone animal model used ($LDLR^{-/-}$ or $ApoE^{-/-}$), it has been observed that the administration of fingolimod induces lymphopenia and does not always prevent the formation of atherosclerotic lesions. The compound, even at low doses, significantly inhibit the Th1-mediated inflammatory response, concurrently triggering an increase in the circulating numbers of Treg and memory T cells[127]. Furthermore, fingolimod inhibits leukocyte infiltration[128], promotes the M1→M2 switch in macrophages and reduces the inflammatory state, reflected in decreased plasma pro-inflammatory cytokines levels[129]. The lipid profile remains unchanged in HFD-fed mice, while Klingenberg et al. observed that $ApoE^{-/-}$ mice fed a normal chow diet exhibited increased levels of VLDL-cholesterol and plasma S1P following fingolimod administration, accompanied by unaltered atherogenesis[130]. $ApoE^{-/-}$ mice develop atherosclerotic lesions regardless of the dietary regimen, suggesting that the high-fat high-cholesterol diet may mask some of the effects of fingolimod. Moreover, Potì et al. demonstrated that selective $S1P_1$ agonists, CYM5442 and KRP-203, induce lymphopenia in mice. However, following the administration of the former, T cell levels in peripheral blood return to baseline within a few hours, indicating reversibility[131]. KRP-203 reduces atherosclerotic lesions without altering plasma lipids[132], while the other agonist fails to prevent atherosclerosis in moderately hypercholesterolemic mice. Lastly, a recent study has demonstrated that the inhibition of $S1P_2$, receptor particularly expressed in the vascular system, reduces endothelial dysfunction, resulting in decreased lipid accumulation, reduced macrophage infiltration and diminished inflammation[133].

Studies investigating the inhibition of various enzymes involved in sphingolipid biosynthesis have shown how the accumulation of intermediates or impaired S1P plasma levels can either decelerate or accelerate the progression of atherosclerosis. The non-selective inhibition of both isoforms of sphingosine kinase results in a reduction of plasma S1P levels in $LDLR^{-/-}$ mice but does not influence the development of atherosclerosis[134]. However, the administration of a selective sphingosine kinase 1 inhibitor (SKI-II) increases in pro-inflammatory cytokines and endothelial adhesion molecules. This leads to an enlargement of the atherosclerotic plaque size, independent of alterations in lymphocyte distribution and reduced levels of plasma triglycerides[135]. Low S1P levels, along with reduced sphingosine and increased sphingomyelin and ceramides, are observed following the inhibition of acid

sphingomyelinase upon the administration of amitriptyline in $LDLR^{-/-}$ mice. These animals exhibit reduced atherosclerosis and downregulation of pro-inflammatory cytokines in macrophages, likely due to decreased levels of S1P as theorized by the authors[136]. Although known for its atheroprotective effects, it was hypothesized that increasing S1P plasma levels could be beneficial in the context of atherosclerosis. However, Keul et al. demonstrated that increasing endogenous S1P levels by inhibiting sphingosine lyase in $ApoE^{-/-}$ mice leads to an exacerbation of the pathology, plaque instability and the development of atherothrombosis. Additionally, sphingosine lyase-deficient macrophages show reduced expression of cholesterol transporters, resulting in decreased lipid efflux[137]. Myriocin is a naturally derived inhibitor of serine palmitoyltransferase with immunosuppressive activity and fingolimod is a derivative of it. The administration of this compound to $ApoE^{-/-}$ mice results in a dose-dependent reduction of plasma sphingomyelin, cholesterol and triglyceride levels due to the modulation of lipid biosynthesis genes. Park et al. observed a regression of atherosclerosis or plaque stabilization, attributed to reduced macrophage infiltration and a simultaneous increase in collagen deposition following myriocin administration[138,139]. Reduced levels of sphingomyelin and ceramides have also been observed in athero-prone mice treated with a glucosylceramide synthase inhibitor (D-PDMP and AMP-DNM). These animals exhibited an altered lipid profile characterized by reduced serum cholesterol and triglycerides, leading to improved atherosclerosis[140,141].

$S1P_1$ and $S1P_3$ signaling in cholesterol efflux: new insight from transgenic mice

Body of evidence supporting the anti-atherogenic effects of S1P primarily came from experiments conducted *in vitro* or *in vivo* using S1PRs knockout mice or synthetic S1P analogues with poorly described side effects. Further studies were necessary to establish the protective effects of endogenous S1P and to investigate the underlying mechanisms. For this purpose, our research group has designed peculiar animal models to enhance S1P signaling and gain a deeper understanding of the protective effects of endogenous S1P against atherosclerosis. Taking advantage of CreLoxP technology, our laboratory developed mice models overexpressing S1PRs, precisely $S1P_1$ or $S1P_3$, in a tissue specific manner, in particular in myeloid cells.

In vivo evaluation of macrophage-to-feces reverse cholesterol transport was conducted using both models overexpressing the receptor $S1P_1$ ($S1P_1$- LysM-Cre mice) or $S1P_3$ ($S1P_3$- LysM-Cre mice) in myeloid cells. Thus, C57BL6/J strain mice were intraperitoneally injected with macrophages derived from $S1P_1$- LysM-Cre or $S1P_3$- LysM-Cre mice, which were radiolabeled with [1,2-^{3}H]-cholesterol and enriched with cholesterol (Acetylated-LDL; AcLDL). *In vivo* RCT was enhanced in mice injected with macrophages from transgenic mice, as evidenced by the increased levels of [1,2-^{3}H]-cholesterol measured in plasma, liver and feces 24 and 48 hours post-injection. These findings represented the first *in vivo* evidence of a close association between endogenous S1P and cholesterol metabolism in macrophages (NOTE: original unpublished data).

However, it is interesting to note that, unexpectedly, the overexpression of $S1P_3$ in hematopoietic stem cells induced acute myelogenous leukemia, partly reversible following fingolimod administration, in mice[54].

Aim

Macrophages play a central role in the development and progression of atherosclerotic lesions. In response to endothelial damage, circulating monocytes infiltrate the vascular wall and differentiate into macrophages. Here, they ingest modified lipoproteins, leading to the formation of foam cells. The accumulation of these foam cells, along with other inflammatory components, results in the development of atherosclerotic plaques. This potential rupture of a plaque can trigger thrombosis and severe cardiovascular events.

Macrophage cholesterol efflux is a central and crucial step in the reverse cholesterol transport. This process contributes to regulate cholesterol levels and prevents the accumulation of excess cholesterol in the arterial walls, reducing the risk of atherosclerosis and cardiovascular diseases. Promising therapeutic approaches aim to reduce macrophage cholesterol accumulation and enhance macrophage-to-feces cholesterol elimination.

Epidemiological studies have demonstrated an inverse relationship between plasma HDL-cholesterol levels and cardiovascular risk. Over the last two decades, it has become increasingly evident that HDLs can interact with nearly every type of cell involved in the pathogenesis of atherosclerosis and functional alterations resulting from such interactions may be directly responsible for the protective effects of these lipoproteins. Furthermore, it has become well-established that sphingosine-1-phosphate (S1P) acts as a mediator for numerous atheroprotective effects attributed to HDLs.

Pharmacological stimulation of S1P receptors (S1PRs) can exert atheroprotective effects. Moreover, it has been demonstrated that, in athero-prone mice, administration of fingolimod, a nonselective modulator of S1PRs, can reduce lesion development. However, these studies have highlighted that fingolimod inhibits atherosclerotic progression through its immunomodulatory activity, regulating the function of lymphocytes and macrophages in terms of activation and secretion of inflammatory cytokines. The impact of this compound on lipid metabolism has not been thoroughly investigated.

An elegant study conducted in our laboratory using a novel murine model modified to amplify S1P signaling through the receptor $S1P_1$ or $S1P_3$ in macrophages has

demonstrated a link between S1P and cell cholesterol metabolism (unpublished data – manuscript in preparation).

It has been observed that *in vivo* macrophage-to-feces reverse cholesterol transport was increased by myeloid overexpression of $S1P_1$ or $S1P_3$, and this suggests that the activation of the S1P/S1PR axis may be involved in cholesterol efflux.

Therefore, the aim of this study was to provide more insights of the impact of S1P/S1PR axis pharmacological modulation on cell cholesterol metabolism. To this purpose, multiple *in vitro* experimental approaches were used to evaluated whether stimulation of S1PRs could affect the expression of cholesterol transporters and their functionality in macrophages.

Materials and Methods

Cell cultures

Every operation concerning cell manipulation was carried out under sterile conditions, using a laminar flow hood. The cells were sub-cultured in 75 cm^2 flasks (Avantor, VWR) and maintained in a humidified cell culture incubator under controlled conditions of temperature (37°C) and CO_2 (5%). Once the confluence was reached, the cells were split into new flasks or seeded into plates.

Murine macrophage cell line, RAW 264.7, were sub-cultured in high-glucose DMEM (Dulbecco's Modified Eagle's Medium; Euroclone) supplemented with 2 mM L-glutamine, 1% penicillin-streptomycin, and 10% fetal calf serum (FCS; Euroclone).

The human monocyte cell line THP-1 were sub-cultured in RPMI 1640 (Roswell Park Memorial Institute Medium; Lonza Bioscience), supplemented with 2 mM L-glutamine, 10% fetal calf serum (FCS; Euroclone) and 1% penicillin-streptomycin. THP-1 cells underwent differentiation into macrophage-like cells, referred to as THP-1 macrophages, through incubation in the presence of Phorbol 12-myristate 13-acetate (PMA).

In all experiments, cells were maintained in serum-reduced medium containing 1% heat-inactivated calf serum.

Analysis of protein expression by Western Blotting

Western Blot analyses were conducted to assess the protein expression of cholesterol transporters ABCA1, ABCG1, and SR-BI, as well as the receptor subtypes 1 and 3 of sphingosine 1-phosphate ($S1P_1$, $S1P_3$).

Macrophages were collected and lysed on ice in RIPA buffer (0.5% sodium deoxycholate, 0.1% sodium dodecyl sulfate (SDS), 1% Triton X-100, 20 mM NaCl, 5 mM EDTA) supplemented with protease inhibitor (cOmplete,™Mini Protease Inhibitor Cocktail, Roche). The protein concentration of the lysates was quantified using BCA protein assay (ThermoFisher Scientific). All protein lysates were reduced using the reducing agent dithiothreitol (DTT [50 mM]), while those used for the assessment of ABCG1 and SR-BI expression were also denatured at 95°C for 2/3 minutes. 40 µg/lane of the prepared protein lysate were loaded and subjected to SDS-polyacrylamide gel

electrophoresis. Subsequently, proteins were transferred onto a polyvinylidene difluoride membrane (PVDF) (BioRad Laboratories, Munich, Germany) and which was then blocked for 1 hour using a solution of 5% non-fat dry milk in Tris-buffered saline containing 0.1% Tween-20 (TBS-T) before the antibody incubation steps to prevent non-specific binding. The PVDF membrane was then incubated overnight at 4°C with the specific primary antibody, diluted in a solution of 5% non-fat dry milk in TBS-T:

- anti- ABCA1, DF 1:250 (NB400-105; Novus Biologicals);
- anti-ABCG1, DF 1:500 (NB400-132; Novus Biologicals);
- anti-SR-BI, DF 1:3000 (NB400-101; Novus Biologicals);
- anti-$S1P_1$, DF 1:500 (MBS8534430; MyBioSource);
- anti-$S1P_3$, DF 1:500 (MBS9704687; MyBioSource);
- anti-β-actin-peroxidase antibody, 1:25000 (A3854; Sigma Aldrich).

Following the overnight incubation, primary antibodies were removed through TBS-T washing. Then, the membrane was incubated with a donkey anti-rabbit IgG/ horseradish peroxidase secondary antibody (DF 1:20000 (Bethyl)) for one hour at room temperature. Enhanced chemi-luminescence (Pierce ECL Western Blotting Substrate; Thermo Fisher Scientific) was utilized for the visualization of the target proteins.

Analysis of gene expression by real-time quantitative RT-PCR

Total RNA samples were isolated from macrophages using Invitrogen TRIzol Reagent (Thermo Fisher Scientific), a ready-to-use reagent consisting of a monophasic solution of phenol, guanidine isothiocyanate, and other components that facilitate RNA isolation while preserving its integrity, according to manufacturer protocol. RNA was eluted in RNAse free water and quantified using NanoDrop ND 1000 (Thermo Scientific). 0,5 µg of total RNA were reverse-transcribed into cDNA using iScript™ cDNA Synthesis Kit (BIO-RAD). Real-time quantitative PCR was performed using SsoFastTM EvaGreen Supermix (BIO-RAD) in presence of gene-specific primers (**Table a**), using CFX96TM Real Time System (BIO-RAD). The relative gene expression was determined using the $2^{-\Delta\Delta Ct}$ method. In brief, the threshold cycle number (Ct) of the target genes was subtracted from the Ct of the geometric mean of housekeeping genes ($Ct_{housekeeping}$) and raised to the 2nd power of this difference.

Immunofluorescence

Macrophages were seeded on appropriate round cover slides at a density of 0.2x106 cells/well. Then, cells were treated with FTY720-P under cholesterol normal or loading conditions (AcLDL) in medium + 1% FCS. After 18 hours, slides were rinsed with PBS, the cells were fixed with cold acetone for 4 minutes and subsequently incubated for 30 minutes at room temperature in PBS + 1% BSA (Sigma Aldrich) to block nonspecific binding sites. The samples were incubated with the primary antibody anti-ABCA1 (NB400-105; Novus Biologicals), diluted 1:100 in a blocking solution (PBS + 1% BSA + 0.1% Triton™ X-100) in a wet chamber in the dark at 4°C overnight. The following day, macrophages were incubated with the secondary antibody mouse anti-rabbit sc-516250 CruzFluor 594 (Santa Cruz Biotechnology), diluted 1:300 in PBS + 1% BSA for one hour at room temperature in the dark. Finally, the slides were washed with PBS, mounted on glass coverslips using a DAPI-containing solution (Fluoroshield with DAPI; Sigma-Aldrich) and observed by confocal fluorescence microscopy (Leica).

Evaluation of lipid accumulation by Oil Red O Staining

Macrophages were seeded on appropriate round cover slides at a density of $0.2x10^6$ cells/well. The cells were incubated with FTY720-P for 18 hours followed by an additional 18-hour incubation either with AcLDL or were treated with FTY720-P under cholesterol normal or loading conditions for 18 hours. Subsequently, the cells were fixed with 4% paraformaldehyde for 20 minutes at room temperature. After a permeabilization step with 60% 2-propanol, macrophages were treated with the Oil Red O solution (ORO; Sigma-Aldrich) for 30 minutes and then washed once with 60% 2-propanol. Stained cells were finally observed under a light microscope and the Oil Red O positive area was calculated using Image J software.

Cell cholesterol efflux assay

Macrophages were seeded in 24-well plates at a density of $0.3x10^6$ cells/well and incubated in suitable medium containing 10% FCS and 2 mM L-glutamine at 37°C and 5% CO_2 for 24 hours. Cells were labeled with 2.0 µCi/mL [1,2-^{3}H]-cholesterol (Perkin Elmer) in medium + 1% FCS + ACAT inhibitor Sandoz 58-035 [2.0 µg/mL] to prevent cellular accumulation of cholesteryl ester. After 24 hours, macrophages were treated with FTY720-P under cholesterol normal or loading conditions (AcLDL) in medium + 0.2% BSA + Sandoz [2.0 µg/mL] for 18 hours. Finally, cholesterol efflux was induced

by adding 2% pool of human normolipidemic sera or human isolated apo-AI (Merk Life Science, Darmstadt, Germany) [10 µg/mL] (acceptors) for 6 hours. To quantify the [1,2-^{3}H]-cholesterol transported from the cells to acceptors, 100 µl of efflux medium was added to in scintillation vials containing 4 ml of scintillation mix (Opti-Fluor) and counted for the radioactivity using beta scintillation spectrometer. Intracellular [1,2-^{3}H]-cholesterol was extracted in 0.6 mL of 2-propanol and left 2-propanol-saturated chamber overnight. Subsequently, 2-propanol was evaporated under N_2. The [1,2-^{3}H]-cholesterol was then resuspended in 1 mL of toluene and quantified by liquid scintillation counting (Insta-Fluor). Cholesterol efflux was expressed as a percentage of the radioactivity released in the supernatant over the total intracellular radioactivity.

Statistical analysis

Data are represented as mean ± SD. Unpaired two-tailed Student's t-test was applied and $p < 0.05$ was considered statistically significant. For comparison involving more than two groups one-way or two-way ANOVA was applied according to the experimental design, followed by post-hoc multiple comparison tests (Tukey).

Table a. qPCR Primer Sequences.

Gene	Forward (5'-3')	Reverse (5'-3')
Hprt	TTGCTCGAGATGTCATGAAGGA	AGCAGGTCAGCAAAGAACTTATAG
Abca1	GGCTGTCCAATTTTGTCTGG	TAGAACGGGCAGGTTGGTAG
Abcg1	GGCTGTCCAATTTTGTCTGG	TAGAACGGGCAGGTTGGTAG
Srb1	TTCTACTTGTCTACT	ATTGAAGGTGATGTTGAC

Results

FTY720-P enhances protein expression but not gene expression of cholesterol transporters in RAW 264.7 murine macrophages

It is known that ABCA1, ABCG1 and SR-BI play an important role in lipid efflux from cells[117]. Macrophages were treated with FTY720-P under cholesterol normal or loading conditions for 18 hours. The expression of ABCA1 protein was almost nonexistent in the absence of stimuli. However, as widely demonstrated[142], stimulation with AcLDL led to a statistically significant increase in the protein expression of the transporter. Likewise, treatment with FTY720-P significantly boosted protein expression, though to a lesser extent compared to AcLDL stimulation. Lastly, even under cholesterol-loading conditions, stimulation with FTY720-P resulted in an elevated ABCA1 expression. Similarly, the protein expression of ABCG1 increased following stimulation with AcLDL (as already extensively demonstrated[143]), and after stimulation with FTY720-P, although to a lesser extent. Furthermore, it was observed that the co-stimulation with AcLDL and FTY720-P significantly further increased the protein expression. As known[144], the protein expression of SR-BI decreased following cholesterol loading. In contrast, cells stimulated with FTY720-P shown an increase in SR-BI protein expression regardless of cholesterol-loading conditions (**Figure 1A**). Subsequently, the expression of ABCA1 was assessed by immunofluorescence. However, the data obtained did not entirely reflect the protein expression observed via Western Blot. Specifically, although a statistically significant increase in ABCA1 expression was observed in cells treated with FTY720-P under cholesterol normal condition, the co-stimulation with AcLDL did not reach statistical significance within the analyzed sampling frames (**Figure 1B**). To evaluate whether the observed variations in protein expression were the result of transcriptional differences, the gene expression of cholesterol transporters in macrophages was evaluated using RT qPCR. While treatment with AcLDL, as known, increased the gene expression of ABCA1 and ABCG1 and decreased SR-BI, no significant differences were observed following stimulation with FTY720-P (**Figure 1C**).

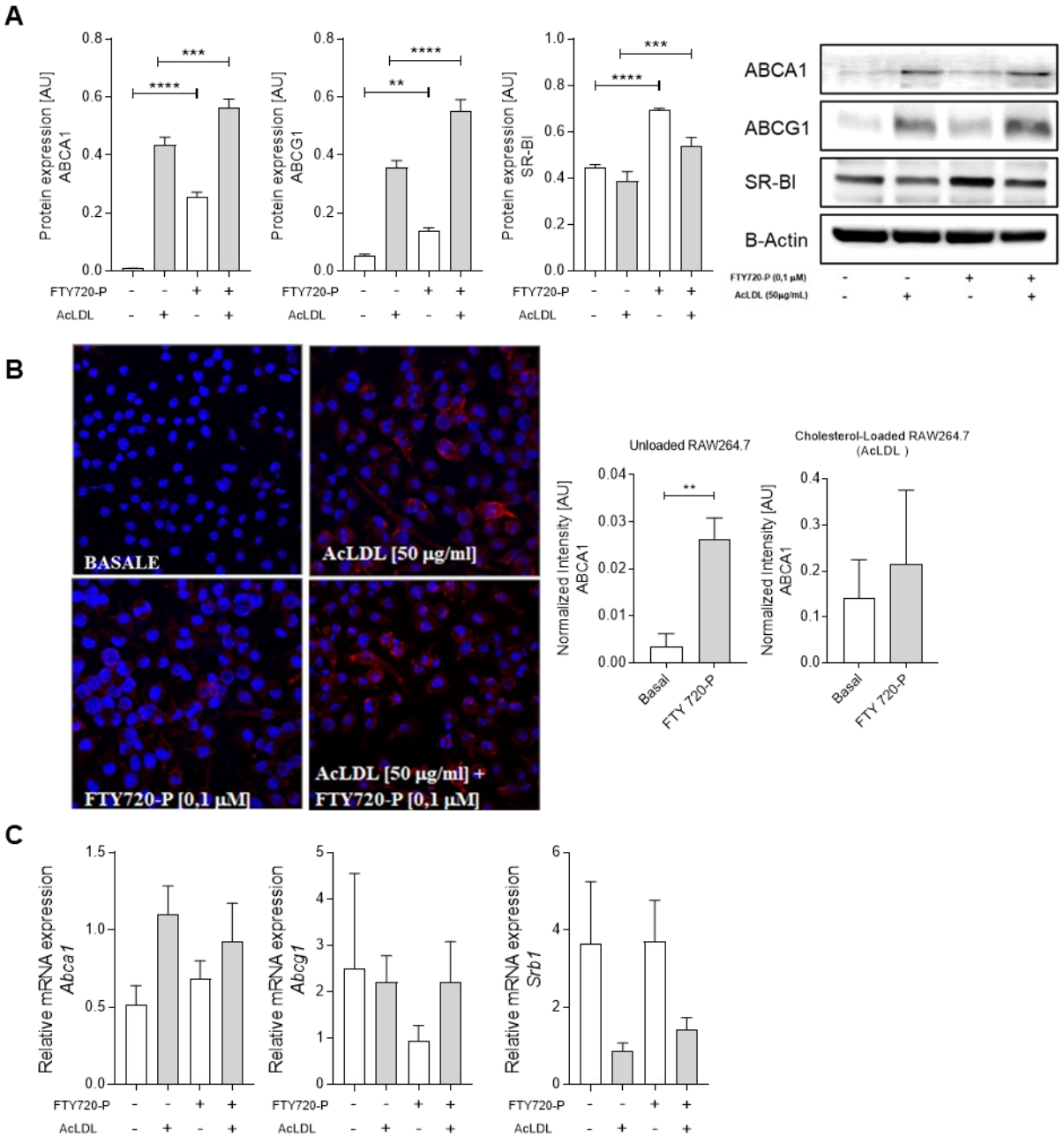

Figure 1. Raw 264.7 macrophages were treated with FTY720-P under cholesterol normal or loading conditions for 18 hours. **(A)** Protein expression of cholesterol transporters ABCA1, ABCG1 and SR-BI. Protein expression was normalized using β-actin as housekeeping gene. **(B)** Protein expression of ABCA1 by immunofluorescence, **(C)** Gene expression of cholesterol transporters ABCA1, ABCG1 and SR-BI.
Data are represented as mean ± SD. *p < 0.05, **p < 0.01, ***p < 0.001, and ****p < 0.0001

FTY720-P reduces lipid accumulation in in RAW 264.7 macrophages

Cellular lipid accumulation in macrophages is one of the pathogenetic events underlying the development of atherosclerosis. Consequently, the effect of FTY720-P treatment on lipid accumulation in macrophages was assessed. Furthermore, the

potential impact of a pre-treatment with the compound was also investigated. Macrophages were incubated with FTY720-P for 18 hours followed by an additional 18-hour incubation either with AcLDL or were treated with FTY720-P under cholesterol normal or loading conditions and intracellular lipid droplet accumulation was determined by Oil Red O staining. We observed a statistically significant reduction in intracellular lipid content in both pre-treated and FTY720-P-treated macrophages compared to the baseline under cholesterol normal condition. However, in AcLDL-loaded macrophages, although a decrease in lipid content was observed, the results did not reach statistical significance (**Figure 2**).

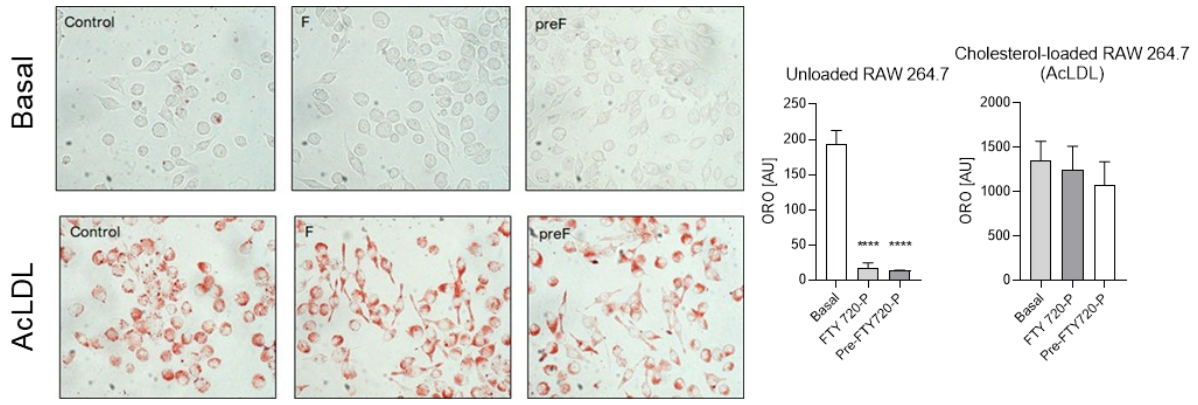

Figure 2. Effect of FTY720-P on lipid droplet accumulation in RAW 264.7 macrophages. The magnification of each panel was ×40.
Data are represented as mean ± SD. ****p < 0.0001

FTY720-P promotes ABCA1-mediated cholesterol efflux in AcLDL-loaded RAW264.7 macrophages

To assess whether the increase in protein expression of cholesterol transporters observed is functional to the cell, the cholesterol efflux to ApoA-I (ABCA1-mediated efflux) and to human whole plasma was evaluated under cholesterol normal or loading conditions. No statistically significant differences were observed, except for an increase in the percentage of efflux mediated by ApoA-I in macrophages co-stimulated with FTY720-P and AcLDL (**Figure 3**).

ABCA1 and ABCG1 upregulation in RAW 264.7 might be $S1P_1$-mediated

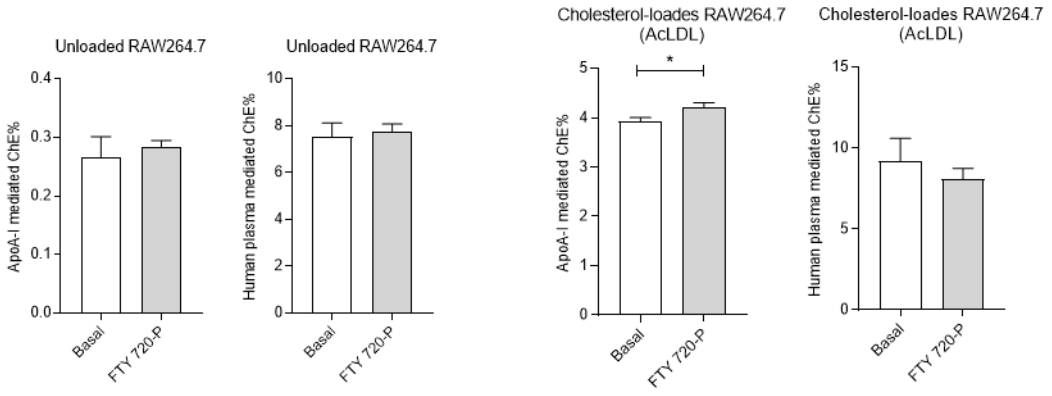

Figure 3. Effect of FTY720-P on cholesterol efflux capacity in RAW 264.7 macrophages. Data are represented as mean ± SD. *p < 0.05

FTY720-P is a non-selective modulator of S1P receptors ($S1P_{1,3–5}$, with a particularly high affinity for $S1P_1$). We further investigated which receptor subtype is involved in the increased protein expression of cholesterol transporters by treating cells with a selective agonist and antagonist. Macrophages were treated with SEW2871, a $S1P_1$-selective agonist, or TY52156, a $S1P_3$-selective antagonist, under cholesterol normal or loading conditions for 18 hours. As previously noted, FTY720-P induced a statistically significant increase in the protein expression of ABCA1. Similarly, SEW2871 also enhanced, albeit to a lesser extent, the protein expression, suggesting a potential activation of the S1P/$S1P_1$ axis. Unexpectedly, treatment with TY52156 leaded to a reduction in ABCA1 protein expression. Lastly, co-stimulation with FTY720-P and the $S1P_3$-antagonist had no influence on the expression of ABCA1. Subsequently, we observed that treatment with FTY720-P, SEW2871, and TY52156 increased the expression of ABCG1, though to a lesser extent compared to AcLDL stimulation (**Figure 4A**). Finally, we evaluated the gene expression of ABCA1 in murine macrophages stimulated with selective modulators of S1PRs. Similar to FTYP720-P, the gene expression of the transporter is not modulated by SEW2871 after 18 hours of treatment. However, macrophage stimulation with TY52156 also decreases mRNA levels, suggesting a potential off-target effect of the compound (**Figure 4 B**).

Figure 4. Raw 264.7 macrophages were treated with FTY720-P, SEW2871 or TY52156 under cholesterol normal or loading conditions for 18 hours. **(A)** Protein expression of cholesterol transporters ABCA1, ABCG1 and SR-BI. Protein expression was normalized using β-actin as housekeeping gene. **(B)** Gene expression of cholesterol transporters ABCA1.
Data are represented as mean ± SD. *p < 0.05, **p < 0.01, ***p < 0.001, and ****p < 0.0001

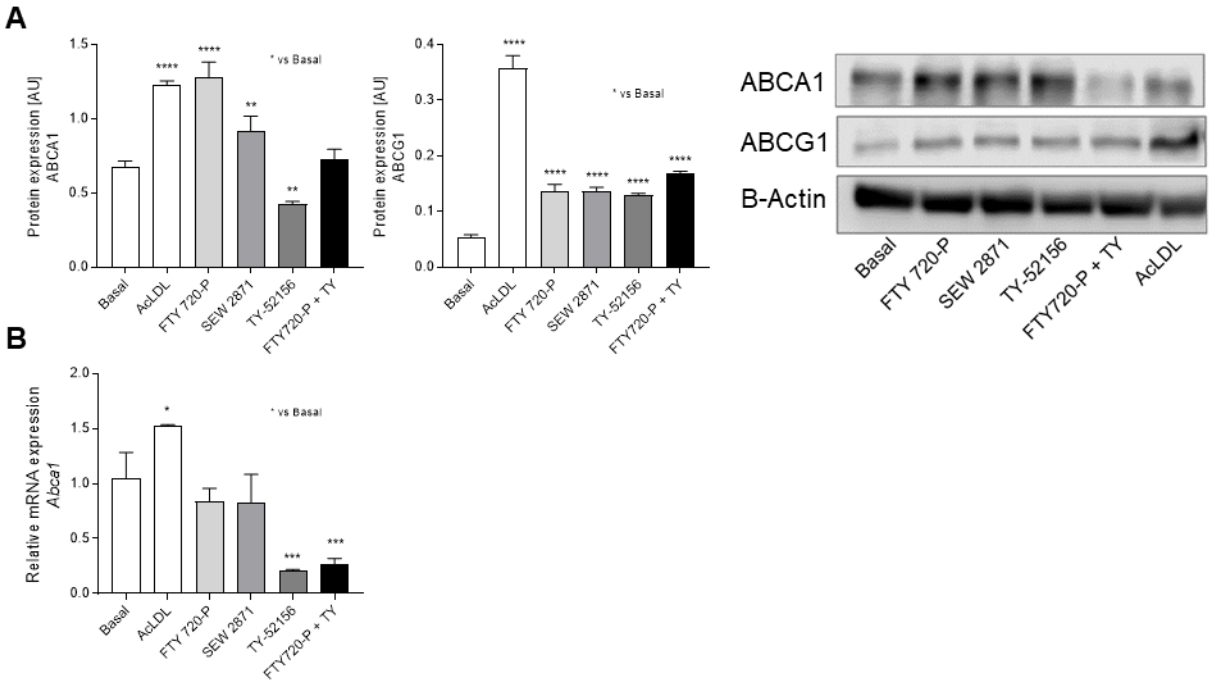

FTY720-P promotes apoA-I-dependent cholesterol efflux through upregulating ABCA1 and reduces lipid accumulation in human macrophages

Mice are the most widely used model for studying immune cells and, in several respects, they closely mirror human biology. However, there are significant differences in terms of metabolic responses. For these reasons, we assessed the effects of S1P/S1PR stimulation on the expression of cholesterol transporters, focusing on ABCA1, in THP-I-derived macrophages. We first examined whether FTY720-P treatment promotes the cholesterol efflux in human macrophage cells and we found that, under cholesterol normal condition, FTY720-P stimulation increased the percentage of efflux mediated by ApoA-I (**Figure 5A**). Since ABCA1 plays a major role in ApoA-I-dependent lipid efflux, we thus examined the expression levels of ABCA1 upon FTY720-P, SEW2871 and TY52156 exposure. As previously reported[145], macrophage stimulation with AcLDL led to a statistically significant increase in the protein expression. FTY720-P treatment significantly enhanced ABCA1 expression compared to the baseline, but not in AcLDL-loaded macrophages. Consistent with observations in murine macrophages, activation of the S1P/$S1P_1$ axis (SEW2871-mediated) enhanced the protein expression of the transporter, whereas the selective $S1P_3$ antagonist reduced it. Interestingly, in FTY720-P – TY52156 co-stimulated human macrophages, the effect of the non-selective modulator predominated (**Figure 5B**). Finally, cellular lipid accumulation was determined by Oil Red O staining. In

AcLDL-loaded THP-I-derived macrophages, we observed that FTY720-P significantly reduces cholesterol accumulation, both when cells were co-stimulated with AcLDL and FTY720-P and when were pre-treated with S1PRs. A slight decrease is also observed under cholesterol normal condition, although statistical significance was not reached (**Figure 5C**).

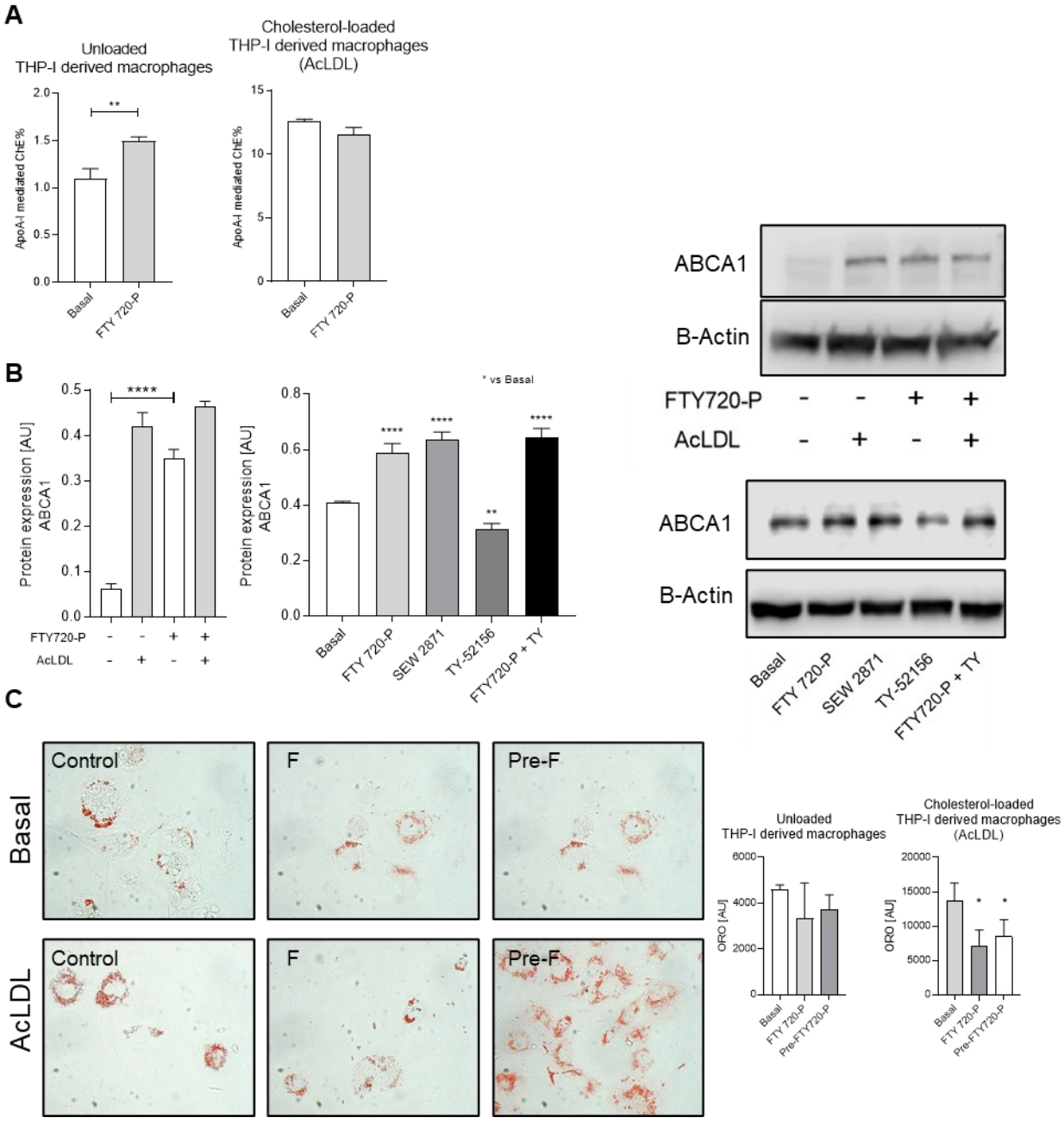

Figure 5. THP-I-derived macrophages were treated with S1PRs modulator under cholesterol normal or loading conditions for 18 hours. **(A)** Effect of FTY720-P on cholesterol efflux capacity. **(B)** Protein expression of cholesterol transporter ABCA1. Protein expression was normalized using β-actin as housekeeping gene. (C) Effect of FTY720-P on lipid droplet accumulation. The magnification of each panel was ×40.
Data are represented as mean ± SD. *p < 0.05, **p < 0.01, ***p < 0.001, and ****p < 0.0001

Discussion

The preliminary data from our study show the potential involvement of the S1P/S1PR axis in cholesterol efflux. In our experimental conditions, fingolimod phosphate reduces cholesterol accumulation in murine and human macrophages. Furthermore, by upregulating the protein expression of the transporter ABCA1, it may enhance lipid efflux mediated by ApoA-I.

The balance between cholesterol uptake and efflux is crucial in maintaining cholesterol homeostasis in macrophages. During the development of atherosclerotic plaque, this balance is significantly altered, promoting the accumulation of cholesterol within the cell, a significant risk factor for atherosclerosis. Although cholesterol efflux from macrophages contributes modestly to the total cholesterol associated with HDLs, it plays a fundamental role in protecting against the development of atherosclerotic plaques. Emerging therapeutic strategies are focused on reducing macrophage cholesterol accumulation and increasing the efficiency of macrophage-to-feces RCT. Therefore, increasing the activity of ABCA1 and ABCG1, key transporters in lipid efflux in macrophages, could be an important strategy in inhibiting the progression of atherosclerosis in subjects with cardiovascular disease high risk. These transporters are induced by the LXR/RXR pathway and finely regulated at the transcriptional, post-transcriptional, and post-translational levels[146]. However, the use of LXR/RXR agonists to induce ABCA1 and ABCG1 and thus improve cholesterol efflux resulted in significant alterations in lipogenic responses and neutrophil effects[147]. A recent study has highlighted the importance of S1P signaling, particularly involving $S1P_3$, in lipid metabolism. Both ceramide and S1P increase the presence of ABCA1 on the plasma membrane, thereby stimulating the efflux of cholesterol to ApoA-I. Additionally, sphingosine kinase 2 plays a pivotal role in this process, as demonstrated by the inhibition and genetic deletion of the enzyme, which suppress the lipid efflux promoted by the LXR agonist[148].

Stimulation with fingolimod phosphate induced an increase in protein expression, but not gene expression, of ABCA1 in murine and human macrophages, and of ABCG1 and SR-BI in murine macrophages under cholesterol normal or loading conditions. These observations suggest that the compound may not directly influence the genetic transcription of cholesterol transporters but instead could exert its effects through

alternative mechanisms. Indeed, it has been demonstrated that the expression of cholesterol transporters can be regulated through three main mechanisms: by increasing genetic transcription, preventing protein degradation, or enhancing mRNA stability. The protein stability of ABCA1 and ABCG1 is intricately regulated by multiple cellular systems, including the proteasomal, lysosomal[149], and calpain pathways[150]. Inhibition of these systems has been shown to lead to a decrease in the protein degradation, facilitating an increased lipid efflux. The interaction of fingolimod phosphate with $S1P_1$ or $S1P_3$ could potentially activate protein kinase C (PCK), leading to the phosphorylation of ABCA1 and subsequent stabilization of the protein. Moreover, post-transcriptionally, the stability of ABCA1 and ABCG1 mRNA is subject to negative regulation by specific microRNAs. Notably, microRNAs such as miR-33a and miR-33b act as suppressors of mRNA stability for both ABCA1 and ABCG1. Additionally, other microRNAs, including miR-17, miR-19b, miR-93, miR-101, and miR-144, have been identified as contributors to the downregulation of ABCA1 mRNA. Immunomodulatory drugs used for treating multiple sclerosis, such as fingolimod, have been shown to modulate the expression of microRNAs[151]. Therefore, investigating this hypothesis could provide additional insights into the involved mechanism.

The increased protein expression of ABCA1 and ABCG1 following treatment with the selective agonist SEW2871 suggests a potential involvement of the S1P/$S1P_1$ axis in the modulation of cholesterol transporter expression. An aspect requiring further investigation is the modulation of ABCA1 expression observed when macrophages were stimulated with TY-52156, a selective antagonist of $S1P_3$. Treatment with TY-52156 yielded unexpected results, leading to a significant decrease in both protein and gene expression of the transporter. Consequently, based on the obtained results, the use of alternative compounds, both agonists and antagonists, will be necessary to investigate the contribution of $S1P_3$ to the effects mediated by fingolimod phosphate.

In conclusion, we demonstrated that fingolimod phosphate, by interacting with S1P receptors, promotes ApoA-I-mediated cholesterol efflux through the upregulation of ABCA1 and reduces lipid accumulation in macrophages. ABCA1 and ABCG1 are integral membrane proteins crucial in cellular cholesterol transport, but they play distinct roles in the efflux of cholesterol from cells. ABCA1 primarily facilitates the efflux of cellular cholesterol to lipid-poor apolipoproteins, typically ApoA-I. On the other hand, ABCG1 is involved in cholesterol efflux to more mature HDL particles and other lipid

acceptors[115]. Although we observed an increase in ABCG1 following stimulation with fingolimod phosphate in murine macrophages, the efflux of lipids to plasma did not rise. One possible explanation could be the high baseline expression of the transporter in resting and non-fingolimod phosphate-stimulated macrophages, leading to a significant percentage of efflux to plasma even in the absence of stimuli. Therefore, despite the compound enhancing the protein expression of the transporter, it is conceivable that the concentration of endogenous ABCG1 had already reached a functionally saturating level. A study, using our identical experimental model, indeed revealed that the impact of ABCG1 overexpression on cholesterol efflux to HDLs was inconsistent[152]

A recent study, published during the data collection phase of this research, demonstrated that fingolimod reduces lipid accumulation by upregulating ABCA1 through an S1P receptor-independent mechanism, in a different murine cell model. The authors show that fingolimod induces the expression of ABCA1 through LXR and sphingosine kinase 2, leading to the acetylation of histone H3 lysine 9 (H3K9)[153]. This, in turn, would result in the suppression of lipid accumulation within macrophages. However, the study lacks support from any functional data, and even though they conducted some experiments in the same cell model used by us, they clearly show that cells respond differently to stimulation with fingolimod. This may reflect the crucial importance of the experimental models in the field of scientific research. However, it's important to acknowledge that the variability in cellular responses to fingolimod stimulation, as highlighted in the mentioned study, underscores the complexity of the system and emphasizes the need to consider different models and experimental approaches to achieve a comprehensive understanding of the involved mechanisms.

In conclusion, the previous data obtained using the peculiar animal model overexpressing $S1P_1$ or $S1P_3$ and the preliminary findings from our *in vitro* study collectively suggest the potential involvement of the S1P/S1PR axis in cholesterol efflux. Despite the availability and clinical use of several drugs for treating and preventing atherosclerotic disease, a significant residual cardiovascular risk still exists. Enhancing ABCA1 and ABCG1 activities may emerge as a potential strategy to inhibit the progression of atherosclerotic plaques. In our experimental conditions, fingolimod phosphate demonstrates a reduction in cholesterol accumulation in two different experimental models. Moreover, upregulating the protein expression of the ABCA1

transporter may enhance ApoA-I-mediated lipid efflux. While this effect could be mediated by $S1P_1$ activation on the current state of our knowledge, we cannot exclude a potential contribution from $S1P_3$. The observed effects underscore the importance of further research to better understand the role of the S1P/S1PR axis in lipid efflux in macrophages and explore potential therapeutic applications.

Chapter 2

Impact of myeloid-Bhlhe40 deficiency in liver fibrosis: exploring Kupffer cells crosstalk with hepatic stellate cells

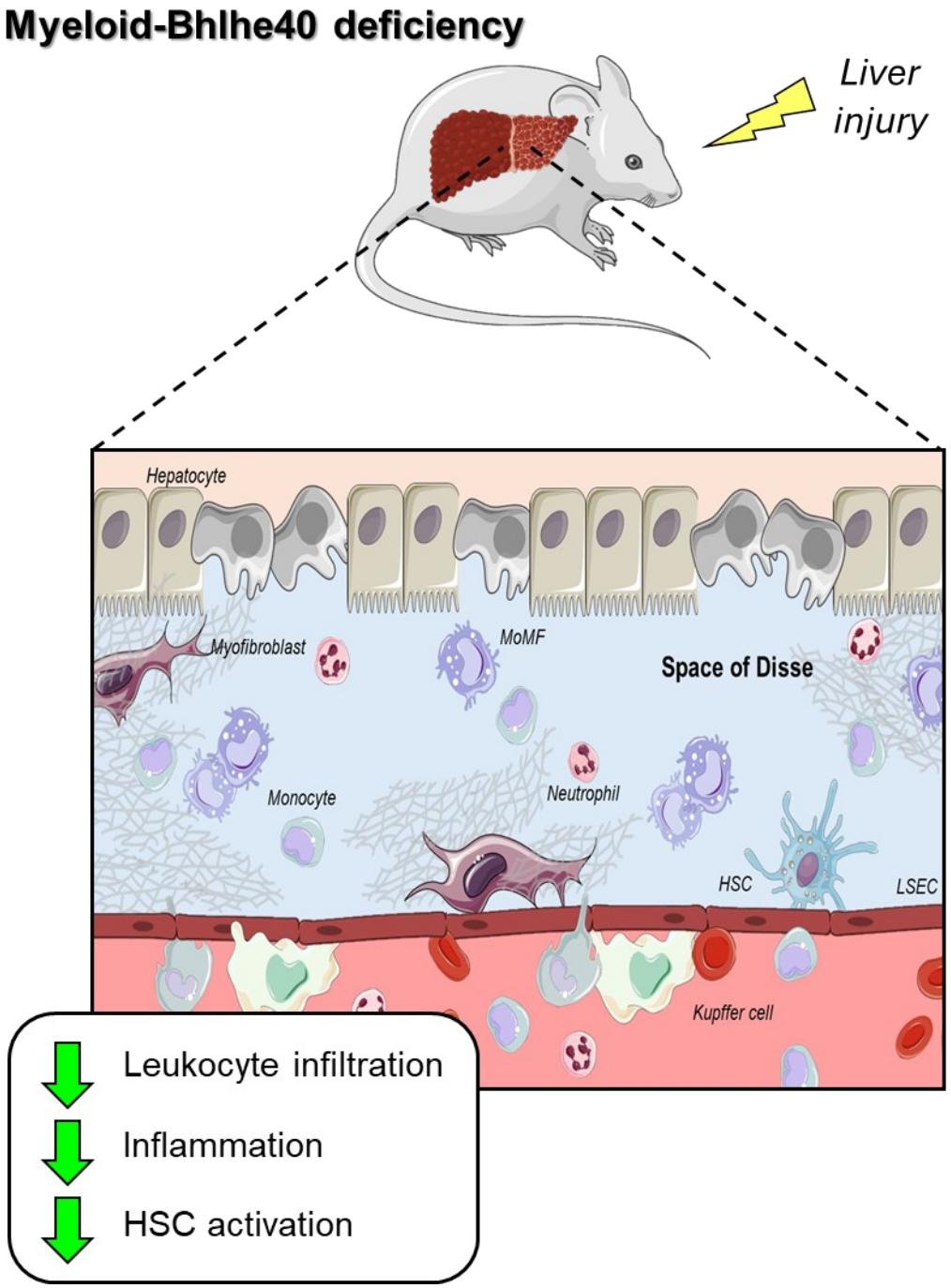

Parts of the figure were drawn by using pictures from Servier Medical Art. Servier Medical Art by Servier is licensed under a Creative Commons Attribution 3.0 Unported License (https://creativecommons.org/licenses/by/3.0/).

Introduction

Liver fibrosis

Chronic liver disease (CLD) represents widespread causes of death worldwide. A recent study has shown that approximately 1.5 billion people globally are affected, mainly as a consequence of nonalcoholic fatty liver disease (NAFLD; 60%), alcohol-related liver disease (ALD; 2%) and hepatitis B (HBV) or C (HCV) virus infections (29% and 9% respectively)[154]. Regardless of the cause, liver damage leads to the development of fibrosis, representing a highly preserved and coordinated protective response to injury, which may progress to cirrhosis and subsequently to hepatocellular carcinoma (HCC)[155].

The onset of hepatic fibrosis involves tissue dysfunction and is defined by the excessive accumulation of collagen and others structural and matricellular proteins (ECM) in the space of Disse, leading to the formation of a fibrotic scar[156]. After tissue injury, immune system cells swiftly infiltrate the liver parenchyma, releasing inflammatory mediators that attract other leukocytes and activate non-parenchymal cells, including hepatic stellate cells (HSCs). HSCs undergo transdifferentiation into myofibroblasts acquiring a wide range of characteristics, including enhanced production ECM, inflammatory and chemotactic mediators, increased proliferation, and contractility, perpetuating inflammation. Moreover, during the development of fibrosis, especially portal fibrosis, myofibroblasts could also originate from peribiliary mesenchymal cells[157–159]. Although this marks a key step in the homeostatic wound-healing response, persistent tissue damage results in chronic cycle of inflammation and angio-architectural changes potentially culminating in organ failure, representing a point-of-no-return[160].

Cell types in liver fibrosis

Hepatocytes

Hepatocytes, the major parenchymal cells, account for about 70% of the entire liver cell population in the steady-state[161]. These specialized cells play a crucial role in the liver's overall functionality, being responsible for various essential functions such as metabolism, protein synthesis and detoxification of various harmful substances to maintain liver homeotasis[162]. In liver disease, hepatocyte change their transcriptomic

profile, which is essential for the liver's adaptive response to injury or stress. Stressed hepatocytes secrete profibrogenic damage-associated molecular patterns (DAMPs) and a variety of profibrogenic mediators such as osteopontin (OPN)[163], Hedgehog ligands[164], TGFβ, Notch[165] and TAZ[166]. In addition, the upregulation of caspases mediates cellular death and the release of chemokines, leading to the recruitment of circulating inflammatory cells to the damaged liver[167].

Liver sinusoidal endothelial cells

Liver sinusoidal endothelial cells (LSECs) develop from common early embryological precursors but exhibit unique characteristics, rendering them distinct from endothelial cells found in other vascular beds[168]. They contain fenestrae organized into sieve plates, whose maintenance requires VEGF[169]. LSECs perform clathrin-mediated endocytosis and secrete paracrine factors that maintain hepatic stellate cells in a quiescent state[170]. After liver damage, changes in hepatic fenestration occur quickly and LSECs undergo capillarization due to the failure of bone marrow-derived LSECs to differentiate[171]. This process is crucial in regulating the recruitment of immune cells into liver tissue[172]. Divergent angiocrine factors from liver sinusoidal endothelial cells promote either regeneration or fibrosis in response to tissue injury[173].

Hepatic immune cells

The liver is a unique immunological organ enriched with several immune cells, which play a fundamental role in both innate and adaptive immunity[160].

Dendritic cells (DCs). Dendritic cells are mononuclear phagocytes that can be primarily classified into two subsets, conventional dendritic cells (conventional type 1 and type 2 DCs) and plasmacytoid dendritic cells (pDCs)[174]. DCs perform many immunological functions and their role in the liver, in establishing hepatic tolerance, is attributed to their ability to evoke tolerogenic responses to antigens[175]. Although several studies have been conducted, the role of dendritic cells in hepatic fibrogenesis is poorly understood and controversial[176–178]. In the setting of NAFLD, Deczkowska et al. recently highlighted an increased presence of cDC1s in both NASH patients and murine disease models, demonstrating a correlation between their abundance and disease severity[179].

Neutrophils. Neutrophils are the most abundant subtype of granulocytes in peripheral circulation that help immune system fight infections (bacteria, fungi, and viruses) and

tissue repair, regulating the innate and adaptive immunity. They are essential contributors that influence the processes of liver injury through proinflammatory cytokines production, activation of Kupffer cells and endothelial cells and promotion of cell adhesion[180]. Furthermore, neutrophils induce a restorative phenotype in macrophages and contribute to collagen degradation, highlighting their key role in the resolution phase of fibrosis[181]. In vivo studies have demonstrated that neutrophil depletion[182] or the deletion of neutrophil chemotactic factors[183,184], such us IL-8, IL-17, CCL3 or CXCL2, ameliorated liver fibrosis.

Monocyte and macrophages. Macrophages are widely distributed in mammalian tissues and are characterized by significant heterogeneity and plasticity depending on the dynamically changing microenvironment. In the liver, two distinct subsets of macrophages can be mainly identified based on their differential cell surface marker expression: Kupffer cells (KCs) and monocyte-derived macrophages (MoMFs). However, there is an additional population of hepatic macrophages residing in the capsule, known as liver capsular macrophages (LCMs). These LCMs are bone marrow-derived and are replenished from circulating monocytes[185]. Capsular phagocytes are $CD11b^{+}F4/80^{+}CD11c^{+}MHC\text{-}II^{+}CSF1R^{+}$ and prevent peritoneal bacteria entering the liver capsule, avoiding pathogens spreading across compartments[185].

Kupffer cells, the liver-resident macrophages located in the hepatic sinusoids, play crucial roles in homeostasis, inflammation, tissue repair, host defense against pathogens and clearance of dead and senescent cells and are the predominant hepatic macrophages in the steady-state. KCs provide primary immune surveillance against gut-derived pathogens and toxins, expressing classic pattern recognition receptors to bind both pathogen-associated molecular patterns (PAMPs) and damage-associated molecular patterns (DAMPs)[186]. They contribute to maintain functional bilirubin[187] and cholesterol metabolism, by reducing LDL-cholesterol and regulating plasma levels of high-density lipoprotein and very low-density lipoprotein through the cholesteryl ester transfer protein (CETP)[188,189]. During homeostasis, in addition, KCs regulate iron metabolism, participating in the clearance of senescent red blood cells (RBCs) and iron recycling, thus preventing damage from excess iron, heme, and hemoglobin deposition in organs[190,191]. These macrophages develop during embryogenesis and sustain themselves through self-renewal mechanisms rather than

on bone marrow-derived progenitors, depending on proliferative signals via. The ability of Kupffer cells to self-renew is highly regulated by particular repressive transcription factors (MafB and cMaf) and enhancers[192]. Based on mouse studies, liver-resident macrophages originate from erythromyeloid progenitors derived from the yolk sac (EMPs) and hematopoietic stem cells[193] that give rise to fetal liver monocytes, which can differentiate into Kupffer cells[194]. Recently, Mass et al. have shown that yolk sac-derived erythroid and myeloid progenitors may generate an intermediate pre-macrophage population (p-Macs) that colonizes the liver and the activation of a specific transcriptional program gives rise to tissue-resident macrophages with specialized functions[195].

Kupffer cells consist of $CD45^+F4/80^+$ $CD64^+CD11b^{int}Clec4F^+CLEC2^+TIMD4^+VISIG4^+$ embryonic KCs (EmKCs) and $CD45^+F4/80^+CD64^+CD11b^{int}Clec4F^{+/-}$ $CLEC2^+TIMD4^{lo}VISIG4^{+/-}$ and monocyte-derived KCs (MoKCs)[196]. Pathological conditions like non-alcoholic steatohepatitis (NASH)[197], excessive intravascular hemolysis[190], bacterial[198], or parasitic[199] infections can cause a reduction in the number of EmKCs, leading to a rapid recruitment of blood monocytes. These monocytes differentiate into MoKCs acquiring a “KC phenotype” in a short time. This process depends on close interactions between KCs and hepatic stellate cells (HSCs), LSECs and hepatocytes that compose the KC niche[200]. Colony-stimulating factor 1 (CSF1), primarily secreted by HSCs in the steady-state liver, plays a crucial role in KCs self-renewal and proliferation, orchestrating the engraftment of monocytes and the imprinting of the KC phenotype. Additionally, Notch signals from LSECs, in coordination with bone morphogenetic protein 9 (BMP9) produced by HSCs, stimulate the production of LXR-α[201] in KCs, a transcription factor crucial for their survival[202,203]. LXR-α also induces the expression of the transcription factor SPI-C, which promotes ferroportin (Slc40a1 or Fpn1), a transmembrane protein essential for maintaining cellular iron homeostasis by promoting iron efflux[204].

Monocyte-derived macrophages are functionally and phenotypically distinct from KCs and only a limited number of MoMFs (except LCMs) populate the liver in the steady-state. However, under pathological states, MoMFs have the capacity to infiltrate and replenish from circulating monocytes which originate from bone marrow $CX3CR1^+CD117^+Lin^-$ progenitor cells[205]. These hematopoietic stem cells further differentiate into common lymphoid progenitors and into granulocyte–monocyte progenitors[206]. After subsequent tightly controlled differentiation steps regulated by

numerous transcription factors and epigenetic DNA methylation mechanisms, functional bone marrow-derived monocytes are identified as $CSF1R^{+}CD11b^{+}LY6C^{+}$ cells[207]. Murine monocytes are divided into two main subpopulations based on Ly6C expression: $LY6C^{+}$ monocytes, which are $CCR2^{+}CX3CR1^{+}CD43^{-}$, and $LY6C^{-}$ monocytes, which are characterized as $CX3CR1^{hi}CCR2^{-}CD43^{+}$ cells[208].

During hepatic injury, the pool of liver macrophages is even expanded by a significant infiltration of bone marrow-derived "classical" $Ly6C^{hi}$ monocytes, dependent on CCL2/CCR2 or CCL1/CCR8 interaction[209,210], that give rise to MoMFs. Both KCs and MoMFs undoubtedly represent the primary macrophage subsets in liver damage[211]. The understanding of liver damage has long overlooked the distinct contributions of KCs and MoMFs, primarily due to a lack of suitable approaches and tools for specific functional assessments. Briefly, during the initial phase of liver damage, activated KCs release pro-inflammatory cytokines and chemokines such as IL-1β, TNF, and CCL2, which sustain tissue injury by inducing apoptosis of hepatocytes or cholangiocytes. Elevated levels of CCL2 promote chemotaxis of $CCR2^{+}$ monocytes to the affected liver. The recruitment of monocytes is crucial for hepatic fibrogenesis. Several studies have demonstrated that the inhibition of CCL2 or the genetic deletion of CCR2 resulted in reduced macrophage infiltration and significantly inhibited liver fibrosis in murine models[212,213]. Moreover, Kupffer cells secrete CXCL1, CXCL2 and CXCL8 to facilitate neutrophils requitment[214]. Likewise, monocyte-derived macrophages secrete different chemokines, which in turn attract other immune cells associated with inflammation and tissue damage. For example, in mouse models of liver fibrosis induced by carbon tetrachloride (CCl4) and a methionine-choline–deficient (MCD) diet, MoMFs secrete CXCL16, recruiting $CXCR6^{+}$ natural killer T (NKT) cells[215]; while in high-fat diet (HFD) fed mice, MoMFs produce CCL5 and CXCL9, leading to the recruitment of $CD4^{+}$ and $CD8^{+}$ T cells, contributing to insulin resistance[216,217]. TLR4 and TLR9 pathways are crucial for hepatic macrophages in producing proinflammatory cytokines such as TNF, IL-6 and IL-1β[218]. In murine models of acetaminophen-induced liver injury, TLR4 deficiency decreases cytokines production and liver injury[219,220]. Similarly, TLR9 deletion suppresses IL-1β production, resulting in reduced steatosis and liver injury in models of diet-induced NASH[221]. Furthermore, TLR4 signaling in KCs is strongly involved in inflammasome activation, including the NLR family pyrin domain containing 3 (NLPR3) inflammasome[222]. In particular, activation of TLR4-dependent NF-κB

signalling promotes ROS production and induce pyroptosis in macrophages, promoting the progression of liver fibrosis[223]. Of particular interest, hepatic macrophages express transforming growth factor beta (TGFβ), a master profibrogenic cytokine which drives HSCs activation, leading to increased expression of tissue inhibitors of matrix metalloproteases[224].

In the liver, macrophages exhibit a dual role in orchestrating the response to fibrotic processes. Indeed, they play a crucial role in both the injury and recovery phases. Using CD11b-DTR transgenic mice, Duffield et al. have shown that depletion of macrophages during fibrosis progression resulted in improved scarring, while their depletion during the resolution phase led to a failure of matrix degradation[225]. Upon cessation of liver injury, Ly6C^{hi} MoMFs differentiate into restorative macrophages, characterized as CD11b^{hi}F4/80^{int}Ly6C^{lo} and exhibiting an anti-inflammatory phenotype. These macrophages express fibrolytic matrix metalloproteinases (MMPs), including MMP12[226] and MMP13[227], phagocytosis-related genes (MARCO)[228], growth factors, such as (HGF and IGF)[229], angiogenesis-related genes (VEGF)[229] and TNF-related apoptosis-inducing ligand (TRAIL)[230]. Phagocytosis of apoptotic cells (efferocytosis), mediated by the STAT3/IL-10/IL-6 signaling pathway, induce the phenotype switching of proinflammatory MoMFs[231]. Recently Bosurgi et al. highlighted the crucial role of IL-4 and IL-13, in coordination with c-met proto-oncogene tyrosine kinase (MerTK)- and/or AXL receptor tyrosine kinase (AXL)-dependent efferocytosis, in driving the differentiation of MoMFs into pro-resolution macrophages[232]. In support of this study, it has been demonstrated that APAP-treated Mer-deficient mice exhibit depletion in hepatoprotective resident macrophages, increased late neutrophils and protracted necrosis[233]. During the recovery phase, activated HSCs induce restorative MoMFs to produce anti-inflammatory cytokines and chemokines, such as IL-10 and IL-6. Furthermore, these pro-resolution macrophages upregulate CX_3C-chemokine receptor 1 (CX_3CR1), depending on CSF1[234], and arginase 1, which have been shown to protect against liver inflammation and fibrosis[235,236], and downregulate CCR2[237].

During liver injury, both MoMFs and KCs play important roles. In addition to increased monocyte infiltration, it has recently been demonstrated that MoKCs replenish and dominate the pool of KCs following depletion of EmKCs due to their enhanced ability to survive in the compromised liver environment. MoKCs play a crucial role in reducing the extent of damage and fibrosis exhibiting increased capacity for proliferation, stronger anti-apoptosis property, enhanced phagocytosis and potentially improved

tissue repair promotion compared with EmKCs[238]. However, the contribution of MoMFs/MoKCs in this study was not fully appreciated. In condition of an injured liver capsule or CCL4-induced acute liver injury, mature F4/80^{hi}GATA6^{+} peritoneal macrophages can also rapidly infiltrate the tissue, helping the liver overcome the damage[239].

Hepatic stellate cells

Hepatic stellate cells (previously named lipocytes, fat-storing, perisinusoidal, or Ito cells), located in the space of Disse between liver sinusoidal endothelial cells and hepatocytes, are resident non-parenchymal liver pericytes. During development, HSCs are derived from the septum transversum mesenchyme, where mesothelial and submesothelial cells of mesenchymal origin migrate ingoing from the embryonic liver surface[240,241]. Best known as vitamin A-storing cells, stellate cells exhibit high plasticity that allows them to regulate physiological and pathological responses. Indeed, these cells play a regulatory role in hepatic growth, immunity, inflammation and homeostasis[242]. Several *in vivo* studies have identified three distinct phenotypes of hepatic stellate cells based on specific markers[243,244]. In response to liver damage, 'quiescent' HSCs (qHSCs) undergo transdifferentiation into activated myofibroblasts[245]. However, after ceases injury, activated HSCs (aHSCs) revert to an inactive phenotype, maintaining epigenetic characteristics that facilitate their reactivation upon subsequent damage[246]. Recent single-cell RNA sequencing studies have revealed that the simplistic classification into 'quiescent,' 'activated,' and 'inactivated' (iHSCs) does not reflect the heterogeneity of stellate cells. Instead, specific clusters within the cell population drive fibrosis, other homeostatic processes, repair or immunomodulation[247].

Quiescent HSCs. qHSCs play a crucial role by providing structural support for hepatic parenchymal cells, acting as a liver scaffold. Moreover, they contribute to the maintenance of the hepatic lobular structure integrity through the synthesis of basal membrane matrix components, including laminin and nonfibrogenic collagen type IV[248]. The crosstalk between hepatic stellate cells and their surrounding environment (hepatocyte/LSECs/HSCs niche) plays a fundamental role in maintaining homeostasis and ensuring the proper functioning of the liver. It regulates the inflammatory response, contributes to the maintenance of cellular physiology and manages the metabolic

functions of the organ[249]. qHSCs participate in retinoid storage in lipid droplets in the liver[250]. Lipid droplets formation depends on the enzymatic activity of lecithin-retinol acyltransferase (Lrat), which converts all-*trans*-retinol into all-*trans*-retinyl esters. The expression of Lrat is linked to the quiescent hepatic stellate cell phenotype, representing a marker for their identification[251]. In the steady-state, qHSCs express neural markers such as glial fibrillary acidic protein (GFAP), synemin, synaptophysin and nerve growth factor receptor 1[252,253], quiescence-associated nuclear receptors (RXR, FXR, LXR and PXR) along with lipogenic genes including Adipor1, Adpf, C/EBPd, which are regulated by PPARγ[254]. Additionally, transcription factors ETS1/2, GATA4/6, and IRF1/2 are identified as lineage-determining transcription factors for HSCs[255].

Activated HSCs. The accumulation of pro-fibrogenic myofibroblasts is a central aspect of tissue fibrosis. Recent studies utilizing bone marrow transplantation techniques in reporter mice demonstrate that liver myofibroblasts primarily originate from the activation of resident mesenchymal cells, such as qHSCs and portal fibroblasts[256,257]. The contribution of other cell populations, such as liver mesothelial cells, liver capsule progenitors, bone marrow-derived fibrocytes or circulating mesenchymal stem cells appears minimal[258]. The composition of myofibroblasts varies depending on the cause of hepatic fibrosis. Toxic liver injury primarily activates HSCs, affecting the centrilobular and perisinusoidal regions[259], while cholestatic liver fibrosis results from periportal injury with contributions from both activated portal fibroblasts and HSCs[260]. In response to chronic liver injury, qHSCs undergo transdifferentiation into activated HSCs characterized by an inflammatory, chemotactic, proliferative and contractile phenotype[261]. Following activation, HSCs migrate from the space of Disse to the fibrotic septa where they further deposit ECM proteins, including collagen type I, and express α-SMA, Col1a1, Col1a2, TGFβRI, TIMP1, Spp1, VIM, LoxL1 and PDGF receptor β (PDGFRβ) [262,263]. Furthermore, in advanced fibrosis, stellate cell autocrine signaling perpetuates their fibrogenic state[264].

Transforming growth factor-β, a potent fibrogenic cytokine released by infiltrating lymphocytes and monocytes, tissue-resident macrophages and damaged hepatocytes, drives HSCs transdifferentiation via SMAD2- and SMAD3- dependent signaling pathway, promoting transcription of fibronectin, type I and type III collagen[265]. In contrast, SMAD7 acts as an endogenous antagonist, inhibiting fibrogenesis[266].

Moreover, in response to TGFβ, p38 mitogen-activated protein kinase and c-jun N-terminal kinase (JNK) activation promote HSCs activation[267,268]. A recent study has shown that TGFβ can partly induce autophagy in HSCs via the ERK and JNK pathways[269]. Autophagy is a key driver of stellate cell activation, producing fatty acids through the cleavage of retinyl esters within cytoplasmic droplets. Genetic inhibition of autophagy in HSCs results in a significant reduction in fibrogenesis and extracellular matrix accumulation in response to CCl4-induced liver injury[270].

The PDGF signaling network is strongly involved during the process of hepatic fibrosis. PDGFRβ is expressed by HSCs after liver damage and its interaction with PDGF, a potent mitogen, mediates proliferation and migration and promotes ECM production and deposition[271]. Kocabayoglu et al have demonstrated that depletion of PDGFRβ in HSCs attenuates liver fibrosis *in vivo*, underlining the importance of this pathway[272].

Vascular endothelial growth factor (VEGF) has been implicated in both profibrogenic functions and liver tissue repair and resolution[273]. It is produced by LSECs, hepatocytes and macrophages and it induces the activation and proliferation of HSCs as well as angiogenesis, resulting in ECM deposition and TGFβ secretion[274].

Metabolic liver injury triggers hepatic stellate cell activation through lipid accumulation, particularly cholesterol and fatty acids. This process involves the release of hedgehog ligands and extracellular vesicles from hepatocytes, inducing HSC proliferation and extracellular matrix production[275]. The hedgehog pathway constitutes an intricate network of ligands, receptors, and transcription factors, playing a crucial role in regulating progenitor cell fate, injury response, tissue repair and fibrosis[276]. It has been demonstrated that conditional disruption of hedgehog signaling in αSMA^{+} cells inhibits liver fibrosis and prevents accumulation of liver progenitor cells[277]. The accumulation of free cholesterol in HSCs, induced by a high-cholesterol diet in conjunction with bile duct ligation (BDL) or CCl4 treatment, accelerates liver fibrosis and activates HSCs. This accumulation enhances HSC sensitivity to TGFβ-induced activation by increasing TLR4-mediated downregulation of the TGFβ pseudoreceptor BAMBI[278,279].

Retinoids, crucial regulators of cell proliferation and differentiation with implications in wound healing and cancer prevention, exhibit a notable role in hepatic stellate cells. The activation of HSCs is associated with a reduction in vitamin A content, facilitated by the downregulation of Lrat, which catalyzes the esterification of retinol into retinyl ester, the storage form of vitamin A. The loss of lipid droplets containing retinyl-esters is a specific hallmark of HSC activation, although this alone is not sufficient to promote

the activation process[280]. Alcohol dehydrogenases (ADHs) in HSCs oxidize retinol to retinaldehyde, which is then metabolized to retinoic acid. Among the 6 different types in the ADH family, ADH3 acts as a positive regulator in the activation of HSCs and concurrently suppresses natural killer cell activity. ADH3 gene deletion or ADH inhibitor improve liver fibrosis induced by bile duct ligation or CCl4, correlating with an increased number of apoptotic HSCs and enhanced activation of NK cells[281].

Induction of endoplasmic reticulum (ER) stress in HSCs has been associated with their activation and the development of liver fibrosis[282]. ER stress-related genes, such as *Atf4*, *Herpud*, and *sXbp1*, show increased expression during HSC activation[283]. Targeted lentiviral delivery of the ER stress marker 78kDa glucose-regulated protein (GRP78) specifically to HSCs reduces fibrosis[282] and inhibiting the IRE1α pathway decreases their activation and autophagic activity, resulting in diminished fibrogenesis[284]. Several studies have demonstrated that reactive oxygen species are pivotal in HSC activation, influencing the regulation of key factors such as collagen type I and TGFβ[285]. Critical regulators of ROS in HSCs include NOX enzymes. In mouse models of fibrosis induced by CCl4 or BDL, HSCs deficient in *Nox1*, *Nox2* or *Nox4* had decreased ROS generation and was associated with attenuated liver injury[286,287]. Additionally, cytoglobin (CYGB), known for scavenging ROS, plays a protective role against fibrogenesis. This has been evidenced in studies utilizing CYGB-deficient mice or CYGB-overexpressing HSCs[288–290].

The crosstalk between hepatic stellate cells and immune cell populations promotes liver fibrogenesis[291]. Myofibroblasts, activated by profibrotic stimuli, release pro-inflammatory cytokines and chemokines, including CCL2, CCL5, macrophage inflammatory proteins CCL3 and CCL4, and macrophage colony-stimulating factor (M-CSF), recruiting immune cells to the inflammatory site. Moreover, they express chemokine receptors (CCR5, CCR7, CXCR3, and CXCR7) and secrete intercellular adhesion molecule 1 (ICAM-1), vascular cell adhesion molecule 1 (VCAM-1), and E-selectin, inducing the migration of Kupffer cells. They also respond to bacterial components through TLR4 and function as non-professional antigen-presenting cells in the injured liver[230,292].

Inactivated HSCs. While the process of hepatic stellate cell activation is well elucidated, there remains a limited understanding of HSC biology during fibrosis regression. An essential mechanism facilitating the spontaneous resolution of liver

fibrosis involves the apoptosis of aHSCs. This process is governed by a complex interplay of pro-apoptotic and pro-survival signals in the recovering liver, resulting in approximately 50% of hepatic stellate cell-derived myofibroblast undergoing cellular death when the etiological cause of hepatic injury is removed[252,293]. Myofibroblast persistence is influenced by anti-apoptotic factors like TGFβ and TIMP1, as well as survival signals mediated by the NF-κB cascade[294]. Alternatively, aHSCs express death receptors, and the withdrawal of fibrogenic signals or stimulation of death receptors by ligands can induce apoptosis. Pro-apoptotic proteins, such as BCL-2-associated X protein (BAX) and B cell lymphoma 2 (BCL-2), also play a role in caspase 9-mediated programmed cell death[230]. Recent studies using genetic tracking techniques (Col-α2(I)$^{Cre\text{-}YFP}$ mice) and single-cell quantitative polymerase chain reaction have reported that the remaining 50% of activated hepatic stellate cell-derived myofibroblasts escape apoptosis, inactivate and acquire a more quiescent phenotype but distinct during the resolution of fibrosis[246,295]. These iHSCs return to the space of Disse, downregulate the expression of fibrogenic genes, including Col1α1, α-SMA, TIMP1, LoxL2 and Spp1, and reacquire features of quiescence, expressing genes like PPARγ and Bambi. However, some specific quiescence-associated genes are not re-expressed in iHSCs, highlighting differences between qHSCs and iHSCs[296]. Chronic liver injury may induce a repetitive cycle of activation and inactivation in hepatic stellate cells, making them more susceptible to fibrogenic stimuli. This is evident in the heightened reactivity of inactivated HSCs to fibrogenic triggers, such as TGFβ, suggesting a potential biological memory[295]. The deactivation of HSCs involves various transcription factors, such as PPARγ and GATA6. Their deficiency in aHSCs impairs HSC inactivation and increased the severity of liver fibrosis[255]. Moreover, an *in vitro* study has demonstrated that the depletion of PPARγ in cultured HSCs induces an activated phenotype, while overexpression of PPARγ in activated HSCs promotes the phenotypic reversal to quiescent HSC[297]. Lastly, GATA4 emerges as a key player in hepatic stellate cell inactivation. Its depletion in mice leads to hepatic stellate cell activation and the development of liver fibrosis, whereas overexpression results in the downregulation of fibrogenic genes, promoting fibrosis regression[298].

Senescent HSCs. In response to chronic liver injury, aHSCs may undergo senescence remaining metabolically active with a gene expression profile indicating cell-cycle exit[299]. These senescent aHSCs, located in the fibrotic liver, release various

biologically active factors, such as senescence-associated secreted proteins (SASPs), influencing immune surveillance, inflammation and tissue homeostasis[300]. SASPs, crucial molecular markers of senescence, include proinflammatory cytokines (IL-1β, IL-6, IL-8), chemokines (CXCL2)[301], and proteases (MMPs). These factors induce inflammation and attract immune cells to eliminate senescent cells. Moreover, IL-22 has been identified as a factor driving the senescent phenotype in HSCs through a STAT3-SOCS3-p53–dependent mechanism[302]. Overexpressing IL-22 induces senescence and reduces liver fibrosis in mice[303]. The HSC senescence-associated phenotype is driven by chromatin instability and DNA damage, linked to the downregulation of DNase2 and TREX1, which normally clear cytoplasmic DNA[304].

Portal fibroblast

Under physiological conditions, portal fibroblast (PFs) constitute only 0.1% of the total liver cell population and are a minor subset of periductular mesenchymal cells, that surround the portal venules and the bile ducts, crucial for maintaining the structural integrity of the portal tract. Fibroblasts participate in wound healing and fibrosis in response to injury and have been identified as contributors to the development of cholestatic liver injury in both mouse models and humans[305]. Activated portal fibroblasts (aPFs) are characterized by specific markers that distinguish them from aHSCs, including ectonucleotidase 2 (NTPDase 2), Thy-1[306], fibulin 2, elastin, mesothelin (Msln) and mucin 16 (Muc16)[249]. Moreover, aPFs do not respond to PDGFβ and NGF. In contrast, these cells, like activated hepatic stellate cells, depend on TGFβ for collagen type I production[262]. The regulation of TGFβ1–TGFβRI–Smad2/3/4-induced fibrogenic responses in aPFs involves the interaction between Msln, Muc16 and Thy-1. Indeed, Thy1 and Muc16 can bind to Msln, forming a Msln-Muc16-Thy1 complex that modulates the TGFβ1 signaling pathway[307]. Thy-1 prevents TGFβ1-mediated PFs activation while Msln plays a crucial role in activation and proliferation of PFs. It has been demonstrated that ablation of Thy-1 exacerbates cholestatic fibrosis and Msln-deficiency significantly suppresses the progression of liver fibrosis[307,308].

In vivo models to study liver fibrosis

Liver fibrosis is a complex condition caused by various factors. Viruses, metabolism, toxins, drugs, alcohol, hereditary factors and cholestasis can all contribute to the

development of chronic liver disease. Given the diverse etiologies impacting the progression of liver fibrosis, the selection of an appropriate model is crucial.

Hepatotoxin-Induced Liver Fibrosis Models

Carbon tetrachloride. Carbon tetrachloride (CCl4) is the most common toxic model for inducing liver fibrosis in rodents. Metabolized to trichloromethyl radical (•CCl3) and trichloromethyl peroxide (•CCl_3O_2) by cytochrome P450 2E1, CCl4 mainly damages liver endothelial cells and hepatic parenchymal cells by disrupting the permeability of lysosomes and mitochondrial membranes. Due to the prevalent expression of CYP2E1 in pericentral zone 3 hepatocytes, hepatotoxic CCl4 metabolites cause mainly severe central lobular necrosis. Liver injury following a single CCl4 injection recovers rapidly and repeated injections are necessary to develop liver fibrosis[309].

CCl4-induced liver injury disrupts the homeostasis of Kupffer cells. It has recently been demonstrated that toxin-induced liver damage significantly reduces the number of EmKCs[310]. This results in the recruitment of monocytes, which, upon differentiation into macrophages, acquire characteristic features of KCs. Specifically, these MoKCs express high levels of KC signature genes, such as *Clec4f*, *Clec1b*, *Vsig4*, *Cd5l*, *C6*, *Folr2*, *Mertk*, *Cdh5*, and *Hmox1*, indicating an advanced state of maturation. In the context of liver damage, MoKCs become predominant in the KC pool due to their ability to survive in the compromised environment and their increased resistance to apoptosis under stress. Furthermore, they contribute to the attenuation of liver fibrosis through various mechanisms. MoKCs exhibit increased phagocytic capacity, attributed to elevated expression of *Cd36* and *Trem2*, and enhanced efferocytosis, despite the reduced expression of the TIM4 receptor[238]. Using scRNA-seq and spatial mapping, Ramachandran et al. have identified in human fibrotic livers a $TREM2^{+}CD9^{+}$ monocyte-derived macrophage (SAMs) population, characterized by a pro-fibrogenic phenotype, within the fibrotic niche. SAMs induce the expression of fibrillar collagen in HSCs and express EGFR ligands, which regulate mesenchymal cell activation. moreover, SAMs promote ex vivo proliferation of primary human HSCs[311].

HSCs are identified as the primary contributors to the myofibroblast pool in CCl4-induced centrilobular injury. The differentiation of qHSCs into aHSCs requires a two-step process. The first phase, initiation, sensitizes qHSCs to cytokines and other extracellular signals, while the second phase, perpetuation, involves the differentiation

into their fully activated phenotype. De Smet et al. investigated the transcriptional programs throughout the entire activation process, from initiation to perpetuation. Their findings revealed that the transcriptional program observed in fully aHSCs is already induced during the initiation phase and initial transcriptional alterations persist through all stages of HSC differentiation[312]. Using single-cell RNA sequencing, recent findings have revealed the spatial distribution of HSCs across the hepatic lobule. HSC zonation has designated portal vein-associated HSCs (PaHSCs) and central vein-associated HSCs (CaHSCs), characterized by a specific gene expression signature. CaHSCs mainly differentiate into pathogenic collagen-producing cells following acute centrilobular liver injury, while quiescent hepatic stellate cells (PaHSCs) play a minor role. CCl4-induced liver injury induces the upregulation of pro-fibrogenic genes (*Col1a1*, *Col1a2*, *Col3a1* and *Lox*) in CaHSCs and the downregulation of uninjured HSC-related genes (*Ecm1*, *Reln*, *Hgf* and *Rgs5*)[313]. A previous study identified four different clusters of hepatic stellate cell-derived myofibroblast. MFB I is characterized by high expression of *Acta2*, transgelin (*Tglna*), *Col1a1*, *Col3a1*, and *Col6a3*; MFB II expresses fewer extracellular matrix-associated genes but shows expression of inflammation-associated genes like *Slpi*, C3, *Saa3*, and *Cd74*; MFB III comprises proliferating fibroblasts expressing components of the activator protein 1 (*Ap1*) transcription factor, such as anti-apoptotic *Jund* and *FosB*; MFB IV exhibits a mixed phenotype with high expression of extracellular matrix modulators (*Mgp*, *Fbln1*) and growth arrest-specific 6 (*Gas6*)[247].

Thioacetamide (TAA). Thioacetamide itself is not hepatotoxic, but its metabolites, TAA sulfoxide and TAA sulfodioxide, converted by CYP2E1, induce oxidative stress covalently binding to proteins and lipids. Toxic metabolites, thus, cause central lobular necrosis, HSCs activation and progressively fibrosis. The TAA model induces portal–portal and portal–central bridging fibrosis development and is therefore better suited for studying the mechanism of hepatic fibrosis compared to spontaneous regression[309,314].

Acetaminophen (APAP). Acetaminophen-induced hepatotoxicity is a leading cause of drug-induced acute liver failure (ALF) in many developed countries. APAP is a widely used over-the-counter drug known for its antipyretic and analgesic properties. Although generally considered safe at therapeutic levels, an overdose can result in severe liver damage, leading to ALF. APAP-induced liver damage results from the

accumulation of N-acetyl-p-phenylquinone imine (NAPQI). Excessive NAPQI depletes glutathione, leading to oxidative stress and mitochondrial dysfunction, ultimately hepatocytes necrosis[315]. Moreover, NAPQI can upregulate the mRNA expression of α-SMA, Col1a1, Col3a1 and TGF-β in HSCs, thereby contributing to the development of hepatic fibrosis[316].

NASH-Induced Fibrosis

Nonalcoholic fatty liver disease (NAFLD, or more recently renamed as Metabolic dysfunction-Associated Steatotic Liver Disease (MASLD)) has emerged as a global healthcare concern with an estimated prevalence rate of 25%. It currently stands as the most prevalent cause of chronic liver disease in adults, but also in children and adolescents, attributable to the increased incidence of overweight and obesity even at a young age[317]. In its progressive form, known as NASH (nonalcoholic steatohepatitis, or MASH for metabolic dysfunction-associated steatohepatitis), NAFLD is characterized by liver injury, inflammation, hepatic steatosis, hepatocyte ballooning and various degrees of fibrosis. Inflammatory processes play a pivotal role in the onset and progression of NASH, increasing the risk of severe conditions such as cirrhosis and hepatocellular carcinoma[318].

Steatosis, an early phase in NAFLD associated with dyslipidemia, obesity and type 2 diabetes, may not progress to NASH without additional stresses such as lipotoxicity, oxidative stress and inflammation. These factors activate cellular stress pathways, leading to hepatocyte death (increased serum alanine aminotransferase levels), inflammation and fibrosis development. Liver steatosis, characterized by increased triglyceride storage, may result from circulating free fatty acids released during adipose tissue lipolysis or hepatic fatty acid synthesis[319]. For studying steatosis, a high-fat diet with 40%–60% fat calories is suitable with a preference for saturated fat known to more effectively promote NASH progression[314]. Despite that, a high concentration of fat (55–60% kcal) may counterproductively induce ketogenesis. Modified high-fat diet offer an alternative approach. Sugar consumption, especially the addition of high-fructose, a key substrate for de novo lipogenesis, in beverages, significantly impacts NAFLD incidence and progression[320]. Liquid fructose promotes extensive liver steatosis and fibrosis, while solid fructose induces a stronger inflammatory response. Recent studies indicate that fructose intake alone can induce

NASH and progress to hepatocellular carcinoma in the NASH-susceptible *MUP-uPA* mouse model[321]. Recent studies emphasize the acceleration of diet-induced NASH in the presence of dietary cholesterol. In mice, increasing dietary cholesterol levels (ranging from 0% to 1%) correlated positively with hepatomegaly, serum ALT, inflammation and fibrosis. Van Rooyen et al. demonstrated that the accumulation of free cholesterol in hepatocytes triggers hepatotoxicity and the progression to NASH in diabetic mice[322]. Moreover, HFD induces caspase-2 activation, which is induced by ER stress. This activation leads to the activation of sterol regulatory element-binding proteins (SREBPs), resulting in cholesterol and triglyceride accumulation within hepatocytes in *MUP-uPA* mice[323]. Additionally, administration of a HFD supplemented with fructose and cholesterol for 6 months induces hepatocellular ballooning, fibrosis and metabolic syndrome[324]. Investigating NASH fibrosis can be also achieved combining a HFD with CCl4 treatment. Although CCl4 may not precisely replicate human NASH, transcriptomic analysis of this model reveals gene expression patterns similar to human disease. A HFD, which is high-fat, high-fructose and high-cholesterol, combined with weekly low-dose CCl4, induces activation of HSCs earlier than western diet treatment alone and accelerates NASH development[325].

Although it is considered less physiological than high-fat, high-sugar diets, the choline-deficient high-fat diet (CD-HFD) induces NASH in mice by impairing hepatic lipid metabolism and glucose homeostasis. The methionine-choline-deficient diet (MCD) successfully reproduces human NASH features, including macrovesicular steatosis, hepatocyte death, lobular inflammation and perisinusoidal fibrosis. MCD diet impairs hepatic lipid export due to the absence of phosphatidylcholine, a key component of very-low-density lipoprotein, and induces lipolysis in white adipose tissue, mobilizing fatty acids to the liver, resulting in weight loss and increased insulin sensitivity. In contrast, the choline-deficient, L-amino acid-defined, high-fat diet (CDAHFD) accelerates NAFLD and NASH progression without inducing obesity or significant weight loss. The CDAHFD significantly increases serum ALT and AST levels, induces hepatic steatosis, ballooning, inflammation, and advanced fibrosis within 12 weeks[326].

Impaired hepatic immune cell landscape, highlighted by a significant increase in monocytes and monocyte-derived cells, contributes to the uncontrolled inflammatory environment driving liver injury and NASH progression in both mice and humans. Especially, macrophages play a crucial role in tissue remodeling and the response to

liver damage. During NASH, inflammatory signals promote the recruitment of blood $CCR2^{+}CX_3CR1^{+}LY6C^{+}$ monocytes to the liver, where they differentiate into monocyte-derived macrophages[327]. Steatohepatitis significantly disrupts the homeostasis of KCs and monocyte differentiation into KCs becomes essential to maintain their numbers. The altered self-maintenance of KCs and the increased death of EmKCs lead to the generation of MoKCs, persisting in the liver after disease regression[196,328,329]. However, their transcriptomic landscape differs from EmKC[330], lacking the complete gene expression spectrum associated with accessory functions like erythrophagocytosis. Moreover, MoKCs display a more pronounced inflammatory profile, are more prone to lipid-induced stress and limit hepatic triglyceride storage by downregulating the expression of the *Scd1*[196]. Besides their role in maintaining the KC pool, monocytes can be recruited during NASH progression and differentiate into MoMFs. In mice, these macrophages share similarities with lipid-associated macrophages (LAMs) isolated in obese white adipose tissue and express elevated levels of *Spp1*, *Cd63*, *Gpnmb*, *Cd9*, and *Trem2*[328]. Hepatic LAMs, located in areas with increased Desmin expression, actively express Osteopontin encoded by *Spp1*. Notably, Osteopontin has recently been identified as a promising biomarker of NASH in patient serum[329].

A crucial mechanism driving fibrosis progression in NASH involves the activation of HSCs. Once activated, these cells undergo transdifferentiation into highly proliferative myofibroblasts, contributing to increased extracellular matrix production. Hepatic lipotoxicity activate macrophages, enhancing their proinflammatory phenotype, triggering HSC activation and promoting NASH pathogenesis[331]. Furthermore, the accumulation of free cholesterol in hepatic stellate cells enhances TLR4 signaling, rendering them more responsive to TGFβ-induced activation[279]. Ballooned hepatocytes play a crucial role in fibrosis development by promoting the activation of HSCs. Fatty acids, specifically palmitic acid, induce hepatocytes to release extracellular vesicles, which, upon uptake by HSCs, activate them, resulting in enhanced proliferation, chemotaxis and expression of profibrotic genes[332]. Additionally, palmitate-treated hepatocytes secrete the profibrotic lipid mediator sphingosine-1-phosphate. In a diet-induced NASH mouse model, administration of Fingolimod, an S1P modulator, prevents NASH development, resulting in reduced hepatocyte ballooning, fibrosis and inflammation[333]. HSC-macrophage crosstalk plays

a significant role in the development and progression of NASH. HSCs, along with LSECs and hepatocytes, drive the recruitment and differentiation of monocyte-derived macrophages, thereby promoting the formation of a more inflammatory and pro-fibrogenic KC population[334].

Biliary Fibrosis Models

Cholestasis refers to an obstruction in both the formation and excretion of bile. Prolonged cholestasis is characterized by increased proliferation of biliary epithelial cells, activation of HSCs, and upregulation of profibrotic gene expression. Bile duct ligation (BDL) surgery is a widely used model for studying cholestatic liver injury in rodents[309]. The 3,5-diethoxycarbonyl-1,4-dihydrocollidine (DDC) diet is an established model to better investigate chronic cholangiopathies and liver fibrosis of the biliary type. By inducing porphyrin secretion into the bile duct, it causes the formation of porphyrin crystals and blockages in the bile ducts, resulting in portal-portal septa and onion skin–like fibrosis in the periductal area after 4–8 weeks of feeding[335]. Finally, genetically modified liver fibrosis mouse models have been developed, including the $Mdr2^{-/-}$ mouse model (mice deficient in the canalicular phospholipid flippase), hepatocyte-specific TGF-β–activated kinase $1^{-/-}$ mice, and adenylate uridylate-rich element–$Del^{-/-}$ mice[314].

Alcohol-Induced Fibrosis Models

Alcoholic liver disease (ALD) develops as a consequence of chronic alcohol consumption. The initial stage often involves the accumulation of fat in the liver, progressing to alcoholic hepatitis, alcoholic liver fibrosis, and ultimately alcoholic cirrhosis. Despite differences in alcohol metabolism, partly due to variations in CYP2E1 activity, and immune system responses between rodents and humans, and although rodents naturally exhibit aversion to alcohol consumption, mouse models have been extensively employed in the study of ALD. Since alcohol administration in drinking water, the Lieber–DeCarli full liquid diet and Tsukamoto–French intragastric feeding model did not succeed in developing liver fibrosis, the combination of ethanol administration with a second stimulus, including specific high fat diet and CCl4 administration has been developed[309,336].

The transcription factor Bhlhe40

As a member of the basic helix-loop-helix transcription factor family, Bhlhe40 exhibits binding affinity for class B E-box DNA sequences characterized by the consensus motif CACGTG[337]. Expressed in several mammalian cell types, including both hematopoietic and nonhematopoietic cells, Bhlhe40 is involved in essential cellular processes, such as cell cycle, circadian rhythm, cell death and differentiation memory CD8+ T cell development, transplant rejection, adipogenesis, skeletal muscle regeneration, and initiation of the DNA damage response[338]. Systemic Bhlhe40-knockout mice are viable and fertile, and detailed evaluations of different tissues, including thymus, spleen, lymph nodes and bone marrow, showed no major differences in the populations of lymphoid and myeloid lineages[339]. Moreover, myeloid-specific deletion did not significantly impact the hematopoietic cell compartment[339].
Bhlhe40 drives inflammation and regulates cytokine production by T cells, impacting immune responses in autoimmunity, transplantation, cancer, and infection. Lin et al. have demonstrated that Bhlhe40 promote neuroinflammation mediated by TH1 and TH17 cells in experimental autoimmune encephalomyelitis (EAE). Bhlhe40$^{-/-}$ mice exhibit resistance to EAE induction. Importantly, Bhlhe40 plays a crucial role in T cell function, positively regulating GM-CSF production while suppressing IL-10[340]. In colorectal cancer, Bhlhe40 is predominantly found in CD4+ T cells[341]. Bhlhe40-CD4 TH1 deficiency reduces colitis development, limits IFNγ production and induce IL-10. Moreover, mice with conditional deletion of Bhlhe40 in T cells are more susceptible to *Toxoplasma gondii*, *Mycobacterium tuberculosis* or *Plasmodium yoelii* infections[342–344].

The role of Bhlhe40 in myeloid cells is not well understood. Recent evidence has shown that the transcription factor is expressed in different populations of resident macrophages, including large peritoneal macrophages (LPMs), small peritoneal macrophages (SPMs), lung alveolar macrophages (AMs), and, to a lesser extent, in Kupffer cells[345,346]. Cook et al. have demonstrated that Bhlhe40 is a tissue-specific regulator of murine resident macrophages. Bhlhe40 plays a crucial role in regulating peritoneal macrophage populations, as evidenced by reduced numbers in Bhlhe40$^{-/-}$ mice during homeostatic conditions. Particularly, Bhlhe40 is intrinsically required for proliferation of large peritoneal macrophages (LPMs) and pleural macrophages in both homeostasis and during type 2 immune responses. The dysfunctional cell cycling

observed in Bhlhe40-deficient LPMs, characterized by a significant proportion expressing the proliferative marker Ki67, implies an aberrant regulatory mechanism compared to wild-type LPMs. Furthermore, authors have shown that Bhlhe40 is indispensable for the self-renewal and maintenance of large peritoneal macrophages (LPMs), but not that of other tissue-resident macrophages[345].

Bhlhe40 emerges as a key driver of widespread pro-inflammatory and glycolytic gene expression in macrophages, inducing HIF1α expression. Moreover, Bhlhe40$^{flox/flox}$ x LysM-Cre mice exhibit reduced recruitment of macrophages and neutrophils at the site of inflammation following zymosan-induced acute lung inflammation[347].

A recent study has investigated the role of Bhlhe40 in the regulation of lipid-associated macrophages genes and pathways. The complete loss or reduced levels of Bhlhe40 in these cells are correlated with increased expression of LAM genes, such as *ApoE*, *Lpl*, *Abca1*, and *Abcg1*, and enhanced activity in LAM cholesterol clearance and lysosomal processing[348].

Aim

Hepatic fibrosis, a pathological feature of various chronic inflammatory diseases, is characterized by the excessive accumulation of extracellular matrix containing fibrin, fibrinogen and fibronectin, underlining tissue dysfunction. The extracellular matrix plays a fundamental role in the development and maintenance of tissue during homeostasis, but excessive production and aberrant turnover result in an imbalance in the wound-healing process. Chronic hepatic damage impairs the regenerative potential of the liver, resulting in the onset of chronic diseases[349].

Chronic liver diseases represent a significant public health problem and contribute to around 2 million deaths annually worldwide. Progressive liver fibrosis can be caused by NASH, alcohol-related liver disease, virus infections or autoimmune or cholestatic disorders, but, regardless of the cause, cirrhosis and subsequently hepatocellular carcinoma is the terminal stage[350].

Despite the similarities in the last-stage pathology, the development of liver fibrosis depends on the etiology of the underlying liver disease. However, several studies using different experimental models have demonstrated that the underlying key mechanisms are common. Liver damage results in the release of soluble mediators into the extracellular environment by damaged or dying cells, leading to a cascade of inflammatory events. Inflammatory cytokines mediate the recruitment of bone marrow-derived inflammatory cells and the production TGFβ and PDGF by activated cells, which, in turn, activate HSCs. Activated HSCs upregulate α-SMA and ECM proteins expression, culminating in the formation of a fibrous scar. An intricate crosstalk between hepatic cell types occurs during fibrogenesis and exploring these interactions could contribute to a deeper understanding of the pathophysiological basis of liver fibrosis and the potential development of novel therapeutic interventions[263].

The transcription factor Bhlhe40 is expressed in both hematopoietic and non-hematopoietic cells and plays a key role in vital cellular processes. Recent evidence has demonstrated that Bhlhe40 is expressed in different populations of resident macrophages, including large peritoneal macrophages, small peritoneal macrophages, lung alveolar macrophages, and, to a lesser extent, in Kupffer cells. Bhlhe40 is an essential cell-intrinsic regulator of proliferation and maintenance in LPMs and could be acquired by monocyte-derived macrophages[345]. Using RNA sequencing, recent findings have revealed that pro-inflammatory gene targets (*Tnfa*,

Ccl2, *Cxcl1*, *Cxcl2*, *Nos2*… etc) were significantly attenuated in thioglycolate-elicited peritoneal macrophages (PMs) derived from myeloid-Bhlhe40 deficient mice stimulated with LPS[347]. Analyzing the sequencing data reported in that manuscript, we found that several genes involved in liver fibrosis were downregulated in Bhlhe40 knockout PMs. As known, $TREM2^{+}CD9^{+}$ monocyte-derived macrophages are associated with fibrotic areas and are characterized by a pro-fibrogenic phenotype[311], while monocytes recruited during NASH progression and differentiated into MoMFs express elevated levels of Spp1 and Gpnmb[328]. Moreover, macrophages can release VEGFα, promoting angiogenesis and fibrosis[351], and MMP-12, which reduces the expression of other matrix metalloproteinases, contributing to the progression of fibrosis[352]. The transcriptomic analyses showed that Trem2, Pdgfβ, VEGFα, Spp1, Fn1, Gpnmb and Mmp12 were largely reduced in activated Bhlhe40 knockout macrophages.

Therefore, the aim of this study was to provide more insights of the impact of myeloid transcription factor Bhlhe40 on hepatic macrophage (KCs and MoMFs) crosstalk with hepatic stellate cells in the context of liver fibrosis.

To this purpose, $Bhlhe40^{flox/flox}$, $Bhlhe40^{flox/flox}$ x LysM-Cre and $Bhlhe40^{flox/flox}$ x Clec4F-Cre were injected intraperitoneally with CCl4 under both acute and chronic conditions or were fed an high fat – high sucrose diet for 24 weeks to induce liver fibrosis. Thus, we performed several *in vivo* analyses to investigate the inflammation level and the liver damage.

Materials and Methods

Animals

All mice were housed in a pathogen-free environment at the local animal facility under a 12-h light/12-h dark cycle and had ad libitum access to food and water. Aged- and sex-matched Bhlhe40$^{flox/flox}$, Bhlhe40$^{flox/flox}$ x LysM-Cre, Bhlhe40$^{flox/flox}$ x Clec4F-Cre, Bhlhe40^{GFP-} and Bhlhe40^{GFP+} littermates were used for experiments. All procedures were conducted following the appropriate guidelines and regulations.

NASH-induced fibrosis: diet and experimental design

Male mice were fed the TD.88137 (Envigo Teklad) diet. This high fat – high sucrose (HF-HS) diet is a milk fat–based diet and its composition is 21.2% fat, 49.1% carbohydrate, 17.3% protein, 5.0% fibre, 3.5% minerals, 0.4% $CaCO_3$, 1% vitamin mix, 0.004% antioxidants, and 0.2% cholesterol.

Bhlhe40$^{flox/flox}$ and Bhlhe40$^{flox/flox}$ x LysM-Cre were fed TD.88137 diet for 24 weeks. Bhlhe40^{GFP-} and Bhlhe40^{GFP+} were fed this HF-HS diet for only 8 weeks.

Mice were weighed once a week. Monthly oral glucose tolerance test was performed and body composition was assessed using quantitative nuclear magnetic resonance spectroscopy. At the conclusion of the experimentation, euthanasia was performed by inhalation of isoflurane (1% - 3%) and cervical dislocation. Blood samples were collected in heparinized tubes, centrifuged at 0.8 rcp, 4 °C, for 20 min, and plasma was stored at -40°C until use.

Oral glucose tolerance test (oGTT)

Mice were subjected to a 5-hour fasting period. Glucose (30%) was administered via gavage at a dose of 2 g/kg. Blood samples were collected and glucose concentration (mg/dL) was measured using a glucometer before glucose administration and at 15, 30, 60, 90, and 120 minutes thereafter. The area under the curve (AUC) was calculated to assess differences in glucose metabolism using GraphPad Prism.

Plasmatic insulin determination

Plasma insulin levels were measured by the commercially available Mouse Ultrasensitive Insulin ELISA (Aplco). The homeostatic model assessment was applied

to evaluate IR (HOMA-IR) and insulin sensitivity check index (QUICKI). The calculation was as follows: HOMA-IR = (fasting glucose × fasting insulin)/22.5; QUICKI = (1/log insulin (mU/L) + log glucose (mg/dL)).

Hepatotoxin (CCl4)-induced fibrosis: experimental design

Acute liver injury (ALI). Female Bhlhe40$^{flox/flox}$, Bhlhe40$^{flox/flox}$ x LysM-Cre or Bhlhe40$^{flox/flox}$ x Clec4F-Cre received a single intraperitoneal injection of CCl4 at 0.8 µL/g body weight resuspended in olive oil. After 40 hours post-injection, euthanasia was performed by inhalation of isoflurane and cervical dislocation. Blood samples were collected in heparinized tubes 24 hours following the CCl4 injection and at the time of sacrifice, centrifuged at 0.8 rcp, 4 °C, for 20 min, and plasma was stored at -40°C until use.

Chronic liver injury. Female Bhlhe40$^{flox/flox}$ and Bhlhe40$^{flox/flox}$ x LysM-Cre were injected intraperitoneally with 0.6 µL/g body weight CCl4 resuspended in olive oil twice weekly for 4 weeks (nine injections). 18 hours after the final CCl4 injection, euthanasia was performed by inhalation of isoflurane and cervical dislocation. Blood samples were collected in heparinized tubes, centrifuged at 0.8 rcp, 4 °C, for 20 min, and plasma was stored at -40°C until use.

Preparation of single-cell suspensions - Liver

After cervical dislocation and following cannulation of the portal vein, the inferior vena cava was cut to allow perfusion with 2 mL of pre-warmed (37°C) phosphate buffered saline (PBS) to wash out blood from liver. After PBS, the mouse liver was perfused with 2 ml of pre-warmed (37°C) Hanks′ Balanced Salt solution (HBSS; Gibco™) with Collagenase D (Roche). Perfused livers were harvested and ~750 mg were used for single-cell suspension preparation. The liver was transferred to a gentleMACS™ C tube (Miltenyi Biotech) containing 3 mL of HBSS with Collagenase D and DNase I (Roche) and gently minced with scissors. After an initial mechanical dissociation using the gentleMACS Dissociators (Miltenyi Biotech), the tissue was subsequently incubated with gentle rocking (120 rpm) for 30 min at 37°C, and then further homogenized. The dissociated suspension was filtered through 100-µm cell strainer (BD Falcon) before staining.

Preparation of single-cell suspensions - Gonadal white adipose tissue

Gonadal white adipose tissue (gWAT) was dissected and placed in tissue culture plate with ice-cold HBSS with Collagenase D and fetal bovine serum. Then, the tissue was cut into small pieces with scissors and incubated with gentle shaking (90 rpm) at 37°C for 30 min. After incubation, the dissociated suspension was filtered through a 100-µm cell strainer and spun down at 1500 rpm for 10 min at 4°C. Supernatant was carefully decanted and pellet resuspended in cold FACS buffer (Ca/Mg2+ free PBS, 1% BSA, 1mM EDTA).

Flow cytometry

After washing, 0.5-5 x 10^6 cells were resuspended in cold FACS buffer and incubated with anti-mouse CD16/32 antibody (BioLegend), to avoid non-specific Fc binding, for 10 min at 4°C. Subsequently, cells were stained extracellularly in dark for 30 min at 4°C (**Table a**). Dead cells were excluded using DRAQ7™ (Alexa Fluor® 700; BioLegend). Bodipy and intracellular Desmin stainings were performed on cells fixed with the Cytofix/Cytoperm™ kit (BD Biosciences). Ki67 staining was performed by fixing and permeabilizing extracellularly stained cells using the FoxP3 Transcription Factor Staining Buffer Kit (eBioscience). To determine absolute cell counts, a fixed number of nonfluorescent beads (10000, 10-µm polybead carboxylate microspheres (Polysciences)) were added to each tube. Data were acquired using a BD LSRFortessa flow cytometer (BD Biosciences) and analyzed with FlowJo software (Tree Star).

Plasma alanine aminotransferase and aspartate aminotransferase activity

Plasma alanine aminotransferase (ALT) and aspartate aminotransferase (AST) activity were determined using a UV test kit (ALAT GPT FS and ASAT GOT FS, Diasys) in plasma run on a Indiko™ Plus Clinical Chemistry Analyzer (Thermo Fisher Scientific).

Liver lipid extraction: total cholesterol and triglycerides determination

Frozen liver samples (~20/25 mg) were homogenized in a chloroform/methanol mixture (3:2) using the Precellys tissue homogenizer from Bertin Technologies. After centrifugation (20 minutes at 2200 rpm) at 20°C, an aliquot of the resulting extract was combined in a 1:1 ratio with 1% Triton in chloroform for triglyceride quantification. Lipid

extraction was performed overnight. After drying, total cholesterol and triglyceride levels were determined using a colorimetric assay with a commercially available kit (Diasys).

Plasma total cholesterol and triglycerides determination

Plasma total cholesterol and triglyceride levels were determined using a colorimetric assay with a commercially available kit (Diasys).

Analysis of gene expression by real-time quantitative RT-PCR

Total RNA isolation was performed using the NucleoSpin RNA Plus kit (MACHEREY-NAGEL). RNA was eluted in RNAse free water and quantified using NanoDrop ND 1000 (Thermo Scientific). 0,5 µg of total RNA were reverse-transcribed into cDNA using the SuperScript™ II Reverse Transcriptase (Thermo Fisher Scientific). Real-time quantitative PCR was performed using LightCycler® 480 ResoLight Dye (Roche) in presence of gene-specific primers (**Table b**), using a LightCycler® 480 real-time PCR system and dedicated software (Roche). Gene expression was normalized using a minimum of three housekeeping genes.

Statistical analysis

Data are represented as mean ± SD. Unpaired two-tailed Student's t-test was applied and $p < 0.05$ was considered statistically significant.

Table a. Antibody combinations and dilutions used for flow cytometry staining.

Name	Conjugate	Target	Host	Source	Fluorescent Dilution
CD140a	Biotin	Mouse	Rat	BioLegend	1:200
F4/80	FITC	Mouse	Rat	BioLegend	1:400
I-A/I-E	Brilliant Violet 510™	Mouse	Rat	BioLegend	1:2000
CD31	PE/Cyanine7	Mouse	Rat	BioLegend	1:6000
Ly-6C	PerCP/Cyanine5.5	Mouse	Rat	BioLegend	1:600-1000
CD9	FITC	Mouse	Rat	BioLegend	1:400
Ly-6G	PE/Dazzle™ 594	Mouse	Rat	BioLegend	1:800-2000
CLEC-2	PE	Mouse	Rat	BioLegend	1:500
CD68	PE	Mouse	Rat	BioLegend	
CD11b	APC/Fire™ 750	Mouse, Human	Rat	BioLegend	1:800
CLEC-2	APC	Mouse	Rat	BioLegend	1:500
Tim-4	APC	Mouse	Rat	BioLegend	1:1000
Streptavidin	Alexa Fluor® 647			BioLegend	1:200
Donkey anti-rabbit IgG	Alexa Fluor® 647	Rabbit	Donkey	BioLegend	1:1000
CD61	PE/Dazzle™ 594	Mouse, Rat	Armenian Hamster	BioLegend	1:400
CD73	FITC	Mouse	Rat	BioLegend	1:100
CD206	Alexa Fluor® 647	Mouse	Rat	BioLegend	1:2000
CD49e	PE/Cyanine7	Mouse	Rat	BioLegend	1:200
CD45	APC/Fire™ 750	Mouse	Rat	BioLegend	1:400
Desmin Recombinant Rabbit Monoclonal Antibody		Human, Mouse, Rat	Rabbit	Invitrogen	1:500
CD9	eFluor™ 450	Mouse	Rat	Invitrogen	1:200
CD163	SuperBright™ 702	Mouse	Rat	Invitrogen	1:6000
VSIG4	PE-Cyanine7	Mouse	Rat	Invitrogen	1:1500
CD115	PE-Cyanine7	Mouse	Rat	Invitrogen	1:800
CD11b	eFluor™ 450	Mouse	Rat	Invitrogen	1:400

F4/80	APC	Mouse	Rat	Invitrogen	1:1000
CD38	eFluor™ 450	Mouse	Rat	Invitrogen	1:400
ICAM-2	PE	Mouse	Rat	Invitrogen	1:400
CD64	PE	Mouse	Mouse	Invitrogen	1:400
CD45	BUV661	Mouse	Rat	BD Biosciences	1:6000
Tim-4	BUV395	Mouse	Rat	BD Biosciences	1:1000

Table b. qPCR Primer Sequences.

Gene	Forward (5'-3')	Reverse (5'-3')
Hprt	TGACACTGGTAA AACAATGC	AACACTTCGAGAGGTCCTTT
Nono	GCTCGTGAGAAGCTGGAGAT	GGGTTATCTTCACACACCATGA
18S	GCAATTATTCCCCATGAACG	GGGACTTAATCAACGCAAGC
Rpl13a	TCCCTGCTGCTCTCAAGG	GCCCCAGGTAAGCAAACTT
Il10	GTCATCGATTTCTCCCCTGT	TCATGGCCTTG AGACACCTT
Il6	CCAGAGATACAAAGAAATGATGG	ACTCCAGAAGACCAGAGGAAA
Tnfa	TCTTCTCATTCCTGCTTGTGG	GGTCTGGGCCATAGAACTGA
Il1b	TGTAATGAAAGACGGCACACC	TCTTCTTTGGGTATTGCTTGG
Il33	GACACATTGAGCATCCAAGG	AACAGATTGGTCATTGTATGTACTCAG
S100a	TCCTTGCGATGGTGATAAAA	GGCCAGAAGCTCTGCTACTC
Saa1	GTCTTCTGCTCCCTGCTCCT	CCTTGGAAAGCCTCGTGAAC
Saa2	GAAGCTGGCTGGAAAGATGG	CCTTTGGGCAGCATCATAGT
Cxcl1	AGACTCCAGCCACACTCCAA	TGACAGCGCAGCTCATTG
Cxcl2	AAAATCATCCAAAAGATACTGAACAA	CTTTGGTTCTTCCGTTGAGG
Pdgfb	CGGCCTGTGACTAGAAGTCC	GAGCTTGAGGCGTCTTGG
Tgfb1	TGGAGCAACATGTGGAACTC	CAGCAGCCGGTTACCAAG
Acta2	CCCACCCAGAGTGGAGAA	ACATAGCTGGAGCAGCGTCT
Hif1a	CATGATGGCTCCCTTTTTCA	GTCACCTGGTTGCTGCAATA
Pck1	ATGTGTGGGCGATGACATT	AACCCGTTTTCTGGGTTGAT
Pck2	CAGGGTCTTATCCGCAAACT	CACATCCTTGGGGTCTGTG
Cpt1a	GACTCCGCTCGCTCATTC	TCTGCCATCTTGAGTGGTGA
Fasn	CCAAGCAGGCACACACAA	CACTCACACCCACCCAGA
Scd1	CTGACCTGAAAGCCGAGAAG	TTTACAAAAGTCTCGCCCCA
Dgat1	TCGTGGTATCCTGAATTGGTG	AGGTTCTCTAAAAATAACCTTGCATT
Dgat2	GGCGCTACTTCCGAGACTAC	TGGTCAGCAGGTTGTGTGTC
Acc1	AGAACCCGAAACTCCCAGAA	TGCAATCTTATCCCCCAAAG

Acly	GTGGCCCCAACTATCAAGAG	ATGGGGATCCCAGTGGTC
Elovl6	CGAGAACGAAGCCATCCA	GCCGACCACCAAAGATAAAG
Srebf1	TGGAGGCAGAGAGCAGAGA	AGCAGGCCAACACTAGTAGTCC
Col1a1	CCCACCCAGAGTGGAGAA	ACATAGCTGGAGCAGCGTCT
Col3a1	AGAACAAGGGTTCACGCCC	TGTAGCCTCACAGTCCTTGG
Lrat	TGGTCTCCAACAAGCGTCTC	GTCTGCTCCGTAGGCAAAGT
Timp1	AGAACAAGGGTTCACGCCC	TGTAGCCTCACAGTCCTTGG

Results

Flow Cytometry Panel Design

To understand the impact of the compromised liver environment following the high fat – high sucrose diet and CCl4 administration on different hepatic cell populations, specific antibody panels have been developed by flow cytometry. Cells were gated based on their forward and sideward scattering. Doublets were excluded from the analysis using FSC-area (FSC-A) and FSC-height (FSC-H) or SSC-area (SSC-A) and SSC-height (SSC-H). We looked for surface markers discriminating KCs from the inflammatory MoMFs found in inflamed livers. As previously reported[196], flow cytometry analysis defined EmKCs as $CD45^+$ (leukocytes) $F4/80^+$ $CLEC2^+$ $TIMD4^+$, MoKCs as $CD45^+$ $F4/80^+$ $CLEC2^+$ $TIMD4^-$ and MoMFs as $CD45^+$ $F4/80^+$ $CLEC2^-$ cells. Due to the significant impact of CCl4 administration on Kupffer cell homeostasis and subsequent alteration in surface marker expression, the gating strategy was adapted to achieve a more precise distinction between KCs and MoMFs (**Figure 1A-B**). Then, we identified HSCs as $CD45^-$ $CLEC2^-$ $CD140^+$ $CD49^+$ $CD9^-$ $CD61^+$ $CD73^+$. Since HSCs are known for their ability to store vitamin A in lipid droplets, HSCs were selected based on the UV light excitation of retinol (**Figure 1C**). Lastly, in the diet-induced hepatic fibrosis model, the macrophage populations in gonadal white adipose tissue were also examined by flow cytometry. Resident macrophages were defined as $CD45^+$ $CD64^+$ $CD11b^+$ $CD38^{hi}$ $CD206^{hi}$ and monocyte-derived macrophages as $CD45^+$ $CD64^+$ $CD11b^+$ $CD38^{lo}$ $CD206^{lo}$ cells[353]. Among the resident macrophages, we characterized three subpopulations based on the surface expression of TIMD4 and CD163 ($TIMD4^+$ $CD163^+$, $TIMD4^-$ $CD163^+$ and $TIMD4^-$ $CD163^-$ cells), while among the monocyte-derived macrophages, two subpopulations were identified ($TIMD4^-$ $CD163^+$ and $TIMD4^-$ $CD163^-$ cells).

Bhlhe40 expression in macrophages

The transcription factor Bhlhe40 is expressed in both hematopoietic and non-hematopoietic cell types, including specific resident macrophage populations[354]. To assess and compare the expression of Bhlhe40 in tissue-recruited and resident macrophages under normal and pathological conditions, we examined macrophages from $Bhlhe40^{GFP}$ reporter mice for Bhlhe40 expression. Mice were analyzed after a 8-week high fat – high sucrose diet or a single intraperitoneal injection of CCl4. As

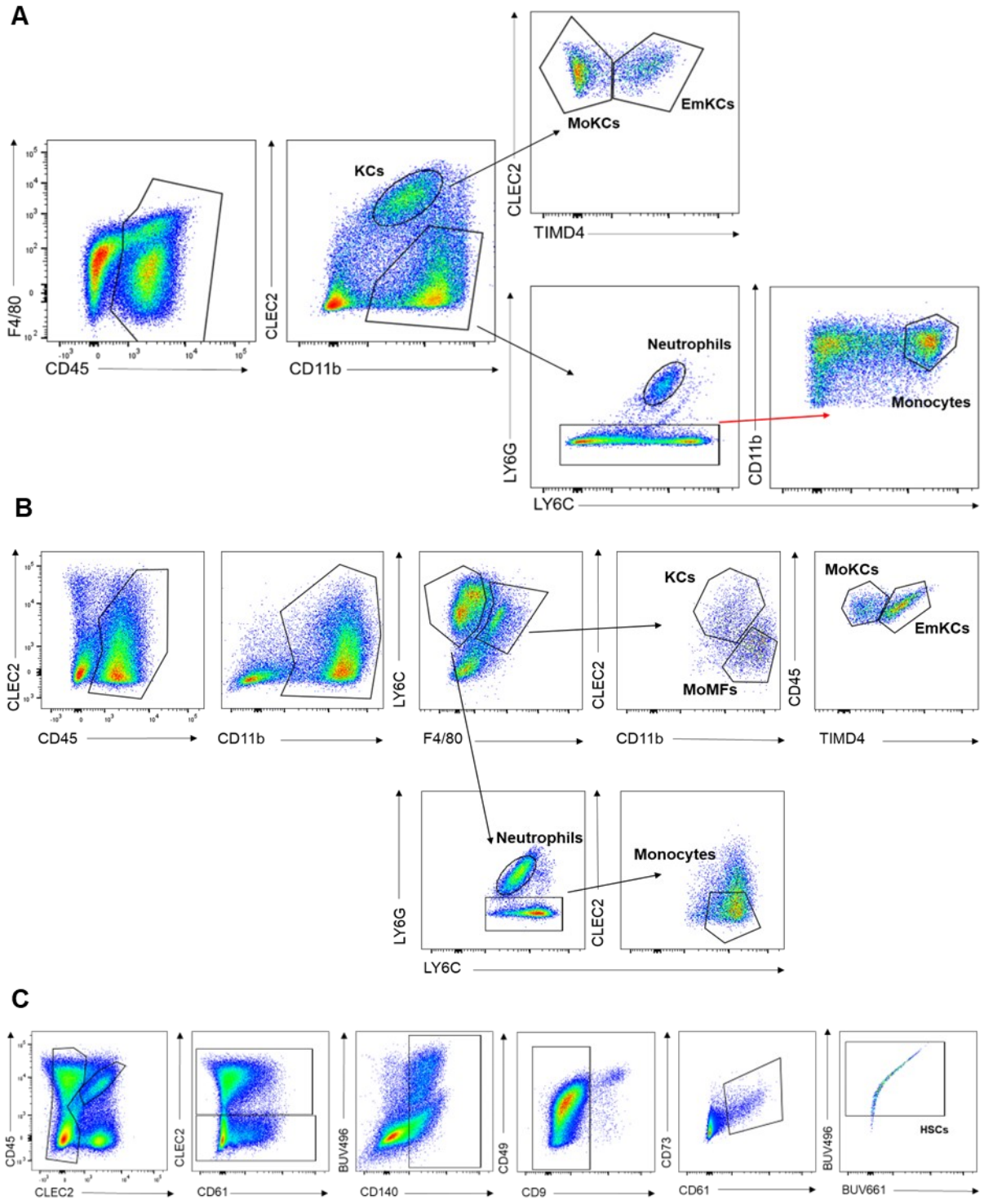

Figure 1. Gating strategy. **(A and B)** Flow cytometry analysis of EmKCs ($CD45^+$ $CLEC2^+$ $TIMD4^+$), MoKCs ($CD45^+$ $CLEC2^+$ $TIMD4^-$) also all positive for F4/80 and MoMFs ($CD45^+$ $CLEC2^-$ $F4/80^+$). **(C)** Flow cytometry analysis of HSCs ($CD45^-$ $CLEC2^-$ $CD140^+$ $CD9^-$ $CD61^+$ $CD73^+$).

previously described[345], we observed high GFP expression in $CD11b^+$ $CD115^+$ $F4/80^+$ $ICAM2^+$ MHC-II^{int} large peritoneal macrophages and $CD11b^+$ $CD115^+$ $F4/80^{lo}$ $ICAM2^{lo}$ MHC-II^{hi} small peritoneal macrophages (**Figure 2A**). Mice fed the HFD diet exhibited

low GFP expression in KCs and gWAT resident macrophages, while it was barely detectable in infiltrating monocyte and neutrophils, as well as in gWAT monocyte-derived macrophages (**Figure 2B**). Finally, we evaluated the expression of GFP in mice injected with a high single dose of CCl4.The control group consisted of animals injected with only vehicle (olive oil). We observed GFP expression in Kupffer cells (in particular in EmKCs) and monocyte-derived macrophages, while infiltrating neutrophils showed very low GFP expression. CCl4 induced a slight increase in GFP expression in macrophage populations (**Figure 2C**). However, it is important to consider that in control animals, monocyte-derived macrophages may include other resident macrophage populations in the liver, such as liver capsular or bile-duct associated macrophages (very low numbers recover with our digestion protocol), since at steady state leukocyte infiltration is almost nonexistent.

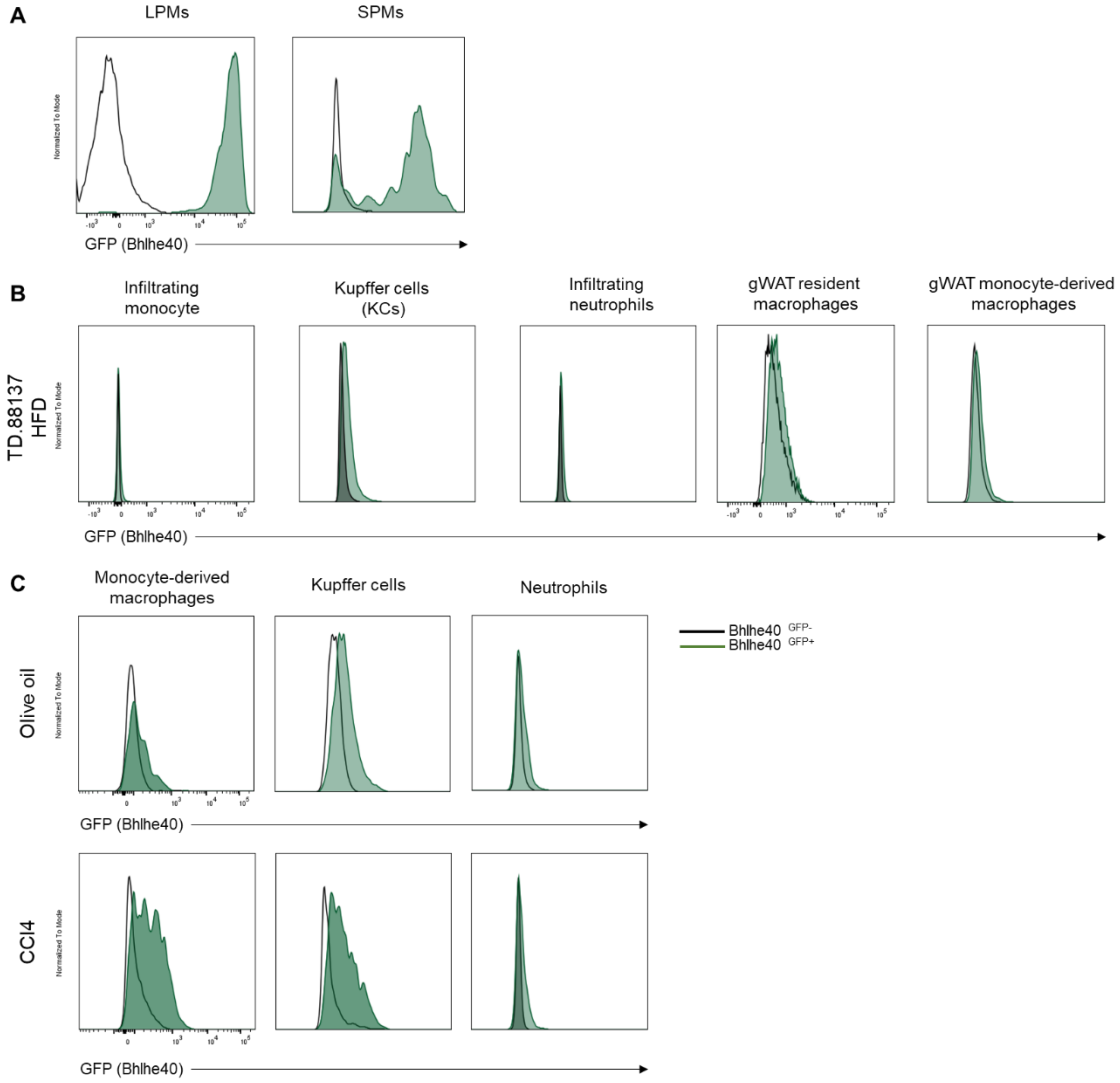

Figure 2. Bhlhe40GFP transgene reporter expression

Myeloid-Bhlhe40 deficiency decreased fasting glycemia after 24 weeks of a high fat – high sucrose diet

Male Bhlhe40$^{flox/flox}$ and Bhlhe40$^{flox/flox}$ x LysM-Cre mice were fed HF-HS diet containing 0.2% cholesterol to develop NASH. After 24 weeks of HFD feeding, mice exhibited around 55–65% increase in body weight. The body weight increase and the body weight gain profiles were similar for both groups (**Figure 3A**). Myeloid-Bhlhe40 deficiency showed no statistically significant effect on body weight, liver and spleen weights, serum and hepatic cholesterol and triglyceride levels and AST activity as compared to control mice. Bhlhe40$^{flox/flox}$ x LysM-Cre mice exhibited higher ALT activity and fasting glycemia than control ones (**Table 1**). Furthermore, we did not observe any differences in the gene expression of selected enzymes involved in fatty acid biosynthesis (*Fasn*, *Scd1*, *Elovl6*, *Acc1*, *Acly*), lipid oxidation (*Cpt1a*), triglyceride synthesis (*Dgat1* and *Dgat2*), regulation of gluconeogenesis (*Pck1* and *Pck2*) and induction of lipogenesis by the liver (*Srebf1*) (**Figure 3B**).

Table 1.

	Bhlhe40$^{fl/fl}$	**Bhlhe40$^{fl/fl}$x LysM-Cre**	
Body weight [g]	44.5 ± 3.5	45.7 ± 1.9	ns
Liver [g]	3.68 ± 0.8	3.87 ± 0.54	ns
Spleen [g]	0.118 ± 0.022	0.112 ± 0.009	ns
ALT [U/L]	373 ± 100	541 ± 73	**p=0.003
AST [U/L]	444 ± 143	472 ± 138	ns
Glycemia (mg/dL)	191 ± 13.6	164 ± 13.5	**p= 0.002
Insulin (mIU/L)	72.4 ± 30.5	66.8 ± 22.1	ns
HOMA-IR	33.7 ± 12.6	26.7 ± 8.0	ns
QUICKI index	0.24 ± 0.01	0.25 ± 0.01	ns
Plasma Total Cholesterol [mg/dL]	252.7 ± 58.2	261.0 ± 34.1	ns
Plasma Triglycerides [mg/dL]	45.0 ± 13.3	42.3 ± 22.9	ns
Hepatic Total Cholesterol [µg/mg]	26.6 ± 10.1	26.5 ± 7.7	ns
Hepatic Triglycerides [µg/mg]	45.9 ± 4.9	43.0 ± 3.0	ns

The percentage of fat mass and lean mass were evaluated every four weeks until the end of the diet. **Figure 3C** shows that both profiles are overlapping between the two

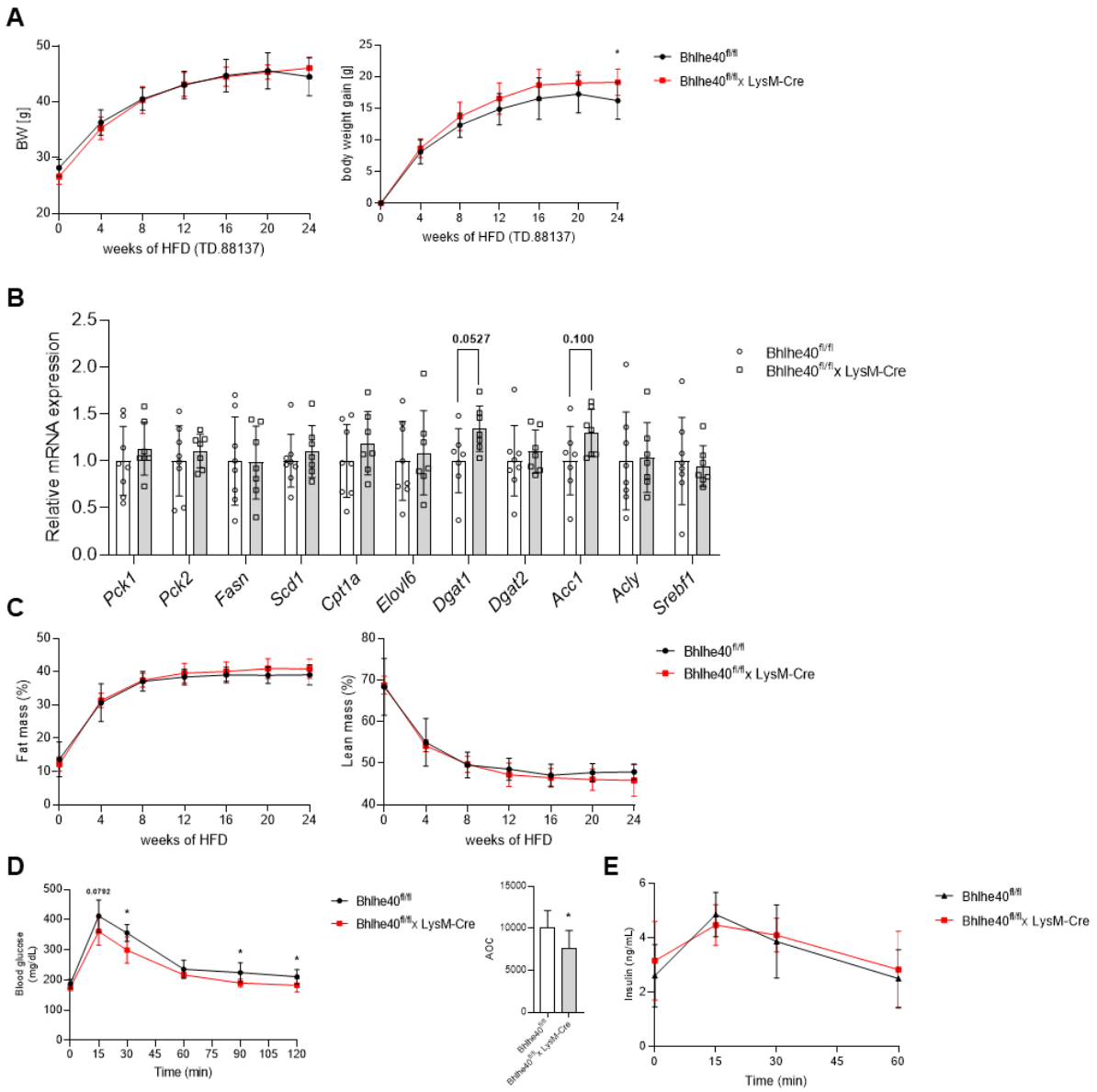

Figure 3. (A) Body weight increase and the body weight gain profiles **(B)** Hepatic mRNA expression of *Pck1*, *Pck2*, *Fasn*, *Scd1*, *Cpt1a*, *Elovl6*, *Dgat1*, *Dgat2*, *Acc1*, *Acly*, *Srebf1*; **(C)** Body fat and body lean percentage; **(D)** Oral glucose tolerance test and area of the curve generated after 20 weeks of HFD; **(E)** Plasma insulin levels related to the oGTT.
Data are represented as mean ± SD. *p < 0.05.

groups. After 20 weeks of HF-HS diet, oGTT results revealed that, after glucose gavage, blood glucose levels increased for both groups, returning to baseline levels after 120 minutes. These results indicated that both groups of mice still exhibited a good glucose tolerance for this duration of high-fat feeding with this diet. However, control mice showed a modestly higher AOC and higher peak glucose levels, suggesting Bhlhe40$^{flox/flox}$ x LysM-Cre mice were slightly more glucose tolerant.

Nevertheless, this difference was not associated with a different insulin response between the two groups (**Figure 3D-E**).

Impact of the high fat – high sucrose TD.88137 diet on hepatic cell populations

TD.88137 diet feeding for 24 weeks induced liver dysfunction, characterized by increased plasma ALT and AST activity and elevated hepatic triglyceride content (**Table 1**). As previously reported, NASH profoundly affects KCs homeostasis. We also observed a recruitment of MoKCs that was comparable in both groups (**Figure 4A**). Monocytes and neutrophils numbers were also comparable between the two groups (**Figure 4B**). MoKCs generated during NASH development are heterogeneous and partially immature with variable expression of specific markers such as VSIG4. In Bhlhe40$^{flox/flox}$ x LysM-Cre mice the fraction of MoKCs which exhibited cell surface expression of VSIG4 was modestly more abundant (~45%) than that of control mice (~38%), although their proliferative state was comparable (**Figure 4C**). Unlike what was observed by Tran et al.[196] with higher proliferation rate of MoKCs as compared to EmKCs in MCD-fed mice, we observed an opposing trend. Nevertheless, EmKCs and MoKCs proliferation rates were comparable in the two groups of mice for each population (**Figure 4D**). It is important to consider that the diet used and its duration may have impacted the homeostasis of KCs differently, potentially leading to a reduction in the proliferative capacity of MoKCs. Flow cytometry analyses also showed no difference in bodipy staining (neutral lipid content) for KC subsets (**Figure 4E**). We did not observe any statistically significant difference between Bhlhe40$^{flox/flox}$ and Bhlhe40$^{flox/flox}$ x LysM-Cre mice in the quantification of HSCs. Mean fluorescence intensity (MFI) measurement was determined in HSCs to evaluate vitamin A content (MFI in UV channel) but also revealed no difference between the two mouse models (**Figure 4F**). Finally, since we observed a slight expression of the transcription factor Bhlhe40 in macrophages of the gonadal white adipose tissue, we proceeded to evaluate specific cellular populations by flow cytometry. No statistically significant difference was observed between the two groups in the quantification of resident and

monocyte-derived macrophages, including different subpopulations characterized by the surface expression of TIMD4 and CD163, as well as in neutrophils (**Figure 4G-H**).

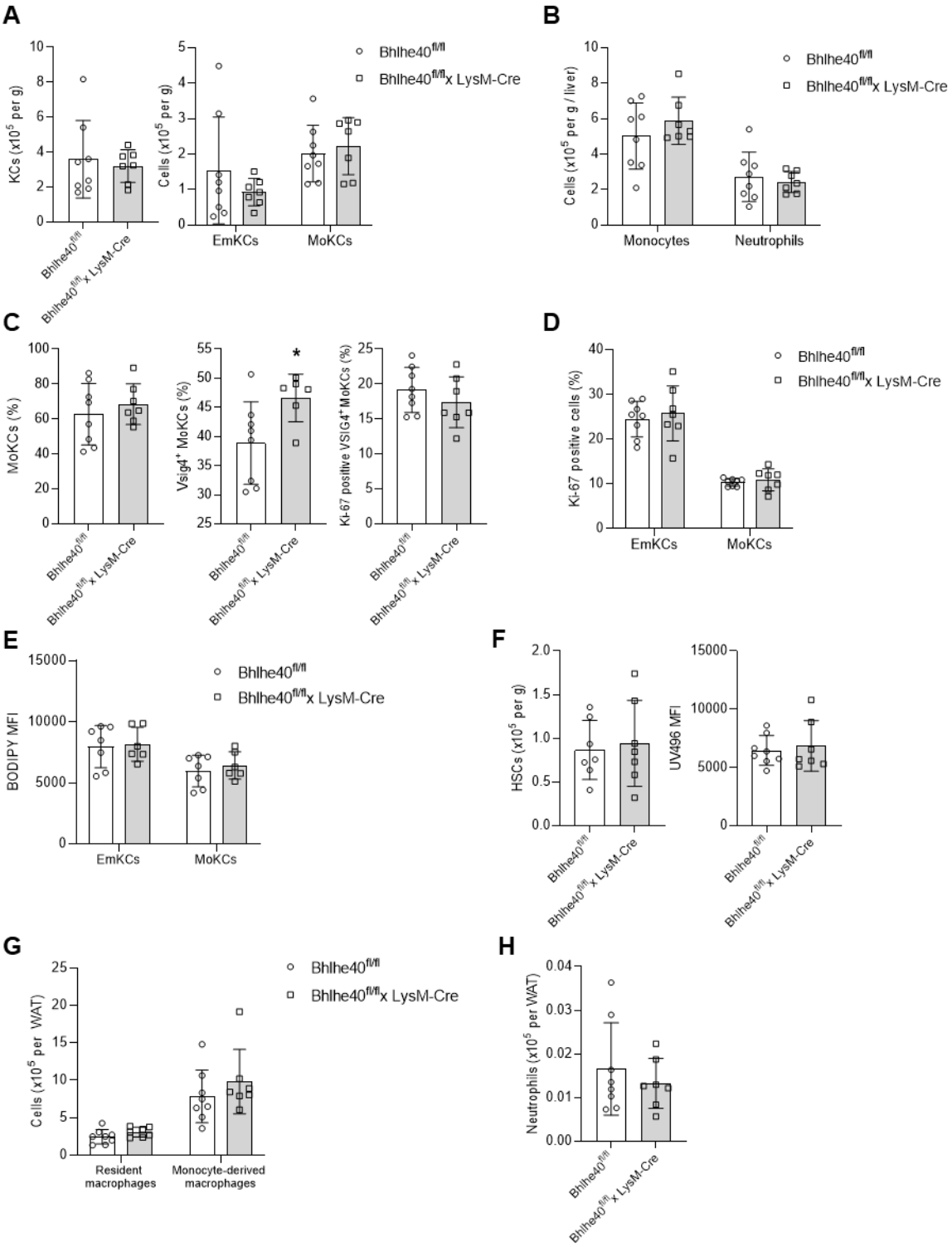

Figure 4. (A) *Total KCs, EmKCs, MoKCs* ***(B)*** *monocytes and neutrophils absolute numbers in livers* ***(C)*** *Percentage of MoKCs, VSIG4⁺ MoKCs and Ki67⁺ VSIG4⁺ MoKCs* ***(D)*** *Percentage of Ki67⁺ EmKCs and MoKCs* ***(E)*** *Intracellular lipids stained by bodipy* ***(F)*** *Total HSCs absolute numbers in livers and UV496 MFI measurements* ***(G)*** *Total resident and monocyte-derived macrophages and* ***(H)*** *neutrophils absolute numbers in gonadal white adipose tissue.*
Data are represented as mean ± SD. *p < 0.05

Myeloid-Bhlhe40 deficiency does not impact the activation of HSCs and the degree of fibrosis after 24 weeks of a high fat – high sucrose diet

We finally sought to investigate the potential consequences of myeloid-Bhlhe40 deficiency on pro-fibrogenic myofibroblasts activation and the consequent development of fibrosis. Thus, we evaluated the expression of key genes associated with HSCs activation and fibrogenesis. Lrat is expressed in quiescent HSCs and downregulated during transdifferentiation into activated myofibroblasts. No difference in *Lrat* mRNA expression was observed after 24 weeks of HF-HS diet (**Figure 5A**), which is potentially consistent with similar autofluorescence in the UV channel (as a marker of retinol content; **Figure 4F**) measured in HSCs of the two groups.

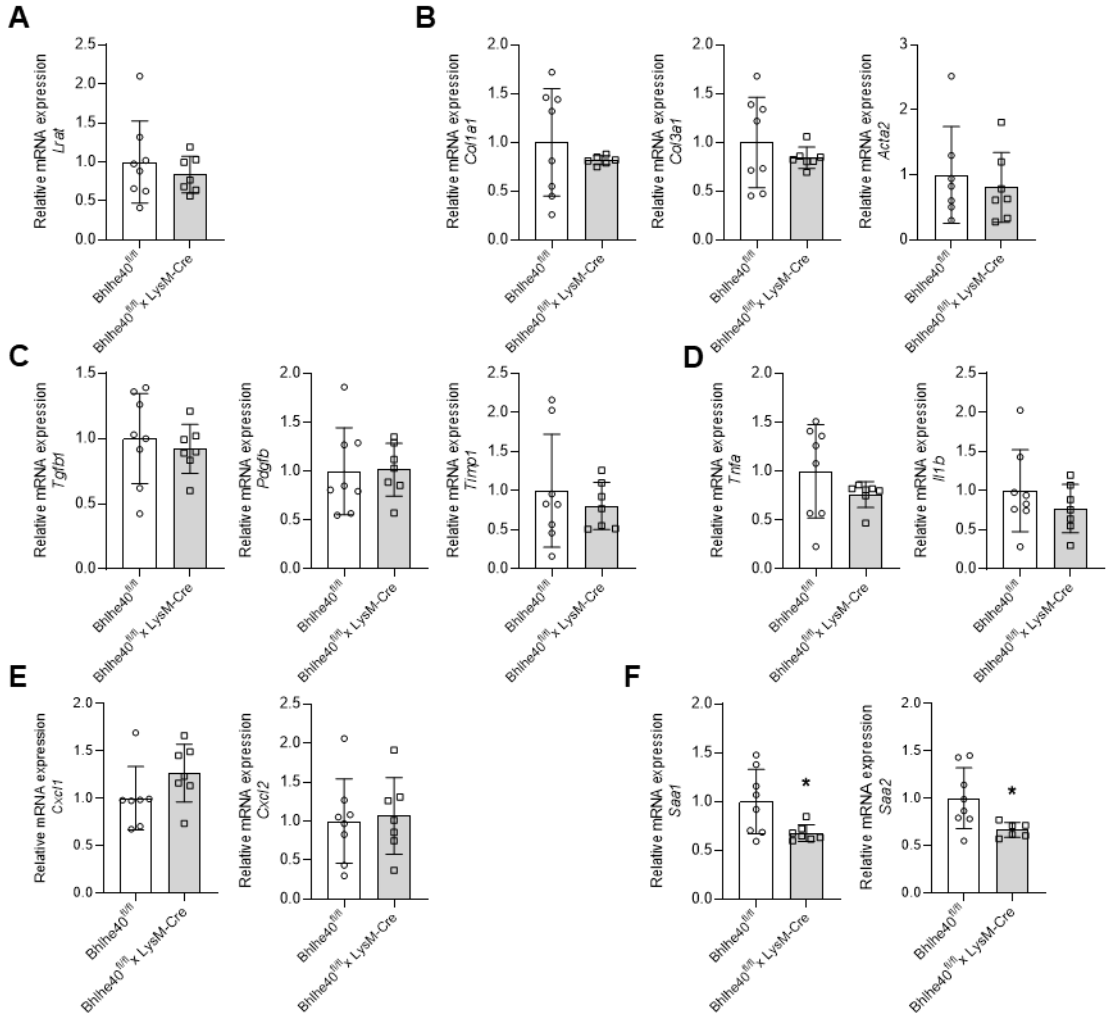

Figure 5. Hepatic mRNA expression of **(A)** *Lrat*, **(B)** *Col1a1*, *Col3a1*, *Acta2*, **(C)** *Tgfb1*, *Pdgfb*, *Timp1*, **(D)** *Tnfa*, *Il1b*, **(E)** *Cxcl1*, *Cxcl2*, **(F)** *Saa1* and *Saa2*.
Data are represented as mean ± SD. *p < 0.05

Then, we analyzed the mRNA expression of genes involved in extracellular matrix deposition, such as collagen encoding genes *Col1a1* and *Col3a1*, and alpha-actin *Acta2* gene. There was no significant difference in the mRNA expression of these pro-fibrotic mediators (**Figure 5B**). mRNA expression levels of genes involved in HSC activation and specific cytokines and chemokine related to fibrosis development were also comparable between the two groups (**Figure 5C-D-E**). If these results suggested no difference in fibrosis development, it must be noted that a few mice in the control group exhibited increased gene activations for *Col1a1* and *Col3a1* suggesting that the pathology was starting to develop stronger in this group. Nevertheless, these expression data will have to be completed by quantitative measurement of fibrosis development in these livers such as Sirius red staining of liver sections and hydroxyproline quantification of liver samples. Finally, activated KCs release proinflammatory cytokines, including the highly expressed acute phase proteins SAA1 and SAA2, normally produced by hepatocytes. Recently, it has been demonstrated that SAA1 induces HSC proliferation and stimulates the production of inflammatory chemokines by HSCs[355]. Interestingly, mRNA levels of *Saa1* and *Saa2* were lower in Bhlhe40$^{flox/flox}$ x LysM-Cre mice.

Myeloid-Bhlhe40 deficiency attenuates myofibroblasts activation after acute liver injury

Previous reports have demonstrated that Bhlhe40 is activated transiently and rapidly in macrophages following LPS stimulation[347]. We utilized the CCl4-induced liver injury model to better understand the role of the transcription factor expressed by myeloid cells following ALI. Flores Molina et al. have shown that wound healing response to ALI (CCL4 model) is characterized by three distinct phases: the necro-inflammatory phase occurs from 0 to 48 hours post-CCl4, the early phase of tissue repair from 48 to 72 hours post-CCl4 and the late repair phase between 72 to 168 hours post-CCl4[211]. Female Bhlhe40$^{flox/flox}$ and Bhlhe40$^{flox/flox}$ x LysM-Cre mice were injected with CCl4 and euthanized 40 hours later, thus straddling the first two phases. All animals lost approximately 10% of their body weight following the injection of CCl4. Myeloid-Bhlhe40 deficiency showed no statistically significant effects on body weight, liver and spleen weights as compared to control mice. We assessed tissue damage by quantifying ALT and AST plasma levels 24 and 48 hours after the administration of CCl4. ALT and AST activities were markedly higher at euthanasia compared to 24

hours post-injection, although no significant differences were observed between the two groups except for plasma AST levels one day post-injection (**Table 2**).

Table 2.

	Bhlhe40$^{fl/fl}$	**Bhlhe40$^{fl/fl}$x LysM-Cre**	
Body weight [g]	20.6 ± 1.6	22.2 ± 2.9	ns
Liver [g]	0.977 ± 0.123	0.982 ± 0.229	ns
Spleen [g]	0.085 ± 0.012	0.098 ± 0.019	ns
ALT [U/L] 24h post-inj	1501 ± 436	2147 ± 961	ns
ALT [U/L] 40h post-inj	12678 ± 3704	11530 ± 4411	ns
AST [U/L] 24h post-inj	1012 ± 259	1428 ± 503	*p=0.04
AST [U/L] 40h post-inj	9143 ± 2918	10137 ± 3073	ns

40 hours after the induction of liver damage, KCs pool homeostasis was markedly changed with the generation of MoKCs that constituted approximately 60% of the KCs pool. A high number of monocytes and neutrophils were also recruited to the injured livers. Moreover, MoMFs emerged as the predominant phagocyte population in those livers (**Figure 6A-C**). We found no difference in KCs pool subsets abundance between Bhlhe40$^{flox/flox}$ and Bhlhe40$^{flox/flox}$ x LysM-Cre mice, nor in monocytes and neutrophils infiltration (**Figure 6B**), consistent with the comparable gene expression levels of typical CXC chemokines (*Cxcl1* and *Cxcl2*) important in immune and inflammatory responses (**Figure 6D**). As it is well-established, toxic liver injury induces HSCs activation and retinyl-ester levels within the cell decrease. Flow cytometry analyses showed no change in the cell density of HSCs, but a trend for increased UV496 autofluorescence was observed in HSCs of Bhlhe40$^{flox/flox}$ x LysM-Cre (**Figure 6E**). Nevertheless, hepatic gene expression levels of *Lrat* were comparable between the two groups (**Figure 6F**). Interestingly, myeloid-Bhlhe40 deficient mice exhibited reduced gene expression of the *Tgfb1* cytokine and growth factor *Pdgfb*, both known factors of the initiation of hepatic stellate cell activation. Concomitantly, lower mRNA levels for *Col1a1*, *Col3a1* and *Acta2* were observed (**Figure 5G-H**). Regarding inflammatory markers, we observed no difference in *Tnfa*, *Il1b* and *Il33* (**Figure 6I**), between the two groups but higher *Il10* (consistent with the repressing role of Bhlhe40

Figure 6. (A) Total KCs, EmKCs, MoKCs **(B)** monocytes and neutrophils absolute numbers in livers **(C)** Percentage of MoKCs, **(D)** hepatic mRNA expression of *Cxcl1* and *Cxcl2*, **(E)** HSCs absolute numbers in livers and UV496 MFI measurements. Hepatic mRNA expression of **(F)** *Lrat*, **(G)** *Tgfb1*, *Pdgfb*, *Timp1*, **(H)** *Col1a1*, *Col3a1*, *Acta2*, **(I)** *Tnfa*, *Il1b*, *Il33*, **(J)** *Il10* and *Il6*.
Data are represented as mean ± SD. *p < 0.05 and **p < 0.01

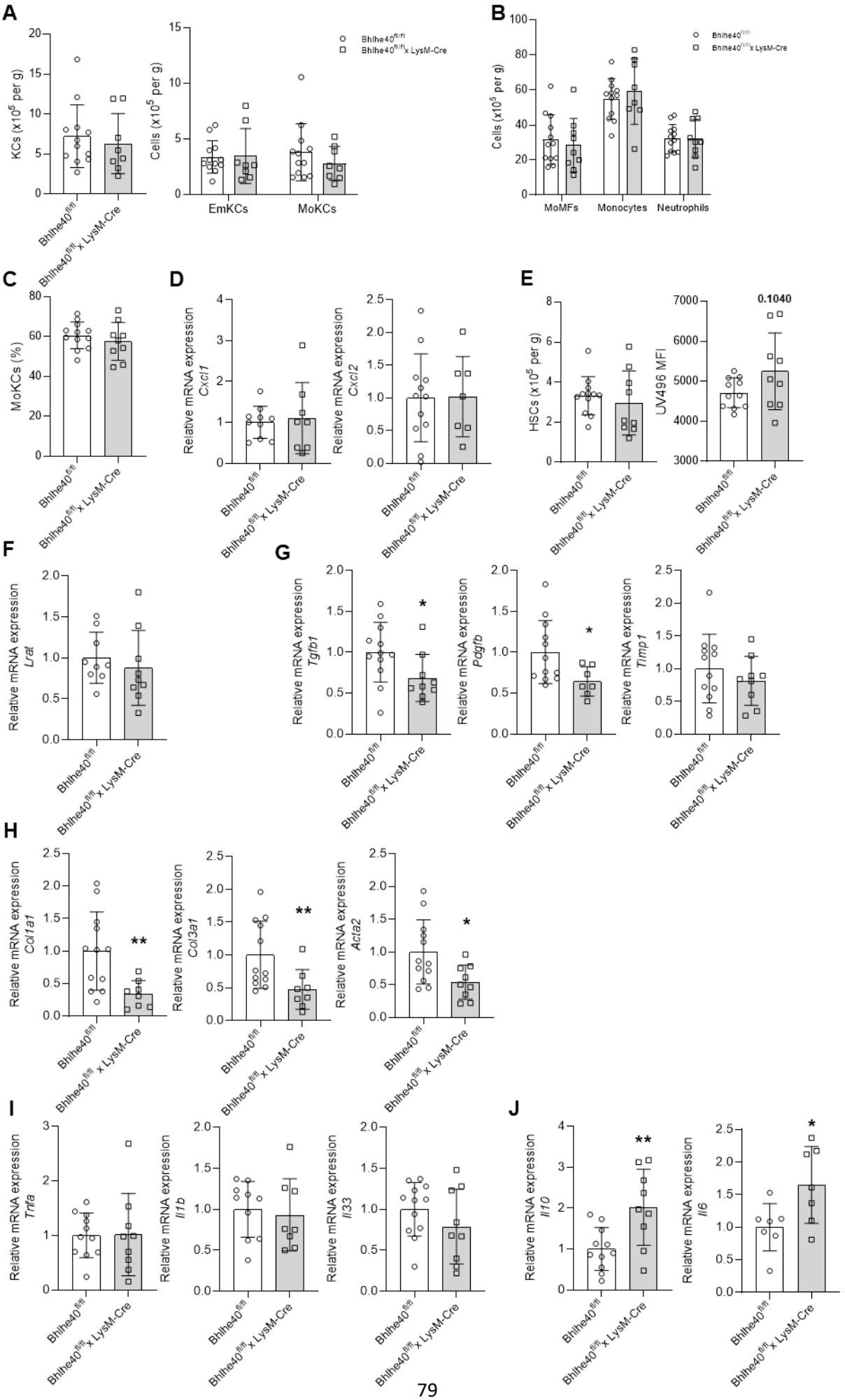
A
KCs (x10^5 per g)
Cells (x10^5 per g)
Bhlhe40fl/fl
Bhlhe40fl/fl x LysM-Cre
EmKCs
MoKCs
B
Cells (x10^5 per g)
MoMFs
Monocytes
Neutrophils
C
MoKCs (%)
D
Relative mRNA expression Cxcl1
Relative mRNA expression Cxcl2
E
HSCs (x10^5 per g)
UV496 MFI
0.1040
F
Relative mRNA expression Lrat
G
Relative mRNA expression Tgfb1
Relative mRNA expression Pdgfb
Relative mRNA expression Timp1
H
Relative mRNA expression Col1a1
Relative mRNA expression Col3a1
Relative mRNA expression Acta2
I
Relative mRNA expression Tnfa
Relative mRNA expression Il1b
Relative mRNA expression Il33
J
Relative mRNA expression Il10
Relative mRNA expression Il6

on IL-10 expression[343]) and *Il6* transcript levels after CCl4 injection in livers of Bhlhe40$^{flox/flox}$ x LysM-Cre mice (**Figure 6J**).

Chronic CCl4 administration decreases hepatic leukocyte infiltration in myeloid-Bhlhe40 deficient mice

We further investigated whether myeloid-Bhlhe40 depletion alleviated CCl4-induced liver fibrosis. Therefore, Bhlhe40$^{flox/flox}$ x LysM-Cre and control mice were intraperitoneally injected with CCl4 (0.6 µL/g body weight) twice a week for four weeks to induce liver fibrosis. 18 hours after the final CCl4 injection, a time of active fibrogenesis, euthanasia was performed. All mice lost approximately 10% to 20% of their body weight in the first two weeks of the experimentation, gradually re-gaining weight thereafter (**Figure 7A**). Serological analysis revealed that levels of plasma ALT and AST, important markers reflecting hepatocyte suffering, were extremely high in both groups and no significant differences were observed in terms of liver and spleen weight (**Table 3**).

Table 3.

	Bhlhe40$^{fl/fl}$	**Bhlhe40$^{fl/fl}$x LysM-Cre**	
Liver [g]	0.928 ± 0.114	0.900 ± 0.095	ns
Spleen [g]	0.131 ± 0.025	0.146 ± 0.030	ns
ALT [U/L]	14032 ± 2086	13976 ± 4311	ns
AST [U/L]	12654 ± 2460	12522 ± 3736	ns

Flow cytometric analysis of KCs revealed no difference in KCs density between the two groups. However, if EmKCs and MoKCs numbers were not different, the proportion of MoKCs in the KC pool was slightly inferior in myeloid-Bhlhe40 deficient mice (**Figure 7B-C**). Myeloid cells infiltration, including monocytes (trend), neutrophils and MoMFs, concomitantly to reduced Cxcl2 chemokine expression were found diminished in Bhlhe40$^{flox/flox}$ x LysM-Cre mice as compared to Bhlhe40$^{flox/flox}$ control mice (**Figure 7D**). Unlike to what was observed at the acute phase, no significant difference in the mRNA expression of genes involved in HSC activation, such as *Tgfb1*, *Pdgfb* and *Timp1*, and in extracellular matrix deposition (*Col1a1*, *Col3a1* and *Acta2*) was observed between the two groups (**Figure 7E-F**). As indicated above for the NASH model, complementary data will have to be done to more thoroughly evaluate fibrosis development in the two CCL4-treated groups (collagen staining on sections and hydroxyproline quantification). Indeed, a snapshot of gene expression profiling

(18h post-CCL4 final injection) may not fully reflect the chronic impact of myeloid-Bhlhe40 deficiency on fibrosis. Finally, and as reported above, *Il10* expression was found more elevated in myeloid-Bhlhe40 deficient mice albeit not to reach statistical significance. A trend for lower levels of *Tnfa* in the liver of these mice was also observed (**Figure 7G**).

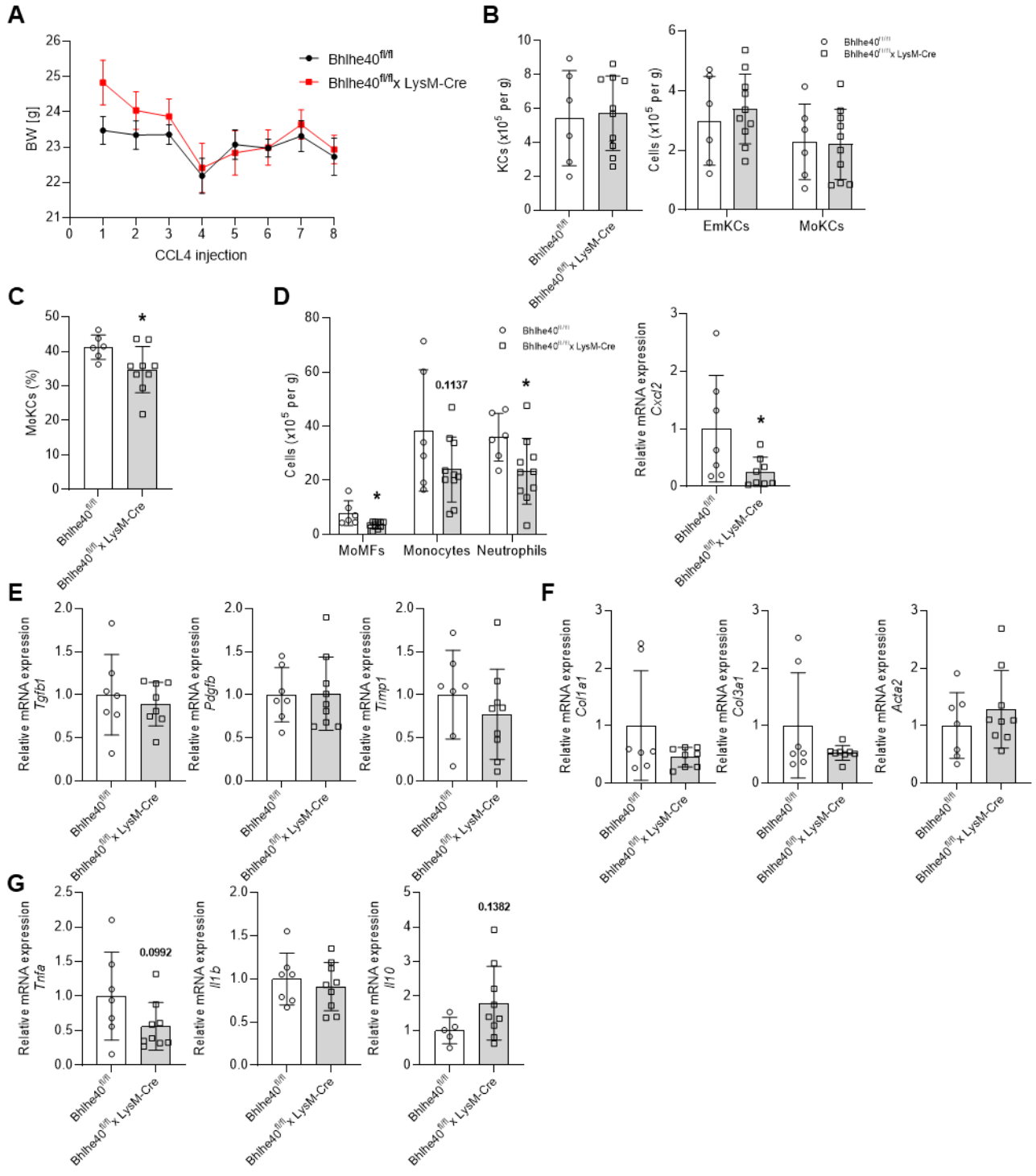

Figure 7. (A) Body weight profile **(B)** Total KCs, EmKCs and MoKCs absolute numbers in livers, **(C)** Percentage of MoKCs, **(D)** monocytes and neutrophils absolute numbers in livers and hepatic mRNA expression of *Cxcl2*. Hepatic mRNA expression of **(E)** *Tgfb1*, *Pdgfb*, *Timp1*, **(F)** *Col1a1*, *Col3a1*, *Acta2*, **(G)** *Tnfa*, *Il1b* and *Il10*.
Data are represented as mean ± SD. *p < 0.05

Specific Kupffer cell-Bhlhe40 deficiency may attenuate CCl4-induced acute liver injury

To potentially reveal different roles played by Bhlhe40 in recruited MoMFs macrophages and KCs, we investigated the impact of Bhlhe40-deficiency specifically in KCs in acute liver injury induced by CCl4. Female Bhlhe40$^{flox/flox}$ and Bhlhe40$^{flox/flox}$ x Clec4F-Cre[203] mice were intraperitoneally injected with CCL4 and euthanized 40 hours later, as described above. KC-Bhlhe40 deficiency showed no statistically significant effects on body weight, liver and spleen weights. We assessed liver damage by quantifying ALT and AST plasma levels 24 and 48 hours after CCL4 administration. Biochemical measurements showed that, compared with the control group, AST plasma concentrations 40 hours post injections in Bhlhe40$^{flox/flox}$ x Clec4F mice were significantly decreased with a similar trend observed with ALT (**Table 4**).

Table 4.

	Bhlhe40$^{fl/fl}$	**Bhlhe40$^{fl/fl}$x Clec4F**	
Body weight [g]	20.6 ± 1.7	21.0 ± 1.0	ns
Liver [g]	0.945 ± 0.187	0.919 ± 0.098	ns
Spleen [g]	0.103 ± 0.021	0.102 ± 0.018	ns
ALT [U/L] 24h post-inj	2527 ± 1579	3435 ± 1592	ns
ALT [U/L] 40h post-inj	8688 ± 4783	5633 ± 1816	ns
AST [U/L] 24h post-inj	2378 ± 1781	2781 ± 1376	ns
AST [U/L] 40h post-inj	8621 ± 4434	4250 ± 1737	*p=0.04

As reported above, CCl4-induced acute liver injury promoted the rapid generation of MoKCs (most likely as a result of partial EmKCs death) and a significant hepatic infiltration of myeloid cells. As previously observed with Bhlhe40$^{flox/flox}$ x LysM-Cre in ALI, KC-Bhlhe40 deficiency had no impact on these parameters (**Figure 8A-C**). Moreover, as observed with Bhlhe40 deficiency in myeloid cells, the specific loss of Bhlhe40 in KCs was associated with reduced expression of genes linked to HSC activations such as *Tgfb1* and *Pdgfb* (borderline statistically significant), but mRNA levels of genes involved in extracellular matrix deposition were not found altered (**Figure 8D-E**). This may potentially be indicative of a specific role played by Bhlhe40

in MoMFs. Finally, we investigated the expression of inflammatory cytokine and chemokine genes. *Il1β*, *Tnfa* and *Il33* cytokine expressions, and those of *Cxcl1* and *Cxcl2* chemokines were found to be less expressed in the livers of Bhlhe40$^{flox/flox}$ x Clec4F-Cre mice following CCl4 administration as compared with control mice. These results could thus suggest that Bhlhe40 expressed by KCs plays an important role in the regulation of inflammation in ALI (**Figure 8F**).

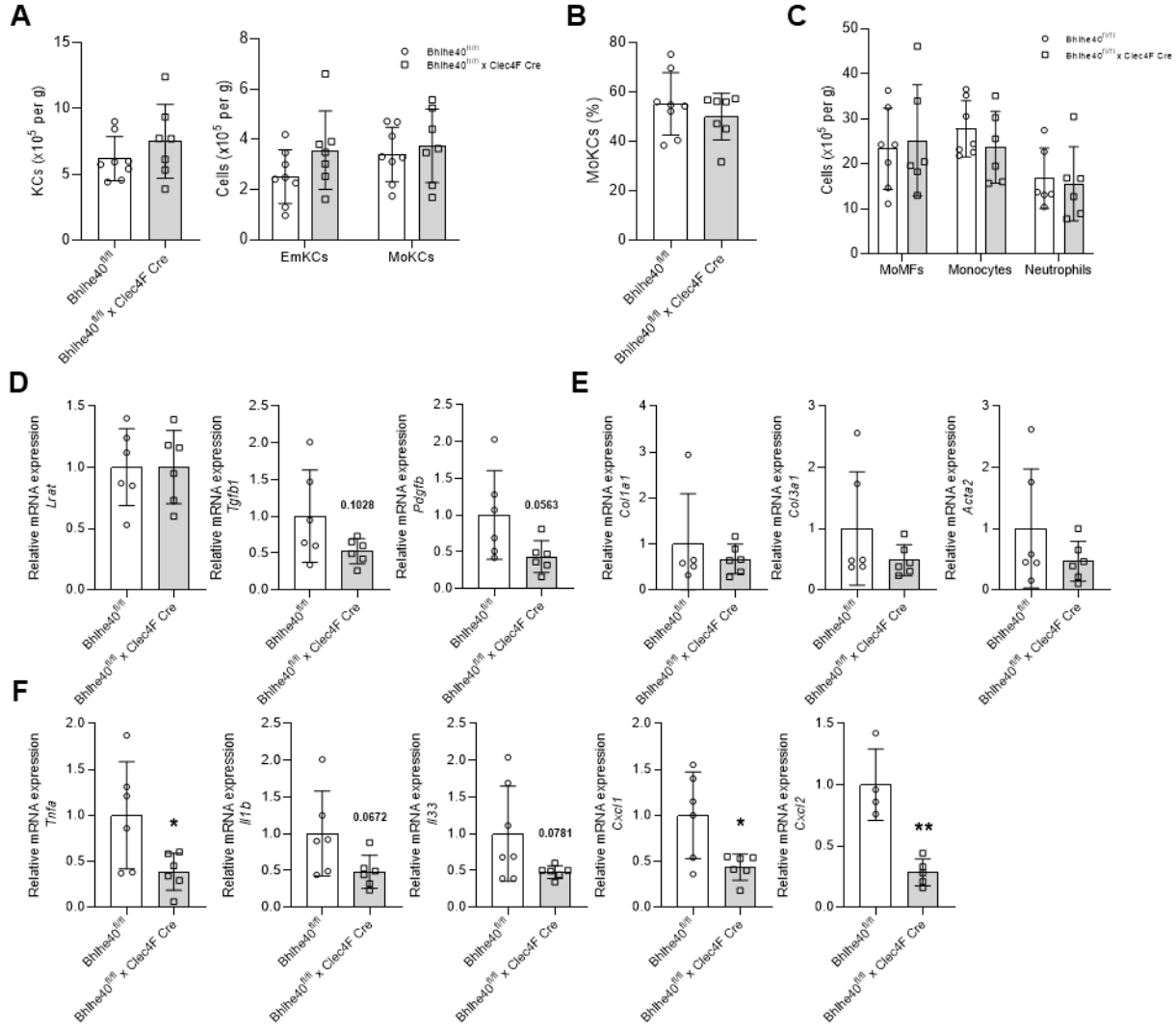

Figure 8. (A) Total KCs, EmKCs and MoKCs absolute numbers in livers, **(B)** Percentage of MoKCs, **(C)** monocytes and neutrophils absolute numbers in livers. Hepatic mRNA expression of **(D)** *Lrat*, *Tgfb1*, *Pdgfb*, **(E)** *Col1a1*, *Col3a1*, *Acta2*, **(G)** *Tnfa*, *Il1b, Il33*, *Cxcl1* and *Cxcl2*.
Data are represented as mean ± SD. *p < 0.05 and **p < 0.01

Discussion

The preliminary data from our study show, for the first time, the potential involvement of the transcription factor Bhlhe40 expressed by myeloid cells in the context of liver fibrosis. Pro-inflammatory genes and genes involved in the initiation of hepatic stellate cell activation and in extracellular matrix deposition are significantly attenuated in myeloid-Bhlhe40 deficient mice. Additionally, the leukocytic infiltration under chronic condition, characteristic of liver damage, appears to be reduced.

Under homeostatic conditions, Bhlhe40 is expressed in large peritoneal macrophages, small peritoneal macrophages, lung alveolar macrophages and, to a lesser extent, in Kupffer cells in mice[345,346]. Activation of macrophages following liver damage resulted in an increased expression of the transcription factor in both resident (KCs) and monocyte-derived macrophages (MoMFs), as observed in Bhlhe40^{GFP} reporter mice. These MoMFs derive from circulating monocytes but could also correspond to infiltrated peritoneal macrophages. Indeed, macrophages from the peritoneal cavity were shown to potentially rapidly infiltrate the liver following CCL4-administration to mice[239]. However, we did not observe in livers of CCL4-treated Bhlhe40^{GFP} reporter mice F4/80^{+} cells with GFP expression levels comparable to those seen in peritoneal macrophages. This could suggest that we did no observe macrophage recruitment into the injured liver via a non-vascular route (peritoneal), or that Bhlhe40 expression in recruited peritoneal macrophages was markedly reduced. Bhlhe40^{GFP} mice also indicated that infiltrating neutrophils and monocytes expressed Bhlhe40 at rather very low levels, suggesting that Bhlhe40 transcription factor may not exert a key function (if any function at all) in these myeloid cell types. Thus, pinpointing macrophages as the main myeloid cell type where Bhlhe40 transcription factor may be active.

Mice fed with a high-fat high-sucrose diet exhibited a significant increase in body weight and in the percentage of fat mass (~40%). The animals developed hepatomegaly, steatosis, dyslipidemia and modest liver damage characterized by elevated plasma levels of ALT/AST. However, 24 weeks of HF-HS feeding were not enough to induce obvious glucose intolerance as shown by the oGTTs. Fasting glucose levels were not significantly different prior to initiation of HF-HS diet. Interestingly, following 24 weeks, myeloid-Bhlhe40 deficient mice exhibited a significant reduction in fasting blood glucose, suggesting a potential involvement of

the transcription factor in glucose metabolism. During fasting, rates of glycolysis in the liver decrease, leading to an increase in hepatic glucose production. Since hepatic gene expression of HIF1α, well-known regulator of key enzymes involved in the glycolysis process[356], was not changed (data not shown), the absence of myeloid Bhlhe40 may have a protective effect on HFD-induced fasting hyperglycemia due to a decreased impact on hepatic gluconeogenic enzymes expression. This will have to be more thoroughly explored.

Kupffer cells are essential to preserve liver homeostasis. They develop embryonically and sustain themselves through self-renewal mechanisms that are independent of circulating monocytes. It has been widely documented that pathological conditions such as NASH or bacterial and parasitic infections lead to the depletion of EmKCs and a quick recruitment of blood monocytes that differentiate into MoKCs, which acquire characteristic features of KCs. In our NASH mouse model, MoKCs were generated and the fraction exhibiting cell surface expression of VSIG4 was significantly higher in myeloid-Bhlhe40 deficient mice. Furthermore, we observed that the percentage of monocyte-derived Kupffer cells was modestly reduced following chronic administration of CCl4. Whether this suggests that the transcription factor may be involved in the processes of MoKCs maturation and recruitment or whether reduced inflammation associated with Bhlhe40 deficiency was responsible for these effects will have to be investigated. The generation of MoKCs during acute liver injury has not been fully elucidated. Zigmond et al. showed that APAP-induced liver damage does not drive MoKCs development[357]. However, in our models of acute liver injury induced by CCl4, we observed a high recruitment of MoKCs, discriminated from MoMFs based on the surface marker expression of CLEC2. Indeed, CLEC2 allows unequivocal identification of Kupffer cells regardless of their origin[196]. These differences may also reflect the cellular pathway involved and/or the cell-specific toxic effects of the molecules used, notably a specific toxicity of CCL4 on EmKCs or cell-types of the KC niche that provide support to EmKCs maintenance.

Bhlhe40 deficiency in myeloid cells, but also specifically in Kupffer cells attenuated inducible pro-inflammatory gene expression (*Tnfa*, *Il1b*, *Cxcl1* and *Cxcl2*), resulting in a potential reduction in leukocytic infiltration that we could eventually evidence in chronic CCL4-treated mice, but not in the HF-HS fed mice. The reduced hepatic expression of *Tgfβ1* and *Pdgfb* in myeloid-Bhlhe40 and KC-deficient deficient mice

could favor decreased hepatic fibrosis due to an attenuated initiation of hepatic stellate cell activation, leading to a reduction in extracellular matrix deposition-associated (*Col1a1*, *Col3a1* and *Acta2*) gene expression. However, the targeted deletion of Bhlhe40 in Kupffer cells did not reduce α-SMA and ECM proteins expression following acute liver injury. This suggests that the transcription factor Bhlhe40 in all cells of the myeloid lineage may be necessary to drive HSC activation, a crucial event in the development of liver fibrosis. Complementary exploration of fibrosis development in both models during chronic hepatic injury will have to be documented to fully assess the impact of Bhlhe40 deficiency in MoMFs and/or KCs.

A recent study has identified scar-associated $CD9^+$ $TREM2^+$ macrophages, which are monocyte-derived, to display a pro-fibrogenic phenotype and expand during hepatic fibrosis[311]. However, other myeloid populations, e.g. associated with obese adipose tissue[358], atherosclerosis[359] and Alzheimer's disease[360], are $CD9^+$ $TREM2^+$ and "scar-associated" does not necessarily imply pro-fibrotic properties. Several studies have demonstrated that TREM2 attenuates fibrotic processes. Indeed, $Trem2^{-/-}$ mice showed increased inflammation and cell death and decreased clearance of lipids and cellular debris, resulting in less fibrosis[361–363]. So, a new set of markers has been identified to distinguish the pathogenic macrophage population more accurately among $CD9^+$ $TREM2^+$ myeloid cells, subsequently named Fab5 SAMs. Fab5 SAMs express SPP1, GPNMP, FABP5 and CD63, genes associated with fibrosis progression, and the $SPP1^+$ $GPNMP^+$ $FABP5^+$ subpopulation is the most abundant in fibrosis. Arising from monocyte, they differentiate by type 3 cytokines (IL-17A and GM-CFS produced by neutrophils and TGF-β in the niche) and co-localize with myofibroblasts and $IL\text{-}17^+$ $GM\text{-}CSF^+$ $MMP9^+$ neutrophils[364]. In our studies myeloid-Bhlhe40 deficient mice exhibited reduced hepatic gene expression of TGF-β, essential for Fab5 SAMs differentiation. Therefore, myeloid-Bhlhe40 deficiency could attenuate the recruitment/generation of Fab5 SAMs that promote clearing normal ECM and pathogenic collagen deposition by activated HSCs and resulting in attenuated liver fibrosis. Interestingly, transcriptomic analyses carried out by Zafar et al.[347] have shown that Trem2, Pdgfb, Spp1 and Gpnmb, key features of Fab5 SAMs, were markedly reduced in activated thioglycolate-elicited peritoneal macrophages derived from myeloid-Bhlhe40 deficient mice. This further supports the idea that myeloid-Bhlhe40

deficiency may impact the functionality of Fab5 SAMs, potentially influencing the regulation of ECM dynamics and collagen deposition in the liver following injury.

Finally, a recent study highlighted the involvement of TREM2 in the process of efferocytosis. Wang et al. demonstrated that hepatic inflammation caused by a HFD results in TREM2 degradation mediated by ADAM17. The loss of TREM2 led to aberrant efferocytosis, exacerbating the production of proinflammatory cytokines[365]. The role of Bhlhe40 has emerged as a key player in driving inflammation by regulating the production of inflammatory cytokines. Moreover, Bhlhe40-deficient macrophages display attenuated gene activation of ADAM17 in vitro (Zafar et al.[347]), which could thus impact TREM2 shedding. This proposed mechanism may enhance macrophage efferocytosis, potentially resulting in reduced fibrosis.

In conclusion, our work revealed the potential involvement of the transcription factor Bhlhe40 in hepatic fibrosis. The modulation of inflammation and the regulation of cytokine production associated with Bhlhe40 deficiency appear to contribute to a noteworthy reduction in leukocyte infiltration and the inhibition of hepatic stellate cells activation. The observed effects underscore the importance of further research to elucidate the precise pathways involved and validate the translational potential of manipulating Bhlhe40 expression in KCs and/or specific infiltrating macrophages sub-populations in the context of liver fibrosis.

References

1. Iessi, E. *et al. On the role of sphingolipids in cell survival and death*. *International Review of Cell and Molecular Biology* **351**, (Elsevier Inc., 2020).
2. Hannun, Y. A. & Obeid, L. M. Principles of bioactive lipid signalling: lessons from sphingolipids. *Nat. Rev. Mol. Cell Biol.* **9**, 139–150 (2008).
3. Futerman, A. H. & Hannun, Y. A. The complex life of simple sphingolipids. *EMBO Rep.* **5**, 777–782 (2004).
4. Gault, C. R., Obeid, L. M. & Hannun, Y. A. An overview of sphingolipid metabolism: from synthesis to breakdown. *Adv. Exp. Med. Biol.* **688**, 1–23 (2010).
5. Pitson, S. M. *et al.* Activation of sphingosine kinase 1 by ERK1/2-mediated phosphorylation. *EMBO J.* **22**, 5491–5500 (2003).
6. Maceyka, M. *et al.* SphK1 and SphK2, Sphingosine Kinase Isoenzymes with Opposing Functions in Sphingolipid Metabolism*. *J. Biol. Chem.* **280**, 37118–37129 (2005).
7. Książek, M., Chacińska, M., Chabowski, A. & Baranowski, M. Sources, metabolism, and regulation of circulating sphingosine-1-phosphate. *J. Lipid Res.* **56**, 1271–1281 (2015).
8. Anada, Y., Igarashi, Y. & Kihara, A. The immunomodulator FTY720 is phosphorylated and released from platelets. *Eur. J. Pharmacol.* **568**, 106–111 (2007).
9. Yatomi, Y. *et al.* Sphingosine 1-Phosphate Breakdown in Platelets. *J. Biochem.* **136**, 495–502 (2004).
10. Tani, M., Sano, T., Ito, M. & Igarashi, Y. Mechanisms of sphingosine and sphingosine 1-phosphate generation in human platelets. *J. Lipid Res.* **46**, 2458–2467 (2005).
11. Ito, K. *et al.* Lack of sphingosine 1-phosphate-degrading enzymes in erythrocytes. *Biochem. Biophys. Res. Commun.* **357**, 212–217 (2007).
12. ULRYCH, T. *et al.* Release of sphingosine-1-phosphate from human platelets is dependent on thromboxane formation. *J. Thromb. Haemost.* **9**, 790–798 (2011).
13. Jonnalagadda, D., Sunkara, M., Morris, A. J. & Whiteheart, S. W. Granule-mediated release of sphingosine-1-phosphate by activated platelets. *Biochim. Biophys. Acta - Mol. Cell Biol. Lipids* **1841**, 1581–1589 (2014).
14. Venkataraman, K. *et al.* Vascular endothelium as a contributor of plasma sphingosine 1-phosphate. *Circ. Res.* **102**, 669–676 (2008).
15. Kobayashi, N. *et al.* MFSD2B is a sphingosine 1-phosphate transporter in erythroid cells. *Sci. Rep.* **8**, 4969 (2018).
16. Vu, T. M. *et al.* Mfsd2b is essential for the sphingosine-1-phosphate export in erythrocytes and platelets. *Nature* **550**, 524–528 (2017).

17. Chandrakanthan, M. *et al.* Deletion of Mfsd2b impairs thrombotic functions of platelets. *Nat. Commun.* **12**, 2286 (2021).

18. Mitra, P. *et al.* Role of ABCC1 in export of sphingosine-1-phosphate from mast cells. *Proc. Natl. Acad. Sci. U. S. A.* **103**, 16394–16399 (2006).

19. Kobayashi, N. *et al.* Sphingosine 1-phosphate is released from the cytosol of rat platelets in a carrier-mediated manner. *J. Lipid Res.* **47**, 614–621 (2006).

20. Hisano, Y., Kobayashi, N., Kawahara, A., Yamaguchi, A. & Nishi, T. The sphingosine 1-phosphate transporter, SPNS2, functions as a transporter of the phosphorylated form of the immunomodulating agent FTY720. *J. Biol. Chem.* **286**, 1758–1766 (2011).

21. Lee, Y.-M., Venkataraman, K., Hwang, S.-I., Han, D. K. & Hla, T. A novel method to quantify sphingosine 1-phosphate by immobilized metal affinity chromatography (IMAC). *Prostaglandins Other Lipid Mediat.* **84**, 154–162 (2007).

22. Kobayashi, N., Kobayashi, N., Yamaguchi, A. & Nishi, T. Characterization of the ATP-dependent sphingosine 1-phosphate transporter in rat erythrocytes. *J. Biol. Chem.* **284**, 21192–21200 (2009).

23. Kawahara, A. *et al.* The sphingolipid transporter spns2 functions in migration of zebrafish myocardial precursors. *Science* **323**, 524–527 (2009).

24. Donoviel, M. S. *et al.* Spinster 2, a sphingosine-1-phosphate transporter, plays a critical role in inflammatory and autoimmune diseases. *FASEB J. Off. Publ. Fed. Am. Soc. Exp. Biol.* **29**, 5018–5028 (2015).

25. Murata, N. *et al.* Interaction of sphingosine 1-phosphate with plasma components, including lipoproteins, regulates the lipid receptor-mediated actions. *Biochem. J.* **352 Pt 3**, 809–815 (2000).

26. Andréani, P. & Gräler, M. H. Comparative quantification of sphingolipids and analogs in biological samples by high-performance liquid chromatography after chloroform extraction. *Anal. Biochem.* **358**, 239–246 (2006).

27. Hammad, S. M., Al Gadban, M. M., Semler, A. J. & Klein, R. L. Sphingosine 1-Phosphate Distribution in Human Plasma: Associations with Lipid Profiles. *J. Lipids* **2012**, 180705 (2012).

28. Ohkawa, R. *et al.* Plasma sphingosine-1-phosphate measurement in healthy subjects: close correlation with red blood cell parameters. *Ann. Clin. Biochem.* **45**, 356–363 (2008).

29. Hammad, S. M. *et al.* Blood sphingolipidomics in healthy humans: impact of sample collection methodology. *J. Lipid Res.* **51**, 3074–3087 (2010).

30. Guo, S. *et al.* Higher level of plasma bioactive molecule sphingosine 1-phosphate in women is associated with estrogen. *Biochim. Biophys. Acta* **1841**, 836–846 (2014).

31. Kowalski, G. M., Carey, A. L., Selathurai, A., Kingwell, B. A. & Bruce, C. R. Plasma sphingosine-1-phosphate is elevated in obesity. *PLoS One* **8**, e72449 (2013).

32. Pappu, R. *et al.* Promotion of lymphocyte egress into blood and lymph by distinct sources of sphingosine-1-phosphate. *Science* **316**, 295–298 (2007).

33. Schwab, S. R. *et al.* Lymphocyte sequestration through S1P lyase inhibition and disruption of S1P gradients. *Science* **309**, 1735–1739 (2005).

34. Hla, T., Venkataraman, K. & Michaud, J. The vascular S1P gradient-cellular sources and biological significance. *Biochim. Biophys. Acta* **1781**, 477–482 (2008).

35. Wilkerson, B. A., Grass, G. D., Wing, S. B., Argraves, W. S. & Argraves, K. M. Sphingosine 1-phosphate (S1P) carrier-dependent regulation of endothelial barrier: high density lipoprotein (HDL)-S1P prolongs endothelial barrier enhancement as compared with albumin-S1P via effects on levels, trafficking, and signaling of S1P1. *J. Biol. Chem.* **287**, 44645–44653 (2012).

36. Christensen, P. M. *et al.* Impaired endothelial barrier function in apolipoprotein M-deficient mice is dependent on sphingosine-1-phosphate receptor 1. *FASEB J. Off. Publ. Fed. Am. Soc. Exp. Biol.* **30**, 2351–2359 (2016).

37. Christoffersen, C. *et al.* Endothelium-protective sphingosine-1-phosphate provided by HDL-associated apolipoprotein M. *Proc. Natl. Acad. Sci. U. S. A.* **108**, 9613–9618 (2011).

38. Mathiesen Janiurek, M., Soylu-Kucharz, R., Christoffersen, C., Kucharz, K. & Lauritzen, M. Apolipoprotein M-bound sphingosine-1-phosphate regulates blood-brain barrier paracellular permeability and transcytosis. *Elife* **8**, (2019).

39. Velagapudi, S. *et al.* Apolipoprotein M and Sphingosine-1-Phosphate Receptor 1 Promote the Transendothelial Transport of High-Density Lipoprotein. *Arterioscler. Thromb. Vasc. Biol.* **41**, e468–e479 (2021).

40. Obinata, H. *et al.* Identification of ApoA4 as a sphingosine 1-phosphate chaperone in ApoM- and albumin-deficient mice. *J. Lipid Res.* **60**, 1912–1921 (2019).

41. Lee, M. J. *et al.* Sphingosine-1-phosphate as a ligand for the G protein-coupled receptor EDG-1. *Science* **279**, 1552–1555 (1998).

42. Chun, J. *et al.* International Union of Pharmacology. XXXIV. Lysophospholipid receptor nomenclature. *Pharmacol. Rev.* **54**, 265–269 (2002).

43. Chun, J., Hla, T., Lynch, K. R., Spiegel, S. & Moolenaar, W. H. International Union of Basic and Clinical Pharmacology. LXXVIII. Lysophospholipid receptor nomenclature. *Pharmacol. Rev.* **62**, 579–587 (2010).

44. Rosen, H. & Goetzl, E. J. Sphingosine 1-phosphate and its receptors: an autocrine and paracrine network. *Nat. Rev. Immunol.* **5**, 560–570 (2005).

45. Kimura, T. *et al.* Sphingosine 1-phosphate stimulates proliferation and migration of human endothelial cells possibly through the lipid receptors, Edg-1 and Edg-3. *Biochem. J.* **348 Pt 1**, 71–76 (2000).

46. Aoki, M., Aoki, H., Ramanathan, R., Hait, N. C. & Takabe, K. Sphingosine-1-Phosphate Signaling in Immune Cells and Inflammation: Roles and Therapeutic Potential. *Mediators Inflamm.* **2016**, 8606878 (2016).

47. Garcia, J. G. *et al.* Sphingosine 1-phosphate promotes endothelial cell barrier integrity by Edg-dependent cytoskeletal rearrangement. *J. Clin. Invest.* **108**, 689–701 (2001).

48. Obinata, H. & Hla, T. Sphingosine 1-phosphate and inflammation. *Int. Immunol.* **31**, 617–625 (2019).

49. Matloubian, M. *et al.* Lymphocyte egress from thymus and peripheral lymphoid organs is dependent on S1P receptor 1. *Nature* **427**, 355–360 (2004).

50. Liu, Y. *et al.* Edg-1, the G protein-coupled receptor for sphingosine-1-phosphate, is essential for vascular maturation. *J. Clin. Invest.* **106**, 951–961 (2000).

51. Skoura, A. *et al.* Sphingosine-1-phosphate receptor-2 function in myeloid cells regulates vascular inflammation and atherosclerosis. *Arterioscler. Thromb. Vasc. Biol.* **31**, 81–85 (2011).

52. Shimizu, T. *et al.* Sphingosine 1-phosphate receptor 2 negatively regulates neointimal formation in mouse arteries. *Circ. Res.* **101**, 995–1000 (2007).

53. Takabe, K., Paugh, S. W., Milstien, S. & Spiegel, S. 'Inside-out' signaling of sphingosine-1-phosphate: therapeutic targets. *Pharmacol. Rev.* **60**, 181–195 (2008).

54. Vorbach, S. *et al.* Enhanced expression of the sphingosine-1-phosphate-receptor-3 causes acute myelogenous leukemia in mice. *Leukemia* **34**, 721–734 (2020).

55. Nofer, J. R. *et al.* Suppression of endothelial cell apoptosis by high density lipoproteins (HDL) and HDL-associated lysosphingolipids. *J. Biol. Chem.* **276**, 34480–34485 (2001).

56. Keul, P. *et al.* Sphingosine-1-phosphate receptor 3 promotes recruitment of monocyte/macrophages in inflammation and atherosclerosis. *Circ. Res.* **108**, 314–323 (2011).

57. Jenne, C. N. *et al.* T-bet-dependent S1P5 expression in NK cells promotes egress from lymph nodes and bone marrow. *J. Exp. Med.* **206**, 2469–2481 (2009).

58. Pournajaf, S., Dargahi, L., Javan, M. & Pourgholami, M. H. Molecular Pharmacology and Novel Potential Therapeutic Applications of Fingolimod. *Front. Pharmacol.* **13**, 807639 (2022).

59. Billich, A. *et al.* Phosphorylation of the immunomodulatory drug FTY720 by sphingosine kinases. *J. Biol. Chem.* **278**, 47408–47415 (2003).

60. Brinkmann, V., Cyster, J. G. & Hla, T. FTY720: Sphingosine 1-Phosphate Receptor-1 in the Control of Lymphocyte Egress and Endothelial Barrier Function. *Am. J. Transplant.* **4**, 1019–1025 (2004).

61. Müller, H. C. *et al.* The Sphingosine-1 Phosphate receptor agonist FTY720 dose dependently affected endothelial integrity in vitro and aggravated ventilator-induced lung injury in mice. *Pulm. Pharmacol. Ther.* **24**, 377–385 (2011).

62. Potì, F. *et al.* Impact of S1P Mimetics on Mesenteric Ischemia/Reperfusion

Injury. *Pharmaceuticals* **13**, (2020).

63. Koyrakh, L., Roman, M. I., Brinkmann, V. & Wickman, K. The Heart Rate Decrease Caused by Acute FTY720 Administration Is Mediated by the G Protein-Gated Potassium Channel IKACh. *Am. J. Transplant.* **5**, 529–536 (2005).

64. DiMarco, J. P. *et al.* First-dose effects of fingolimod: Pooled safety data from three phase 3 studies. *Mult. Scler. Relat. Disord.* **3**, 629–638 (2014).

65. Camm, J., Hla, T., Bakshi, R. & Brinkmann, V. Cardiac and vascular effects of fingolimod: mechanistic basis and clinical implications. *Am. Heart J.* **168**, 632–644 (2014).

66. Tölle, M. *et al.* Immunomodulator FTY720 Induces eNOS-dependent arterial vasodilatation via the lysophospholipid receptor S1P3. *Circ. Res.* **96**, 913–920 (2005).

67. Bryan, A. M. *et al.* FTY720 reactivates cryptococcal granulomas in mice through S1P receptor 3 on macrophages. *J. Clin. Invest.* **130**, 4546–4560 (2020).

68. Zhao, Z., Lv, Y., Gu, Z.-C., Ma, C.-L. & Zhong, M.-K. Risk for Cardiovascular Adverse Events Associated With Sphingosine-1-Phosphate Receptor Modulators in Patients With Multiple Sclerosis: Insights From a Pooled Analysis of 15 Randomised Controlled Trials. *Front. Immunol.* **12**, 795574 (2021).

69. Rauma, I., Huhtala, H., Soilu-Hänninen, M. & Kuusisto, H. Lipid Profile Alterations during Fingolimod Treatment in Multiple Sclerosis Patients. *Journal of neuroimmune pharmacology : the official journal of the Society on NeuroImmune Pharmacology* **15**, 567–569 (2020).

70. Ferret-Sena, V. *et al.* Fingolimod treatment modulates PPARγ and CD36 gene expression in women with multiple sclerosis. *Front. Mol. Neurosci.* **15**, 1077381 (2022).

71. World Health Organization. Cardiovascular diseases (CVDs) Fact Sheet. (2021).

72. Gaudio, E., Carpino, G., Grassi, M. & Musca, A. [Morphological aspects of atherosclerosis lesion: past and present]. *Clin. Ter.* **157**, 135–142 (2006).

73. Weber, C. & Noels, H. Atherosclerosis: current pathogenesis and therapeutic options. *Nat. Med.* **17**, 1410–1422 (2011).

74. Fruchart, J. C., Nierman, M. C., Stroes, E. S. G., Kastelein, J. J. P. & Duriez, P. New risk factors for atherosclerosis and patient risk assessment. *Circulation* (2004).

75. Goldstein, J. A., Chandra, H. R. & O'Neill, W. W. Relation of number of complex coronary lesions to serum C-reactive protein levels and major adverse cardiovascular events at one year. *Am. J. Cardiol.* **96**, 56–60 (2005).

76. Zakynthinos, E. & Pappa, N. Inflammatory biomarkers in coronary artery disease. *J. Cardiol.* **53**, 317–333 (2009).

77. Björkegren, J. L. M. & Lusis, A. J. Atherosclerosis: Recent developments. *Cell*

185, 1630–1645 (2022).

78. Gimbrone, M. A. J. & García-Cardeña, G. Endothelial Cell Dysfunction and the Pathobiology of Atherosclerosis. *Circ. Res.* **118**, 620–636 (2016).

79. Haidari, M. *et al.* Increased oxidative stress in atherosclerosis-predisposed regions of the mouse aorta. *Life Sci.* **87**, 100–110 (2010).

80. Robbins, C. S. *et al.* Local proliferation dominates lesional macrophage accumulation in atherosclerosis. *Nat. Med.* **19**, 1166–1172 (2013).

81. Glass, C. K. & Witztum, J. L. Atherosclerosis. the road ahead. *Cell* **104**, 503–516 (2001).

82. Saigusa, R., Winkels, H. & Ley, K. T cell subsets and functions in atherosclerosis. *Nat. Rev. Cardiol.* **17**, 387–401 (2020).

83. Libby, P. *et al.* Atherosclerosis. *Nat. Rev. Dis. Prim.* **5**, 56 (2019).

84. Gerlach, B. D. *et al.* Efferocytosis induces macrophage proliferation to help resolve tissue injury. *Cell Metab.* **33**, 2445-2463.e8 (2021).

85. Jebari-Benslaiman, S. *et al.* Pathophysiology of Atherosclerosis. *Int. J. Mol. Sci.* **23**, (2022).

86. Chinetti-Gbaguidi, G., Colin, S. & Staels, B. Macrophage subsets in atherosclerosis. *Nat. Rev. Cardiol.* **12**, 10–17 (2015).

87. Hashimoto, D. *et al.* Tissue-resident macrophages self-maintain locally throughout adult life with minimal contribution from circulating monocytes. *Immunity* **38**, 792–804 (2013).

88. Frodermann, V. & Nahrendorf, M. Macrophages and Cardiovascular Health. *Physiol. Rev.* **98**, 2523–2569 (2018).

89. von Ehr, A., Bode, C. & Hilgendorf, I. Macrophages in Atheromatous Plaque Developmental Stages. *Front. Cardiovasc. Med.* **9**, 865367 (2022).

90. Barringhaus, K. G. *et al.* Alpha4beta1 integrin (VLA-4) blockade attenuates both early and late leukocyte recruitment and neointimal growth following carotid injury in apolipoprotein E (-/-) mice. *J. Vasc. Res.* **41**, 252–260 (2004).

91. Watanabe, T. & Fan, J. Atherosclerosis and inflammation mononuclear cell recruitment and adhesion molecules with reference to the implication of ICAM-1/LFA-1 pathway in atherogenesis. *Int. J. Cardiol.* **66 Suppl 1**, S45-53; discussion S55 (1998).

92. Rolin, J. & Maghazachi, A. A. Implications of chemokines, chemokine receptors, and inflammatory lipids in atherosclerosis. *J. Leukoc. Biol.* **95**, 575–585 (2014).

93. Hou, P. *et al.* Macrophage polarization and metabolism in atherosclerosis. *Cell Death Dis.* **14**, 691 (2023).

94. Auffray, C., Sieweke, M. H. & Geissmann, F. Blood monocytes: development, heterogeneity, and relationship with dendritic cells. *Annu. Rev. Immunol.* **27**, 669–692 (2009).

95. Rahman, K. *et al.* Inflammatory Ly6Chi monocytes and their conversion to M2

macrophages drive atherosclerosis regression. *J. Clin. Invest.* **127**, 2904–2915 (2017).

96. Murray, P. J. *et al.* Macrophage Activation and Polarization: Nomenclature and Experimental Guidelines. *Immunity* **41**, 14–20 (2014).

97. Duewell, P. *et al.* NLRP3 inflammasomes are required for atherogenesis and activated by cholesterol crystals. *Nature* **464**, 1357–1361 (2010).

98. Hirose, K. *et al.* Different responses to oxidized low-density lipoproteins in human polarized macrophages. *Lipids Health Dis.* **10**, 1 (2011).

99. Verreck, F. A. W. *et al.* Human IL-23-producing type 1 macrophages promote but IL-10-producing type 2 macrophages subvert immunity to (myco)bacteria. *Proc. Natl. Acad. Sci. U. S. A.* **101**, 4560–4565 (2004).

100. Mosser, D. M. The many faces of macrophage activation. *J. Leukoc. Biol.* **73**, 209–212 (2003).

101. Martinez, F. O., Sica, A., Mantovani, A. & Locati, M. Macrophage activation and polarization. *Front. Biosci.* **13**, 453–461 (2008).

102. Ferrante, C. J. *et al.* The adenosine-dependent angiogenic switch of macrophages to an M2-like phenotype is independent of interleukin-4 receptor alpha (IL-4Rα) signaling. *Inflammation* **36**, 921–931 (2013).

103. Finn, A. V *et al.* Hemoglobin directs macrophage differentiation and prevents foam cell formation in human atherosclerotic plaques. *J. Am. Coll. Cardiol.* **59**, 166–177 (2012).

104. Guo, L. *et al.* CD163+ macrophages promote angiogenesis and vascular permeability accompanied by inflammation in atherosclerosis. *J. Clin. Invest.* **128**, 1106–1124 (2018).

105. Boyle, J. J. *et al.* Activating transcription factor 1 directs Mhem atheroprotective macrophages through coordinated iron handling and foam cell protection. *Circ. Res.* **110**, 20–33 (2012).

106. Kadl, A. *et al.* Identification of a novel macrophage phenotype that develops in response to atherogenic phospholipids via Nrf2. *Circ. Res.* **107**, 737–746 (2010).

107. Erbel, C. *et al.* CXCL4-induced plaque macrophages can be specifically identified by co-expression of MMP7+S100A8+ in vitro and in vivo. *Innate Immun.* **21**, 255–265 (2015).

108. Erbel, C. *et al.* Prevalence of M4 macrophages within human coronary atherosclerotic plaques is associated with features of plaque instability. *Int. J. Cardiol.* **186**, 219–225 (2015).

109. Feingold, K. R. & Grunfeld, C. *Introduction to Lipids and Lipoproteins*. *Endotext* (2000).

110. Kontush, A. *et al.* Structure of HDL: particle subclasses and molecular components. *Handb. Exp. Pharmacol.* **224**, 3–51 (2015).

111. Gordon, T., Castelli, W. P., Hjortland, M. C., Kannel, W. B. & Dawber, T. R. High

density lipoprotein as a protective factor against coronary heart disease. The Framingham Study. *Am. J. Med.* **62**, 707–714 (1977).

112. Voight, B. F. *et al.* Plasma HDL cholesterol and risk of myocardial infarction: a mendelian randomisation study. *Lancet (London, England)* **380**, 572–580 (2012).

113. Madsen, C. M., Varbo, A. & Nordestgaard, B. G. Novel Insights From Human Studies on the Role of High-Density Lipoprotein in Mortality and Noncardiovascular Disease. *Arterioscler. Thromb. Vasc. Biol.* **41**, 128–140 (2021).

114. von Eckardstein, A., Nofer, J. R. & Assmann, G. High density lipoproteins and arteriosclerosis. Role of cholesterol efflux and reverse cholesterol transport. *Arterioscler. Thromb. Vasc. Biol.* **21**, 13–27 (2001).

115. Favari, E. *et al.* Cholesterol efflux and reverse cholesterol transport. in *Handbook of Experimental Pharmacology* (2015). doi:10.1007/978-3-319-09665-0_4

116. Zanotti, I. *et al.* Macrophage, but not systemic, apolipoprotein E is necessary for macrophage reverse cholesterol transport in vivo. *Arterioscler. Thromb. Vasc. Biol.* **31**, 74–80 (2011).

117. Adorni, M. P. *et al.* The roles of different pathways in the release of cholesterol from macrophages. *J. Lipid Res.* **48**, 2453–2462 (2007).

118. Marques, L. R. *et al.* Reverse cholesterol transport: Molecular mechanisms and the non-medical approach to enhance HDL cholesterol. *Frontiers in Physiology* (2018). doi:10.3389/fphys.2018.00526

119. Parthasarathy, S., Barnett, J. & Fong, L. G. High-density lipoprotein inhibits the oxidative modification of low-density lipoprotein. *Biochim. Biophys. Acta* **1044**, 275–283 (1990).

120. Swertfeger, D. K. *et al.* Feasibility of a plasma bioassay to assess oxidative protection of low-density lipoproteins by high-density lipoproteins. *J. Clin. Lipidol.* **12**, 1539–1548 (2018).

121. Tang, C., Liu, Y., Kessler, P. S., Vaughan, A. M. & Oram, J. F. The macrophage cholesterol exporter ABCA1 functions as an anti-inflammatory receptor. *J. Biol. Chem.* **284**, 32336–32343 (2009).

122. Liu, D. *et al.* Human apolipoprotein A-I induces cyclooxygenase-2 expression and prostaglandin I-2 release in endothelial cells through ATP-binding cassette transporter A1. *Am. J. Physiol. Cell Physiol.* **301**, C739-48 (2011).

123. Kimura, T. *et al.* Role of scavenger receptor class B type I and sphingosine 1-phosphate receptors in high density lipoprotein-induced inhibition of adhesion molecule expression in endothelial cells. *J. Biol. Chem.* **281**, 37457–37467 (2006).

124. Nofer, J.-R. *et al.* High density lipoprotein-associated lysosphingolipids reduce E-selectin expression in human endothelial cells. *Biochem. Biophys. Res. Commun.* **310**, 98–103 (2003).

125. Kimura, T. *et al.* High-density lipoprotein stimulates endothelial cell migration and survival through sphingosine 1-phosphate and its receptors. *Arterioscler. Thromb. Vasc. Biol.* **23**, 1283–1288 (2003).

126. Mineo, C., Deguchi, H., Griffin, J. H. & Shaul, P. W. Endothelial and antithrombotic actions of HDL. *Circ. Res.* **98**, 1352–1364 (2006).

127. Huang, K. *et al.* Oral FTY720 administration induces immune tolerance and inhibits early development of atherosclerosis in apolipoprotein E-deficient mice. *Int. J. Immunopathol. Pharmacol.* **25**, 397–406 (2012).

128. Keul, P. *et al.* The sphingosine-1-phosphate analogue FTY720 reduces atherosclerosis in apolipoprotein E-deficient mice. *Arterioscler. Thromb. Vasc. Biol.* **27**, 607–613 (2007).

129. Nofer, J.-R. *et al.* FTY720, a synthetic sphingosine 1 phosphate analogue, inhibits development of atherosclerosis in low-density lipoprotein receptor-deficient mice. *Circulation* **115**, 501–508 (2007).

130. Klingenberg, R. *et al.* Sphingosine-1-phosphate analogue FTY720 causes lymphocyte redistribution and hypercholesterolemia in ApoE-deficient mice. *Arterioscler. Thromb. Vasc. Biol.* **27**, 2392–2399 (2007).

131. Poti, F. *et al.* Effect of sphingosine 1-phosphate (S1P) receptor agonists FTY720 and CYM5442 on atherosclerosis development in LDL receptor deficient (LDL-R-/-) mice. *Vascul. Pharmacol.* **57**, 56–64 (2012).

132. Potì, F. *et al.* KRP-203, sphingosine 1-phosphate receptor type 1 agonist, ameliorates atherosclerosis in LDL-R-/- mice. *Arterioscler. Thromb. Vasc. Biol.* **33**, 1505–1512 (2013).

133. Ganbaatar, B. *et al.* Inhibition of S1P Receptor 2 Attenuates Endothelial Dysfunction and Inhibits Atherogenesis in Apolipoprotein E-Deficient Mice. *J. Atheroscler. Thromb.* **28**, 630–642 (2021).

134. Poti, F. *et al.* Sphingosine kinase inhibition exerts both pro- and anti-atherogenic effects in low-density lipoprotein receptor-deficient (LDL-R(-/-)) mice. *Thromb. Haemost.* **107**, 552–561 (2012).

135. Potì, F., Ceglarek, U., Burkhardt, R., Simoni, M. & Nofer, J.-R. SKI-II – a sphingosine kinase 1 inhibitor – exacerbates atherosclerosis in low-density lipoprotein receptor-deficient (LDL-R−/−) mice on high cholesterol diet. *Atherosclerosis* **240**, 212–215 (2015).

136. Lu, Z. *et al.* Amitriptyline inhibits nonalcoholic steatohepatitis and atherosclerosis induced by high-fat diet and LPS through modulation of sphingolipid metabolism. *Am. J. Physiol. Endocrinol. Metab.* **318**, E131–E144 (2020).

137. Keul, P. *et al.* Sphingosine-1-Phosphate (S1P) Lyase Inhibition Aggravates Atherosclerosis and Induces Plaque Rupture in ApoE(-/-)Mice. *Int. J. Mol. Sci.* **23**, (2022).

138. Park, T.-S., Rosebury, W., Kindt, E. K., Kowala, M. C. & Panek, R. L. Serine palmitoyltransferase inhibitor myriocin induces the regression of atherosclerotic plaques in hyperlipidemic ApoE-deficient mice. *Pharmacol. Res.* **58**, 45–51

(2008).

139. Park, T.-S. *et al.* Modulation of lipoprotein metabolism by inhibition of sphingomyelin synthesis in ApoE knockout mice. *Atherosclerosis* **189**, 264–272 (2006).

140. Bietrix, F. *et al.* Inhibition of glycosphingolipid synthesis induces a profound reduction of plasma cholesterol and inhibits atherosclerosis development in APOE*3 Leiden and low-density lipoprotein receptor-/- mice. *Arterioscler. Thromb. Vasc. Biol.* **30**, 931–937 (2010).

141. Chatterjee, S. *et al.* Inhibition of Glycosphingolipid Synthesis Ameliorates Atherosclerosis and Arterial Stiffness in Apolipoprotein E−/− Mice and Rabbits Fed a High-Fat and -Cholesterol Diet. *Circulation* **129**, 2403–2413 (2014).

142. Wang, M.-D. *et al.* Different cellular traffic of LDL-cholesterol and acetylated LDL-cholesterol leads to distinct reverse cholesterol transport pathways. *J. Lipid Res.* **48**, 633–645 (2007).

143. Klucken, J. *et al.* ABCG1 (ABC8), the human homolog of the Drosophila white gene, is a regulator of macrophage cholesterol and phospholipid transport. *Proc. Natl. Acad. Sci. U. S. A.* **97**, 817–822 (2000).

144. Han, J. *et al.* Oxidized low density lipoprotein decreases macrophage expression of scavenger receptor B-I. *J. Biol. Chem.* **276**, 16567–16572 (2001).

145. Wang, M.-D. *et al.* Different cellular traffic of LDL-cholesterol and acetylated LDL-cholesterol leads to distinct reverse cholesterol transport pathwayss. *J. Lipid Res.* **48**, 633–645 (2007).

146. Matsuo, M. ABCA1 and ABCG1 as potential therapeutic targets for the prevention of atherosclerosis. *J. Pharmacol. Sci.* **148**, 197–203 (2022).

147. Kirchgessner, T. G. *et al.* Beneficial and Adverse Effects of an LXR Agonist on Human Lipid and Lipoprotein Metabolism and Circulating Neutrophils. *Cell Metab.* **24**, 223–233 (2016).

148. Vaidya, M. *et al.* Regulation of ABCA1-mediated cholesterol efflux by sphingosine-1-phosphate signaling in macrophages. *J. Lipid Res.* **60**, 506–515 (2019).

149. Wang, D. *et al.* 6-Dihydroparadol, a Ginger Constituent, Enhances Cholesterol Efflux from THP-1-Derived Macrophages. *Mol. Nutr. Food Res.* **62**, e1800011 (2018).

150. Li, X. *et al.* Paeonol suppresses lipid accumulation in macrophages via upregulation of the ATP-binding cassette transporter A1 and downregulation of the cluster of differentiation 36. *Int. J. Oncol.* **46**, 764–774 (2015).

151. Marangon, D., Raffaele, S., Fumagalli, M. & Lecca, D. MicroRNAs change the games in central nervous system pharmacology. *Biochem. Pharmacol.* **168**, 162–172 (2019).

152. Mukhamedova, N. *et al.* Enhancing apolipoprotein A-I-dependent cholesterol efflux elevates cholesterol export from macrophages in vivo. *J. Lipid Res.* **49**, 2312–2322 (2008).

153. Tachibana, K. *et al.* FTY720 Reduces Lipid Accumulation by Upregulating ABCA1 through Liver X Receptor and Sphingosine Kinase 2 Signaling in Macrophages. *Int. J. Mol. Sci.* **23**, (2022).

154. Moon, A. M., Singal, A. G. & Tapper, E. B. Contemporary Epidemiology of Chronic Liver Disease and Cirrhosis. *Clin. Gastroenterol. Hepatol. Off. Clin. Pract. J. Am. Gastroenterol. Assoc.* **18**, 2650–2666 (2020).

155. Bhattacharya, M. & Ramachandran, P. Immunology of human fibrosis. *Nat. Immunol.* **24**, 1423–1433 (2023).

156. Henderson, N. C., Rieder, F. & Wynn, T. A. Fibrosis: from mechanisms to medicines. *Nature* **587**, 555–566 (2020).

157. Lei, L. *et al.* Portal fibroblasts with mesenchymal stem cell features form a reservoir of proliferative myofibroblasts in liver fibrosis. *Hepatology* **76**, 1360–1375 (2022).

158. Kramann, R. *et al.* Perivascular Gli1+ progenitors are key contributors to injury-induced organ fibrosis. *Cell Stem Cell* **16**, 51–66 (2015).

159. Gupta, V., Gupta, I., Park, J., Bram, Y. & Schwartz, R. E. Hedgehog Signaling Demarcates a Niche of Fibrogenic Peribiliary Mesenchymal Cells. *Gastroenterology* **159**, 624-638.e9 (2020).

160. Hammerich, L. & Tacke, F. Hepatic inflammatory responses in liver fibrosis. *Nat. Rev. Gastroenterol. Hepatol.* **20**, 633–646 (2023).

161. Si-Tayeb, K., Lemaigre, F. P. & Duncan, S. A. Organogenesis and Development of the Liver. *Dev. Cell* **18**, 175–189 (2010).

162. Gong, J., Tu, W., Liu, J. & Tian, D. Hepatocytes: A key role in liver inflammation. *Front. Immunol.* **13**, 1083780 (2022).

163. Arriazu, E. *et al.* Signalling via the osteopontin and high mobility group box-1 axis drives the fibrogenic response to liver injury. *Gut* **66**, 1123–1137 (2017).

164. Xie, G. *et al.* Cross-talk between Notch and Hedgehog regulates hepatic stellate cell fate in mice. *Hepatology* **58**, 1801–1813 (2013).

165. Zhu, C. *et al.* Hepatocyte Notch activation induces liver fibrosis in nonalcoholic steatohepatitis. *Sci. Transl. Med.* **10**, (2018).

166. Wang, X. *et al.* Hepatocyte TAZ/WWTR1 Promotes Inflammation and Fibrosis in Nonalcoholic Steatohepatitis. *Cell Metab.* **24**, 848–862 (2016).

167. Gao, B., Ahmad, M. F., Nagy, L. E. & Tsukamoto, H. Inflammatory pathways in alcoholic steatohepatitis. *J. Hepatol.* **70**, 249–259 (2019).

168. Shetty, S., Lalor, P. F. & Adams, D. H. Liver sinusoidal endothelial cells — gatekeepers of hepatic immunity. *Nat. Rev. Gastroenterol. Hepatol.* **15**, 555–567 (2018).

169. DeLeve, L. D. Liver sinusoidal endothelial cells in hepatic fibrosis. *Hepatology* **61**, 1740–1746 (2015).

170. Deleve, L. D., Wang, X. & Guo, Y. Sinusoidal endothelial cells prevent rat

stellate cell activation and promote reversion to quiescence. *Hepatology* **48**, 920–930 (2008).

171. Maretti-Mira, A. C., Wang, X., Wang, L. & DeLeve, L. D. Incomplete Differentiation of Engrafted Bone Marrow Endothelial Progenitor Cells Initiates Hepatic Fibrosis in the Rat. *Hepatology* **69**, 1259–1272 (2019).

172. Shields, P. L. *et al.* Chemokine and chemokine receptor interactions provide a mechanism for selective T cell recruitment to specific liver compartments within hepatitis C-infected liver. *J. Immunol.* **163**, 6236–6243 (1999).

173. Ding, B.-S. *et al.* Divergent angiocrine signals from vascular niche balance liver regeneration and fibrosis. *Nature* **505**, 97–102 (2014).

174. Bosteels, C. *et al.* Inflammatory Type 2 cDCs Acquire Features of cDC1s and Macrophages to Orchestrate Immunity to Respiratory Virus Infection. *Immunity* **52**, 1039-1056.e9 (2020).

175. Goubier, A. *et al.* Plasmacytoid dendritic cells mediate oral tolerance. *Immunity* **29**, 464–475 (2008).

176. Pradere, J.-P. *et al.* Hepatic macrophages but not dendritic cells contribute to liver fibrosis by promoting the survival of activated hepatic stellate cells in mice. *Hepatology* **58**, 1461–1473 (2013).

177. Henning, J. R. *et al.* Dendritic cells limit fibroinflammatory injury in nonalcoholic steatohepatitis in mice. *Hepatology* **58**, 589–602 (2013).

178. Sutti, S. *et al.* CX(3)CR1 Mediates the Development of Monocyte-Derived Dendritic Cells during Hepatic Inflammation. *Cells* **8**, (2019).

179. Deczkowska, A. *et al.* XCR1(+) type 1 conventional dendritic cells drive liver pathology in non-alcoholic steatohepatitis. *Nat. Med.* **27**, 1043–1054 (2021).

180. Liu, K., Wang, F.-S. & Xu, R. Neutrophils in liver diseases: pathogenesis and therapeutic targets. *Cell. Mol. Immunol.* **18**, 38–44 (2021).

181. Tang, J., Yan, Z., Feng, Q., Yu, L. & Wang, H. The Roles of Neutrophils in the Pathogenesis of Liver Diseases. *Front. Immunol.* **12**, 625472 (2021).

182. Saijou, E. *et al.* Neutrophils alleviate fibrosis in the CCl(4)-induced mouse chronic liver injury model. *Hepatol. Commun.* **2**, 703–717 (2018).

183. Gao, B. & Bataller, R. Alcoholic Liver Disease: Pathogenesis and New Therapeutic Targets. *Gastroenterology* **141**, 1572–1585 (2011).

184. Moles, A. *et al.* A TLR2/S100A9/CXCL-2 signaling network is necessary for neutrophil recruitment in acute and chronic liver injury in the mouse. *J. Hepatol.* **60**, 782–791 (2014).

185. Sierro, F. *et al.* A Liver Capsular Network of Monocyte-Derived Macrophages Restricts Hepatic Dissemination of Intraperitoneal Bacteria by Neutrophil Recruitment. *Immunity* **47**, 374-388.e6 (2017).

186. Kulle, A., Thanabalasuriar, A., Cohen, T. S. & Szydlowska, M. Resident macrophages of the lung and liver: The guardians of our tissues. *Front. Immunol.* **13**, 1029085 (2022).

187. Naito, M., Hasegawa, G., Ebe, Y. & Yamamoto, T. Differentiation and function of Kupffer cells. *Med. Electron Microsc.* **37**, 16–28 (2004).

188. Demetz, E. *et al.* The haemochromatosis gene Hfe and Kupffer cells control LDL cholesterol homeostasis and impact on atherosclerosis development. *Eur. Heart J.* **41**, 3949–3959 (2020).

189. Wang, Y. *et al.* Plasma cholesteryl ester transfer protein is predominantly derived from Kupffer cells. *Hepatology* **62**, 1710–1722 (2015).

190. Theurl, I. *et al.* On-demand erythrocyte disposal and iron recycling requires transient macrophages in the liver. *Nat. Med.* **22**, 945–951 (2016).

191. Gammella, E., Buratti, P., Cairo, G. & Recalcati, S. Macrophages: central regulators of iron balance. *Metallomics* **6**, 1336–1345 (2014).

192. Soucie, E. L. *et al.* Lineage-specific enhancers activate self-renewal genes in macrophages and embryonic stem cells. *Science* **351**, aad5510 (2016).

193. Sheng, J., Ruedl, C. & Karjalainen, K. Fetal HSCs versus EMP2s. *Immunity* **43**, 1025 (2015).

194. Kim, K.-W., Zhang, N., Choi, K. & Randolph, G. J. Homegrown Macrophages. *Immunity* **45**, 468–470 (2016).

195. Mass, E. *et al.* Specification of tissue-resident macrophages during organogenesis. *Science* **353**, (2016).

196. Tran, S. *et al.* Impaired Kupffer Cell Self-Renewal Alters the Liver Response to Lipid Overload during Non-alcoholic Steatohepatitis. *Immunity* **53**, 627-640.e5 (2020).

197. Seidman, J. S. *et al.* Niche-Specific Reprogramming of Epigenetic Landscapes Drives Myeloid Cell Diversity in Nonalcoholic Steatohepatitis. *Immunity* **52**, 1057-1074.e7 (2020).

198. Blériot, C. *et al.* Liver-resident macrophage necroptosis orchestrates type 1 microbicidal inflammation and type-2-mediated tissue repair during bacterial infection. *Immunity* **42**, 145–158 (2015).

199. Lai, S. M. *et al.* Organ-Specific Fate, Recruitment, and Refilling Dynamics of Tissue-Resident Macrophages during Blood-Stage Malaria. *Cell Rep.* **25**, 3099-3109.e3 (2018).

200. Wen, Y., Lambrecht, J., Ju, C. & Tacke, F. Hepatic macrophages in liver homeostasis and diseases-diversity, plasticity and therapeutic opportunities. *Cell. Mol. Immunol.* **18**, 45–56 (2021).

201. Bonnardel, J. *et al.* Stellate Cells, Hepatocytes, and Endothelial Cells Imprint the Kupffer Cell Identity on Monocytes Colonizing the Liver Macrophage Niche. *Immunity* **51**, 638-654.e9 (2019).

202. Scott, C. L. *et al.* The Transcription Factor ZEB2 Is Required to Maintain the Tissue-Specific Identities of Macrophages. *Immunity* **49**, 312-325.e5 (2018).

203. Sakai, M. *et al.* Liver-Derived Signals Sequentially Reprogram Myeloid Enhancers to Initiate and Maintain Kupffer Cell Identity. *Immunity* **51**, 655-

670.e8 (2019).

204. Drakesmith, H., Nemeth, E. & Ganz, T. Ironing out Ferroportin. *Cell Metab.* **22**, 777–787 (2015).

205. Fogg, D. K. *et al.* A clonogenic bone marrow progenitor specific for macrophages and dendritic cells. *Science* **311**, 83–87 (2006).

206. Auffray, C. *et al.* CX3CR1+ CD115+ CD135+ common macrophage/DC precursors and the role of CX3CR1 in their response to inflammation. *J. Exp. Med.* **206**, 595–606 (2009).

207. Eaves, C. J. Hematopoietic stem cells: concepts, definitions, and the new reality. *Blood* **125**, 2605–2613 (2015).

208. Varol, C., Mildner, A. & Jung, S. Macrophages: development and tissue specialization. *Annu. Rev. Immunol.* **33**, 643–675 (2015).

209. Karlmark, K. R. *et al.* Hepatic recruitment of the inflammatory Gr1+ monocyte subset upon liver injury promotes hepatic fibrosis. *Hepatology* **50**, 261–274 (2009).

210. Heymann, F. *et al.* Hepatic macrophage migration and differentiation critical for liver fibrosis is mediated by the chemokine receptor C-C motif chemokine receptor 8 in mice. *Hepatology* **55**, (2012).

211. Flores Molina, M. *et al.* Distinct spatial distribution and roles of Kupffer cells and monocyte-derived macrophages in mouse acute liver injury. *Front. Immunol.* **13**, 994480 (2022).

212. Imamura, M., Ogawa, T., Sasaguri, Y., Chayama, K. & Ueno, H. Suppression of macrophage infiltration inhibits activation of hepatic stellate cells and liver fibrogenesis in rats. *Gastroenterology* **128**, 138–146 (2005).

213. Mitchell, C. *et al.* Dual role of CCR2 in the constitution and the resolution of liver fibrosis in mice. *Am. J. Pathol.* **174**, 1766–1775 (2009).

214. Marra, F. & Tacke, F. Roles for chemokines in liver disease. *Gastroenterology* **147**, 577-594.e1 (2014).

215. Wehr, A. *et al.* Chemokine receptor CXCR6-dependent hepatic NK T Cell accumulation promotes inflammation and liver fibrosis. *J. Immunol.* **190**, 5226–5236 (2013).

216. Xia, C. *et al.* MRP14 enhances the ability of macrophage to recruit T cells and promotes obesity-induced insulin resistance. *Int. J. Obes. (Lond).* **43**, 2434–2447 (2019).

217. Mossanen, J. C. *et al.* Chemokine (C-C motif) receptor 2-positive monocytes aggravate the early phase of acetaminophen-induced acute liver injury. *Hepatology* **64**, 1667–1682 (2016).

218. Kim, S. Y. *et al.* Pro-inflammatory hepatic macrophages generate ROS through NADPH oxidase 2 via endocytosis of monomeric TLR4-MD2 complex. *Nat. Commun.* **8**, 2247 (2017).

219. Inokuchi, S. *et al.* Toll-like receptor 4 mediates alcohol-induced steatohepatitis

through bone marrow-derived and endogenous liver cells in mice. *Alcohol. Clin. Exp. Res.* **35**, 1509–1518 (2011).

220. Zhang, C. *et al.* Macrophage-derived IL-1α promotes sterile inflammation in a mouse model of acetaminophen hepatotoxicity. *Cell. Mol. Immunol.* **15**, 973–982 (2018).

221. Miura, K. *et al.* Toll-like receptor 9 promotes steatohepatitis by induction of interleukin-1beta in mice. *Gastroenterology* **139**, 323–34.e7 (2010).

222. Sharma, S., Le Guillou, D. & Chen, J. Y. Cellular stress in the pathogenesis of nonalcoholic steatohepatitis and liver fibrosis. *Nat. Rev. Gastroenterol. Hepatol.* **20**, 662–678 (2023).

223. Liu, Y. *et al.* S100A8-Mediated NLRP3 Inflammasome-Dependent Pyroptosis in Macrophages Facilitates Liver Fibrosis Progression. *Cells* **11**, (2022).

224. Wynn, T. A. & Barron, L. Macrophages: master regulators of inflammation and fibrosis. *Semin. Liver Dis.* **30**, 245–257 (2010).

225. Duffield, J. S. *et al.* Selective depletion of macrophages reveals distinct, opposing roles during liver injury and repair. *J. Clin. Invest.* **115**, 56–65 (2005).

226. Pellicoro, A. *et al.* Elastin accumulation is regulated at the level of degradation by macrophage metalloelastase (MMP-12) during experimental liver fibrosis. *Hepatology* **55**, 1965–1975 (2012).

227. Fallowfield, J. A. *et al.* Scar-associated macrophages are a major source of hepatic matrix metalloproteinase-13 and facilitate the resolution of murine hepatic fibrosis. *J. Immunol.* **178**, 5288–5295 (2007).

228. MacParland, S. A. *et al.* Single cell RNA sequencing of human liver reveals distinct intrahepatic macrophage populations. *Nat. Commun.* **9**, 4383 (2018).

229. Wang, M. *et al.* Chronic alcohol ingestion modulates hepatic macrophage populations and functions in mice. *J. Leukoc. Biol.* **96**, 657–665 (2014).

230. Pellicoro, A., Ramachandran, P., Iredale, J. P. & Fallowfield, J. A. Liver fibrosis and repair: immune regulation of wound healing in a solid organ. *Nat. Rev. Immunol.* **14**, 181–194 (2014).

231. Campana, L. *et al.* The STAT3-IL-10-IL-6 Pathway Is a Novel Regulator of Macrophage Efferocytosis and Phenotypic Conversion in Sterile Liver Injury. *J. Immunol.* **200**, 1169–1187 (2018).

232. Bosurgi, L. *et al.* Macrophage function in tissue repair and remodeling requires IL-4 or IL-13 with apoptotic cells. *Science* **356**, 1072–1076 (2017).

233. Triantafyllou, E. *et al.* MerTK expressing hepatic macrophages promote the resolution of inflammation in acute liver failure. *Gut* **67**, 333–347 (2018).

234. Stutchfield, B. M. *et al.* CSF1 Restores Innate Immunity After Liver Injury in Mice and Serum Levels Indicate Outcomes of Patients With Acute Liver Failure. *Gastroenterology* **149**, 1896-1909.e14 (2015).

235. Karlmark, K. R. *et al.* The fractalkine receptor CX_3CR1 protects against liver fibrosis by controlling differentiation and survival of infiltrating hepatic

monocytes. *Hepatology* **52**, 1769–1782 (2010).

236. Aoyama, T., Inokuchi, S., Brenner, D. A. & Seki, E. CX3CL1-CX3CR1 interaction prevents carbon tetrachloride-induced liver inflammation and fibrosis in mice. *Hepatology* **52**, 1390–1400 (2010).

237. Dal-Secco, D. *et al.* A dynamic spectrum of monocytes arising from the in situ reprogramming of CCR2+ monocytes at a site of sterile injury. *J. Exp. Med.* **212**, 447–456 (2015).

238. Li, W., Yang, Y., Yang, L., Chang, N. & Li, L. Monocyte-derived Kupffer cells dominate in the Kupffer cell pool during liver injury. *Cell Rep.* **42**, 113164 (2023).

239. Wang, J. & Kubes, P. A Reservoir of Mature Cavity Macrophages that Can Rapidly Invade Visceral Organs to Affect Tissue Repair. *Cell* **165**, 668–678 (2016).

240. Asahina, K., Zhou, B., Pu, W. T. & Tsukamoto, H. Septum transversum-derived mesothelium gives rise to hepatic stellate cells and perivascular mesenchymal cells in developing mouse liver. *Hepatology* **53**, 983–995 (2011).

241. Asahina, K. *et al.* Mesenchymal origin of hepatic stellate cells, submesothelial cells, and perivascular mesenchymal cells during mouse liver development. *Hepatology* **49**, 998–1011 (2009).

242. Trivedi, P., Wang, S. & Friedman, S. L. The Power of Plasticity-Metabolic Regulation of Hepatic Stellate Cells. *Cell Metab.* **33**, 242–257 (2021).

243. Liu, X., Xu, J., Brenner, D. A. & Kisseleva, T. Reversibility of Liver Fibrosis and Inactivation of Fibrogenic Myofibroblasts. *Curr. Pathobiol. Rep.* **1**, 209–214 (2013).

244. Mederacke, I. *et al.* Fate tracing reveals hepatic stellate cells as dominant contributors to liver fibrosis independent of its aetiology. *Nat. Commun.* **4**, 2823 (2013).

245. Tsuchida, T. & Friedman, S. L. Mechanisms of hepatic stellate cell activation. *Nat. Rev. Gastroenterol. Hepatol.* **14**, 397–411 (2017).

246. Troeger, J. S. *et al.* Deactivation of hepatic stellate cells during liver fibrosis resolution in mice. *Gastroenterology* **143**, 1073–83.e22 (2012).

247. Krenkel, O., Hundertmark, J., Ritz, T. P., Weiskirchen, R. & Tacke, F. Single Cell RNA Sequencing Identifies Subsets of Hepatic Stellate Cells and Myofibroblasts in Liver Fibrosis. 1–10

248. Weiskirchen, R. & Tacke, F. Cellular and molecular functions of hepatic stellate cells in inflammatory responses and liver immunology. *Hepatobiliary Surg. Nutr.* **3**, 344–363 (2014).

249. Kim, H. Y. *et al.* The Origin and Fate of Liver Myofibroblasts. *Cell. Mol. Gastroenterol. Hepatol.* **17**, 93–106 (2023).

250. Hendriks, H. F. J., Verhoofstad, W. A. M. M., Brouwer, A., De Leeuw, A. M. & Knook, D. L. Perisinusoidal fat-storing cells are the main vitamin A storage sites in rat liver. *Exp. Cell Res.* **160**, 138–149 (1985).

251. Batten, M. L. *et al.* Lecithin-retinol Acyltransferase Is Essential for Accumulation of All-trans-Retinyl Esters in the Eye and in the Liver*. *J. Biol. Chem.* **279**, 10422–10432 (2004).

252. Kendall, T. J. *et al.* p75 neurotrophin receptor signaling regulates hepatic myofibroblast proliferation and apoptosis in recovery from rodent liver fibrosis. *Hepatology* **49**, 901–910 (2009).

253. Sachs, B. D. *et al.* p75 neurotrophin receptor regulates tissue fibrosis through inhibition of plasminogen activation via a PDE4/cAMP/PKA pathway. *J. Cell Biol.* **177**, 1119–1132 (2007).

254. Hazra, S. *et al.* Peroxisome Proliferator-activated Receptor γ Induces a Phenotypic Switch from Activated to Quiescent Hepatic Stellate Cells*. *J. Biol. Chem.* **279**, 11392–11401 (2004).

255. Liu, X. *et al.* Identification of Lineage-Specific Transcription Factors That Prevent Activation of Hepatic Stellate Cells and Promote Fibrosis Resolution. *Gastroenterology* **158**, 1728-1744.e14 (2020).

256. Dranoff, J. A. & Wells, R. G. Portal fibroblasts: Underappreciated mediators of biliary fibrosis. *Hepatology* **51**, 1438–1444 (2010).

257. Friedman, S. L., Roll, F. J., Boyles, J. & Bissell, D. M. Hepatic lipocytes: the principal collagen-producing cells of normal rat liver. *Proc. Natl. Acad. Sci. U. S. A.* **82**, 8681–8685 (1985).

258. Brenner, D. A. *et al.* Origin of myofibroblasts in liver fibrosis. *Fibrogenesis Tissue Repair* **5**, S17 (2012).

259. Iwaisako, K. *et al.* Origin of myofibroblasts in the fibrotic liver in mice. *Proc. Natl. Acad. Sci. U. S. A.* **111**, E3297-305 (2014).

260. Nishio, T. *et al.* Activated hepatic stellate cells and portal fibroblasts contribute to cholestatic liver fibrosis in MDR2 knockout mice. *J. Hepatol.* **71**, 573–585 (2019).

261. Puche, J. E., Saiman, Y. & Friedman, S. L. Hepatic stellate cells and liver fibrosis. *Compr. Physiol.* **3**, 1473–1492 (2013).

262. Kisseleva, T. & Brenner, D. Molecular and cellular mechanisms of liver fibrosis and its regression. *Nat. Rev. Gastroenterol. Hepatol.* **18**, 151–166 (2021).

263. Bataller, R. & Brenner, D. A. Liver fibrosis. *J. Clin. Invest.* **115**, 209–218 (2005).

264. Wang, S. *et al.* An autocrine signaling circuit in hepatic stellate cells underlies advanced fibrosis in nonalcoholic steatohepatitis. *Sci. Transl. Med.* **15**, eadd3949 (2023).

265. Breitkopf, K., Godoy, P., Ciuclan, L., Singer, M. V & Dooley, S. TGF-beta/Smad signaling in the injured liver. *Z. Gastroenterol.* **44**, 57–66 (2006).

266. Dooley, S. *et al.* Smad7 prevents activation of hepatic stellate cells and liver fibrosis in rats. *Gastroenterology* **125**, 178–191 (2003).

267. Hanafusa, H. *et al.* Involvement of the p38 mitogen-activated protein kinase pathway in transforming growth factor-beta-induced gene expression. *J. Biol.*

Chem. **274**, 27161–27167 (1999).

268. Engel, M. E., McDonnell, M. A., Law, B. K. & Moses, H. L. Interdependent SMAD and JNK signaling in transforming growth factor-beta-mediated transcription. *J. Biol. Chem.* **274**, 37413–37420 (1999).

269. Zhang, J., Jiang, N., Ping, J. & Xu, L. TGF-β1-induced autophagy activates hepatic stellate cells via the ERK and JNK signaling pathways. *Int. J. Mol. Med.* **47**, 256–266 (2021).

270. Hernández-Gea, V. *et al.* Autophagy releases lipid that promotes fibrogenesis by activated hepatic stellate cells in mice and in human tissues. *Gastroenterology* **142**, 938–946 (2012).

271. Pinzani, M. PDGF and signal transduction in hepatic stellate cells. *Front. Biosci.* **7**, d1720-6 (2002).

272. Kocabayoglu, P. *et al.* β-PDGF receptor expressed by hepatic stellate cells regulates fibrosis in murine liver injury, but not carcinogenesis. *J. Hepatol.* **63**, 141–147 (2015).

273. Yang, L. *et al.* Vascular endothelial growth factor promotes fibrosis resolution and repair in mice. *Gastroenterology* **146**, 1339–50.e1 (2014).

274. Huang, Y. *et al.* Bevacizumab attenuates hepatic fibrosis in rats by inhibiting activation of hepatic stellate cells. *PLoS One* **8**, e73492 (2013).

275. Rangwala, F. *et al.* Increased production of sonic hedgehog by ballooned hepatocytes. *J. Pathol.* **224**, 401–410 (2011).

276. Omenetti, A., Choi, S., Michelotti, G. & Diehl, A. M. Hedgehog signaling in the liver. *J. Hepatol.* **54**, 366–373 (2011).

277. Michelotti, G. A. *et al.* Smoothened is a master regulator of adult liver repair. *J. Clin. Invest.* **123**, 2380–2394 (2013).

278. Tomita, K. *et al.* Free cholesterol accumulation in hepatic stellate cells: mechanism of liver fibrosis aggravation in nonalcoholic steatohepatitis in mice. *Hepatology* **59**, 154–169 (2014).

279. Teratani, T. *et al.* A high-cholesterol diet exacerbates liver fibrosis in mice via accumulation of free cholesterol in hepatic stellate cells. *Gastroenterology* **142**, 152-164.e10 (2012).

280. Kluwe, J. *et al.* Absence of hepatic stellate cell retinoid lipid droplets does not enhance hepatic fibrosis but decreases hepatic carcinogenesis. *Gut* **60**, 1260 LP – 1268 (2011).

281. Yi, H.-S. *et al.* Alcohol dehydrogenase III exacerbates liver fibrosis by enhancing stellate cell activation and suppressing natural killer cells in mice. *Hepatology* **60**, 1044–1053 (2014).

282. Koo, J. H., Lee, H. J., Kim, W. & Kim, S. G. Endoplasmic Reticulum Stress in Hepatic Stellate Cells Promotes Liver Fibrosis via PERK-Mediated Degradation of HNRNPA1 and Up-regulation of SMAD2. *Gastroenterology* **150**, 181-193.e8 (2016).

283. Mannaerts, I. *et al.* Unfolded protein response is an early, non-critical event during hepatic stellate cell activation. *Cell Death Dis.* **10**, 98 (2019).

284. Hernández-Gea, V. *et al.* Endoplasmic reticulum stress induces fibrogenic activity in hepatic stellate cells through autophagy. *J. Hepatol.* **59**, 98–104 (2013).

285. Greenwel, P., Domínguez-Rosales, J. A., Mavi, G., Rivas-Estilla, A. M. & Rojkind, M. Hydrogen peroxide: a link between acetaldehyde-elicited alpha1(I) collagen gene up-regulation and oxidative stress in mouse hepatic stellate cells. *Hepatology* **31**, 109–116 (2000).

286. Paik, Y.-H. *et al.* The nicotinamide adenine dinucleotide phosphate oxidase (NOX) homologues NOX1 and NOX2/gp91(phox) mediate hepatic fibrosis in mice. *Hepatology* **53**, 1730–1741 (2011).

287. Lan, T., Kisseleva, T. & Brenner, D. A. Deficiency of NOX1 or NOX4 Prevents Liver Inflammation and Fibrosis in Mice through Inhibition of Hepatic Stellate Cell Activation. *PLoS One* **10**, e0129743 (2015).

288. Van Thuy, T. T., Thuy, L. T. T., Yoshizato, K. & Kawada, N. Possible Involvement of Nitric Oxide in Enhanced Liver Injury and Fibrogenesis during Cholestasis in Cytoglobin-deficient Mice. *Sci. Rep.* **7**, 41888 (2017).

289. Thuy, L. T. T. *et al.* Cytoglobin deficiency promotes liver cancer development from hepatosteatosis through activation of the oxidative stress pathway. *Am. J. Pathol.* **185**, 1045–1060 (2015).

290. Thuy, L. T. T. *et al.* Absence of cytoglobin promotes multiple organ abnormalities in aged mice. *Sci. Rep.* **6**, 24990 (2016).

291. Iredale, J. P. Models of liver fibrosis: exploring the dynamic nature of inflammation and repair in a solid organ. *J. Clin. Invest.* **117**, 539–548 (2007).

292. Yang, F. *et al.* Crosstalk between hepatic stellate cells and surrounding cells in hepatic fibrosis. *Int. Immunopharmacol.* **99**, 108051 (2021).

293. Iredale, J. P. *et al.* Mechanisms of spontaneous resolution of rat liver fibrosis. Hepatic stellate cell apoptosis and reduced hepatic expression of metalloproteinase inhibitors. *J. Clin. Invest.* **102**, 538–549 (1998).

294. Elsharkawy, A. M., Oakley, F. & Mann, D. A. The role and regulation of hepatic stellate cell apoptosis in reversal of liver fibrosis. *Apoptosis* **10**, 927–939 (2005).

295. Kisseleva, T. *et al.* Myofibroblasts revert to an inactive phenotype during regression of liver fibrosis. *Proc. Natl. Acad. Sci.* **109**, 9448–9453 (2012).

296. Kisseleva, T. & Brenner, D. A. Inactivation of myofibroblasts during regression of liver fibrosis. *Cell cycle (Georgetown, Tex.)* **12**, 381–382 (2013).

297. She, H., Xiong, S., Hazra, S. & Tsukamoto, H. Adipogenic transcriptional regulation of hepatic stellate cells. *J. Biol. Chem.* **280**, 4959–4967 (2005).

298. Arroyo, N. *et al.* GATA4 induces liver fibrosis regression by deactivating hepatic stellate cells. *JCI insight* **6**, (2021).

299. Schrader, J., Fallowfield, J. & Iredale, J. P. Senescence of activated stellate

cells: not just early retirement. *Hepatology* **49**, 1045–1047 (2009).

300. Krizhanovsky, V. *et al.* Senescence of activated stellate cells limits liver fibrosis. *Cell* **134**, 657–667 (2008).

301. Cheng, N., Kim, K.-H. & Lau, L. F. Senescent hepatic stellate cells promote liver regeneration through IL-6 and ligands of CXCR2. *JCI insight* **7**, (2022).

302. Kong, X. *et al.* Interleukin-22 induces hepatic stellate cell senescence and restricts liver fibrosis in mice. *Hepatology* **56**, 1150–1159 (2012).

303. Kong, X., Feng, D., Mathews, S. & Gao, B. Hepatoprotective and anti-fibrotic functions of interleukin-22: therapeutic potential for the treatment of alcoholic liver disease. *J. Gastroenterol. Hepatol.* **28 Suppl 1**, 56–60 (2013).

304. Takahashi, A. *et al.* Downregulation of cytoplasmic DNases is implicated in cytoplasmic DNA accumulation and SASP in senescent cells. *Nat. Commun.* **9**, 1249 (2018).

305. Wells, R. G. The Portal Fibroblast: Not Just a Poor Man's Stellate Cell. *Gastroenterology* **147**, 41–47 (2014).

306. Dudas, J., Mansuroglu, T., Batusic, D., Saile, B. & Ramadori, G. Thy-1 is an in vivo and in vitro marker of liver myofibroblasts. *Cell Tissue Res.* **329**, 503–514 (2007).

307. Koyama, Y. *et al.* Mesothelin/mucin 16 signaling in activated portal fibroblasts regulates cholestatic liver fibrosis. *J. Clin. Invest.* **127**, 1254–1270 (2017).

308. Nishio, T. *et al.* The Role of Mesothelin in Activation of Portal Fibroblasts in Cholestatic Liver Injury. *Biology (Basel).* **11**, (2022).

309. Bao, Y. *et al.* Animal and Organoid Models of Liver Fibrosis. *Front. Physiol.* **12**, (2021).

310. Ramachandran, P. *et al.* Differential Ly-6C expression identifies the recruited macrophage phenotype, which orchestrates the regression of murine liver fibrosis. *Proc. Natl. Acad. Sci.* **109**, E3186–E3195 (2012).

311. Ramachandran, P. *et al.* Resolving the fibrotic niche of human liver cirrhosis at single-cell level. *Nature* **575**, 512–518 (2019).

312. De Smet, V. *et al.* Initiation of hepatic stellate cell activation extends into chronic liver disease. *Cell Death Dis.* **12**, 1110 (2021).

313. Dobie, R. *et al.* Single-Cell Transcriptomics Uncovers Zonation of Function in the Mesenchyme during Liver Fibrosis. *Cell Rep.* **29**, 1832-1847.e8 (2019).

314. Lee, Y.-S. & Seki, E. In Vivo and In Vitro Models to Study Liver Fibrosis: Mechanisms and Limitations. *Cell. Mol. Gastroenterol. Hepatol.* **16**, 355–367 (2023).

315. Yan, M., Huo, Y., Yin, S. & Hu, H. Mechanisms of acetaminophen-induced liver injury and its implications for therapeutic interventions. *Redox Biol.* **17**, 274–283 (2018).

316. Bai, Q. *et al.* Long-term acetaminophen treatment induced liver fibrosis in mice

and the involvement of Egr-1. *Toxicology* **382**, 47–58 (2017).

317. Schuster, S., Cabrera, D., Arrese, M. & Feldstein, A. E. Triggering and resolution of inflammation in NASH. *Nat. Rev. Gastroenterol. Hepatol.* **15**, 349–364 (2018).

318. 10.

319. Donnelly, K. L. *et al.* Sources of fatty acids stored in liver and secreted via lipoproteins in patients with nonalcoholic fatty liver disease. *J. Clin. Invest.* **115**, 1343–1351 (2005).

320. Chen, H. *et al.* Consumption of Sugar-Sweetened Beverages Has a Dose-Dependent Effect on the Risk of Non-Alcoholic Fatty Liver Disease: An Updated Systematic Review and Dose-Response Meta-Analysis. *International Journal of Environmental Research and Public Health* **16**, (2019).

321. Todoric, J. *et al.* Fructose stimulated de novo lipogenesis is promoted by inflammation. *Nat. Metab.* **2**, 1034–1045 (2020).

322. Van Rooyen, D. M. *et al.* Hepatic Free Cholesterol Accumulates in Obese, Diabetic Mice and Causes Nonalcoholic Steatohepatitis. *Gastroenterology* **141**, 1393-1403.e5 (2011).

323. Kim, J. Y. *et al.* ER Stress Drives Lipogenesis and Steatohepatitis via Caspase-2 Activation of S1P. *Cell* **175**, 133-145.e15 (2018).

324. Charlton, M. *et al.* Fast food diet mouse: novel small animal model of NASH with ballooning, progressive fibrosis, and high physiological fidelity to the human condition. *Am. J. Physiol. Liver Physiol.* **301**, G825–G834 (2011).

325. Tsuchida, T. *et al.* A simple diet- and chemical-induced murine NASH model with rapid progression of steatohepatitis, fibrosis and liver cancer. *J. Hepatol.* **69**, 385–395 (2018).

326. Gallage, S. *et al.* A researcher's guide to preclinical mouse NASH models. *Nat. Metab.* **4**, 1632–1649 (2022).

327. Huby, T. & Gautier, E. L. Immune cell-mediated features of non-alcoholic steatohepatitis. *Nat. Rev. Immunol.* **22**, 429–443 (2022).

328. Daemen, S. *et al.* Dynamic Shifts in the Composition of Resident and Recruited Macrophages Influence Tissue Remodeling in NASH. *Cell Rep.* **34**, 108626 (2021).

329. Remmerie, A. *et al.* Osteopontin Expression Identifies a Subset of Recruited Macrophages Distinct from Kupffer Cells in the Fatty Liver. *Immunity* **53**, 641-657.e14 (2020).

330. Seidman, J. S. *et al.* Niche-Specific Reprogramming of Epigenetic Landscapes Drives Myeloid Cell Diversity in Nonalcoholic Steatohepatitis. *Immunity* **52**, 1057-1074.e7 (2020).

331. Wiering, L., Subramanian, P. & Hammerich, L. Hepatic Stellate Cells: Dictating Outcome in Nonalcoholic Fatty Liver Disease. *Cell. Mol. Gastroenterol. Hepatol.* **15**, 1277–1292 (2023).

332. Povero, D. *et al.* Lipid-induced hepatocyte-derived extracellular vesicles

regulate hepatic stellate cell via microRNAs targeting PPAR-γ. *Cell. Mol. Gastroenterol. Hepatol.* **1**, 646-663.e4 (2015).

333. Mauer, A. S., Hirsova, P., Maiers, J. L., Shah, V. H. & Malhi, H. Inhibition of sphingosine 1-phosphate signaling ameliorates murine nonalcoholic steatohepatitis. *Am. J. Physiol. Gastrointest. Liver Physiol.* **312**, G300–G313 (2017).

334. Carter, J. K. & Friedman, S. L. Hepatic Stellate Cell-Immune Interactions in NASH. *Front. Endocrinol. (Lausanne).* **13**, 867940 (2022).

335. Fickert, P. *et al.* A New Xenobiotic-Induced Mouse Model of Sclerosing Cholangitis and Biliary Fibrosis. *Am. J. Pathol.* **171**, 525–536 (2007).

336. Yanguas, S. C. *et al.* Experimental models of liver fibrosis. *Arch. Toxicol.* **90**, 1025–1048 (2016).

337. Cook, M. E., Jarjour, N. N., Lin, C.-C. & Edelson, B. T. Transcription Factor Bhlhe40 in Immunity and Autoimmunity. *Trends Immunol.* **41**, 1023–1036 (2020).

338. Ow, J. R., Tan, Y. H., Jin, Y., Bahirvani, A. G. & Taneja, R. Stra13 and Sharp-1, the non-grouchy regulators of development and disease. *Curr. Top. Dev. Biol.* **110**, 317–338 (2014).

339. Sun, H., Lu, B., Li, R. Q., Flavell, R. A. & Taneja, R. Defective T cell activation and autoimmune disorder in Stra13-deficient mice. *Nat. Immunol.* **2**, 1040–1047 (2001).

340. Lin, C.-C. *et al.* Bhlhe40 controls cytokine production by T cells and is essential for pathogenicity in autoimmune neuroinflammation. *Nat. Commun.* **5**, 3551 (2014).

341. Zhang, L. *et al.* Lineage tracking reveals dynamic relationships of T cells in colorectal cancer. *Nature* **564**, 268–272 (2018).

342. Yu, F. *et al.* The transcription factor Bhlhe40 is a switch of inflammatory versus antiinflammatory Th1 cell fate determination. *J. Exp. Med.* **215**, 1813–1821 (2018).

343. Huynh, J. P. *et al.* Bhlhe40 is an essential repressor of IL-10 during Mycobacterium tuberculosis infection. *J. Exp. Med.* **215**, 1823–1838 (2018).

344. O'Neal, K. A., Zeltner, S. L., Foscue, C. L. & Stumhofer, J. S. Bhlhe40 limits early IL-10 production from CD4(+) T cells during Plasmodium yoelii 17X infection. *Infect. Immun.* **91**, e0036723 (2023).

345. Jarjour, N. N. *et al.* Bhlhe40 mediates tissue-specific control of macrophage proliferation in homeostasis and type 2 immunity. *Nat. Immunol.* **20**, 687–700 (2019).

346. Rauschmeier, R. *et al.* Bhlhe40 and Bhlhe41 transcription factors regulate alveolar macrophage self-renewal and identity. *EMBO J.* **38**, e101233 (2019).

347. Zafar, A., Ng, H. P., Kim, G.-D., Chan, E. R. & Mahabeleshwar, G. H. BHLHE40 promotes macrophage pro-inflammatory gene expression and functions.

FASEB J. **35**, e21940 (2021).

348. Podlesny-Drabiniok, A. *et al.* BHLHE40/41 regulate macrophage/microglia responses associated with Alzheimer's disease and other disorders of lipid-rich tissues. *bioRxiv : the preprint server for biology* (2023). doi:10.1101/2023.02.13.528372

349. Ortiz, C. *et al.* Extracellular Matrix Remodeling in Chronic Liver Disease. *Curr. Tissue Microenviron. Reports* **2**, 41–52 (2021).

350. Asrani, S. K., Devarbhavi, H., Eaton, J. & Kamath, P. S. Burden of liver diseases in the world. *J. Hepatol.* **70**, 151–171 (2019).

351. Kantari-Mimoun, C. *et al.* Resolution of liver fibrosis requires myeloid cell-driven sinusoidal angiogenesis. *Hepatology* **61**, 2042–2055 (2015).

352. Roeb, E. Matrix metalloproteinases and liver fibrosis (translational aspects). *Matrix Biol.* **68**–**69**, 463–473 (2018).

353. Askia, H. *et al.* Obesity-elicited macrophages shape CD9^{hi} progenitor fate to promote adipose tissue fibrosis and dysfunction. *bioRxiv* 2023.09.26.559540 (2023). doi:10.1101/2023.09.26.559540

354. Gautier, E. L. *et al.* Gene-expression profiles and transcriptional regulatory pathways that underlie the identity and diversity of mouse tissue macrophages. *Nat. Immunol.* **13**, 1118–1128 (2012).

355. Getachew, A. *et al.* SAA1/TLR2 axis directs chemotactic migration of hepatic stellate cells responding to injury. *iScience* **24**, 102483 (2021).

356. Semenza, G. L., Roth, P. H., Fang, H. M. & Wang, G. L. Transcriptional regulation of genes encoding glycolytic enzymes by hypoxia-inducible factor 1. *J. Biol. Chem.* **269**, 23757–23763 (1994).

357. Zigmond, E. *et al.* Infiltrating Monocyte-Derived Macrophages and Resident Kupffer Cells Display Different Ontogeny and Functions in Acute Liver Injury. *J. Immunol.* **193**, 344–353 (2014).

358. Jaitin, D. A. *et al.* Lipid-Associated Macrophages Control Metabolic Homeostasis in a Trem2-Dependent Manner. *Cell* **178**, 686-698.e14 (2019).

359. Cochain, C. *et al.* Single-Cell RNA-Seq Reveals the Transcriptional Landscape and Heterogeneity of Aortic Macrophages in Murine Atherosclerosis. *Circ. Res.* **122**, 1661–1674 (2018).

360. Keren-Shaul, H. *et al.* A Unique Microglia Type Associated with Restricting Development of Alzheimer's Disease. *Cell* **169**, 1276-1290.e17 (2017).

361. Labiano, I. *et al.* TREM-2 plays a protective role in cholestasis by acting as a negative regulator of inflammation. *J. Hepatol.* **77**, 991–1004 (2022).

362. Hendrikx, T. *et al.* Soluble TREM2 levels reflect the recruitment and expansion of TREM2(+) macrophages that localize to fibrotic areas and limit NASH. *J. Hepatol.* **77**, 1373–1385 (2022).

363. Perugorria, M. J. *et al.* Non-parenchymal TREM-2 protects the liver from

immune-mediated hepatocellular damage. *Gut* **68**, 533–546 (2019).

364. Fabre, T. *et al.* Identification of a broadly fibrogenic macrophage subset induced by type 3 inflammation. *Sci. Immunol.* **8**, eadd8945 (2023).

365. Wang, X. *et al.* Prolonged hypernutrition impairs TREM2-dependent efferocytosis to license chronic liver inflammation and NASH development. *Immunity* **56**, 58-77.e11 (2023).